UNIVERSITA' DEGLI STUDI DI PADOVA

DIPARTIMENTO DI INGEGNERIA INDUSTRIALE

CORSO DI LAUREA MAGISTRALE IN CHEMICAL AND PROCESS ENGINEERING

Tesi di Laurea Magistrale in
Chemical and Process Engineering

Valorisation of Dairy Industry By-Products Through Mixotrophic and Heterotrophic Cultivation of *Galdiera sulphuraria*: A Techno-Economic Perspective

Relatore: Prof. Elena Barbera

Correlatore: Leonardo Pattaro

Laureando: IVÁN GONZÁLEZ ALONSO

ANNO ACCADEMICO 2025/26

Abstract

The valorisation of industrial by-products represents a key strategy for improving the sustainability and economic viability of biotechnological processes. In this context, the thermo-acidophilic microalga *Galdieria sulphuraria* is of particular interest because of its metabolic versatility and its ability to grow under both heterotrophic and mixotrophic conditions. This thesis investigates the use of dairy industry by-products, namely milk permeate and second cheese whey (SCW), as substrates for the cultivation of *G. sulphuraria*, combining laboratory-scale experimentation with process design and preliminary techno-economic assessment.

The experimental work focuses on the continuous cultivation of *G. sulphuraria* on milk permeate under heterotrophic and mixotrophic conditions. In parallel, milk permeate and SCW are characterised in terms of carbon, nitrogen, and phosphorus content to support process calculations. Under the tested conditions, heterotrophic cultivation achieves a biomass productivity of 2.83 ± 0.05 g L^{-1} d^{-1}, whereas the highest productivity obtained under mixotrophic conditions is 1.56 ± 0.16 g L^{-1} d^{-1}, indicating that heterotrophic cultivation is more favourable for biomass production under the investigated conditions.

The experimental results are then used as the basis for conceptual plant design, mass and energy balances, process simulation, and techno-economic assessment. Three process configurations are evaluated: a large-scale heterotrophic process based on milk permeate, a small-scale heterotrophic process based on SCW, and a sequential small-scale heterotrophic and mixotrophic process based on SCW with C-phycocyanin recovery. Among the analysed scenarios, the large-scale heterotrophic permeate configuration proves to be the most favourable, with a biomass production of 453 kg h^{-1} and an NPV of 65.5 M€. By contrast, the small-scale heterotrophic SCW scenario is not economically feasible in its current form, with an NPV of −0.15 M€. However, the sequential heterotrophic and mixotrophic SCW configuration improves the economic performance by enabling the recovery of 0.18 kg h^{-1} of C-phycocyanin as a higher-value product and reaches an NPV of 0.83 M€.

Overall, the results show that dairy by-products can be valorised through the cultivation of *G. sulphuraria*, although the final outcome depends strongly on cultivation regime, process scale, and product portfolio.

Declaration of usage of generative AI and AI-assisted technologies

AI-assisted technologies were used to support the review of scientific and technical literature, including the translation of selected papers and technical sources when needed. They were also used to generate and modify some images, as well as to assist in the revision of grammar and language throughout the thesis.

The author reviewed and edited the thesis as needed and take full responsibility for its content.

Acknowledgments

Con este trabajo no solo concluye este máster, sino también una etapa muy importante de mi vida: mi etapa como estudiante. La recta final de este camino no ha sido fácil; ha habido momentos difíciles, y el máster ha supuesto una experiencia muy exigente, tanto a nivel académico como personal. Aun así, me gustaría expresar mi más sincero agradecimiento a la Universidad de Padova y a sus profesores, porque, sin ninguna duda, han contribuido a convertirme en un mejor ingeniero.

En primer lugar, quiero agradecer profundamente a mis padres, Pilar Alonso López y Ángel González Serrano, por haber estado siempre a mi lado cuando más lo he necesitado. No solo me han brindado su apoyo incondicional, sino que también me han dado la oportunidad de cursar este máster, algo que no habría sido posible sin ellos. Cuando todo iba bien, el camino parecía más sencillo, pero ha sido especialmente en los momentos difíciles —que los ha habido, y muchos más de los que me hubiera gustado— cuando más he sentido su apoyo, su paciencia y su ayuda en todas las formas posibles. Siento sinceramente que, sin vosotros, este máster no habría sido posible; por eso, este logro también es vuestro.

También quiero dar las gracias a mi hermano, David, que, aunque a veces pueda parecer más ausente, sé que siempre está ahí para mí y que siempre me desea lo mejor.

A mis abuelos, Abilio e Isabel, quiero agradecerles de una manera muy especial todo lo que han significado para mí. Sé que, en muchas ocasiones, se alegran incluso más que yo de cada examen aprobado y sufren aún más que yo cuando las cosas no salen bien. Por eso, y por toda la educación, los valores y el cariño que me han dado, y que han contribuido a convertirme en la persona que soy hoy, les estaré siempre profundamente agradecido.

También quiero agradecer al resto de mi familia, tanto a la de Vitoria como a la de Madrid, por su apoyo y su cariño. Muchas gracias a todos.

Asimismo, me gustaría dar las gracias a la persona que ha sido mi mayor apoyo aquí en Italia: mi novia, Veronica Zoe Piazza. Solo quiero decirte gracias. Gracias por haber estado siempre ahí cuando más lo he necesitado y gracias por la santa paciencia que tienes a veces conmigo. Sabes que, para mí, esta etapa no ha sido nada fácil y que ha habido muchos momentos difíciles. Sin embargo, tanto en la distancia, cuando estabas en Canadá, como aquí, cerca de mí, en Marghera, hemos sabido estar siempre el uno para el otro. Siento que este logro también es, en parte, gracias a ti.

También me gustaría dedicar unas palabras especiales a mis amigos de Vitoria, que, desde la distancia, de una manera directa o indirecta, siempre han estado ahí, en cada llamada y en cada mensaje. Ha habido momentos en los que no me encontraba bien y ellos, sin saberlo, con una llamada o simplemente contándome cómo iban las cosas por allí, conseguían animarme. Quiero mencionar de

forma especial a algunos de ellos, por estar siempre ahí y por haber venido a visitarme, algo que me ha hecho una especial ilusión y que valoro profundamente por el esfuerzo que han hecho para venir a verme. Gracias, Iñaki, Asier, Adrián, Aitor, Ander, Iker, Ari y Anne.

De mi estancia en Padova, quiero dar las gracias a mis compañeros de piso canarios del primer año, a mis compañeros del máster y, en general, a todas las personas que han formado parte de esta etapa de mi vida en Italia. Entre todas ellas, quiero destacar especialmente a Tommaso. No sé qué habría hecho sin él. Gracias a él, siento que todo mi recorrido en el máster ha sido más fácil, porque no solo encontré un compañero, sino también un gran amigo. Ha hecho que mi vida fuera mejor tanto dentro como fuera de las aulas y, sinceramente, considero que, sin su ayuda y su apoyo, no habría terminado el máster ahora y probablemente me habría costado mucho más. Gracias.

Table of contents

Introduction *1*

Chapter 1 Theorical Background and State of Art *5*

1.1 The dairy industry and its by-products **5**

1.1.1 Overview of dairy processing 5

1.1.2 By-products of dairy industry 8

1.1.3 Permeate and second cheese whey (SCW) 9

1.1.4 Regulations and environmental compliance for dairy by-products 12

1.1.5 Valorisation of dairy by-products 14

1.2 Microalgae and their industrial potential **16**

1.2.1 Nutrition and feed applications 17

1.2.2 Cosmetics 18

1.2.3 Pigment production 18

1.2.4 Biofuel technologies 18

1.2.5 Environmental remediation technologies 19

1.3 Microalgae cultivation **20**

1.3.1 Cultivation regimes: autotrophic, heterotrophic and mixotrophic 20

1.3.2 Growth factors affecting microalgae 21

1.3.2.1 Nutrients availability 21

1.3.2.2 Light 22

1.3.2.3 pH 23

1.3.2.4 Temperature 24

1.3.3 Cultivation strategies 25

1.3.3.1 Batch 25

1.3.3.2 Continuous 26

1.3.4 Cultivation systems 26

1.3.4.1 Open systems 26

1.3.4.2 Closed systems 27

1.3.5 Cultivation equipment and scale-up considerations 27

1.4 *Galdieria sulphuraria* **30**

1.4.1 Taxonomy and physiology 31

1.4.2 Growth conditions and nutrient requirements 31

1.4.3 Biotechnological relevance 31

1.5 Objective of the thesis **33**

Chapter 2 Materials and Methods 35

2.1 Algal strain and acclimation conditions 35

2.2 Continuous cultivation 36

2.2.1 Mixotrophic experiments 38

2.2.2 Heterotrophic cultivation 39

2.3 Monitoring, analytical methods and measurements 40

2.3.1 Optical density 40

2.3.2 Dry weight 41

2.3.3 Total organic carbon and total nitrogen 41

2.3.4 Phosphates analysis 42

2.4 Material balances 43

2.4.1 Carbon balances 44

2.4.2 Nitrogen balances 45

2.4.3 Phosphorus balances 46

2.5 Process simulation and conceptual plant design 46

2.5.1 Large-scale process design 47

2.5.1.1 Process flow diagram and process description 47

2.5.1.2 Main equipment and operating conditions 50

2.5.2 Small-scale process design 51

2.5.2.1 Process flow diagram and process description 51

2.5.2.2 Main equipment and operating conditions 57

2.6 Energy balances 60

2.7 Methodology for economic analysis 61

Chapter 3 Laboratory Results and Discussion 65

3.1 Characterisation of the by-products and culture media 65

3.1.1 Milk permeate 65

3.1.2 Second cheese whey 66

3.1.3 Representative inlet compositions adopted for process calculations 67

3.2 Results of the continuous heterotrophic cultivation 68

3.3 Results of the continuous mixotrophic cultivation 70

3.3.1 Biomass productivity 70

3.3.2 TOC and TN 72

3.3.3 Phosphorus content 73

3.3.4 Experimental yield coefficients 73

3.4 Comparison between heterotrophic and mixotrophic cultivation 74

3.5 Productivity and yield coefficients selected for process design 74

Chapter 4 Techno-Economic Results and Discussion 77

4.1 Large-scale scenario: heterotrophic cultivation 77

4.1.1 Process performance and stream compositions 78

4.1.2 Economic performance and feasibility 79

4.2 Small-scale scenario: heterotrophic cultivation 81

4.2.1 Process performance and stream compositions 81

4.2.2 Economic performance and feasibility 82

4.3 Small-scale scenario: sequential heterotrophic and mixotrophic cultivation 83

4.3.1 Process performance and stream compositions 84

4.3.2 Economic performance and feasibility 87

4.3.3 Sensitivity analysis 88

4.3.3.1 Electricity price 88

4.3.3.2 C-phycocyanin content 89

4.4 Comparative discussion of the three scenarios 90

4.4.1 CAPEX and OPEX 91

4.4.2 Comparison of profitability indicators 91

Conclusions 93

Appendix 97

A Survey for inlet determination 97

B Estimation procedure for productivity and light intensity evaluation in mixotrophic conditions 98

B.1 Productivity 98

B.2 Light intensity 99

C Economic formulas 99

C.1 Reactor installed cost calculation 99

C.2 Heat exchangers and impellers installed cost calculation 99

C.3 Heating water stream calculations for heat exchangers 100

C.4 Reactor and other equipment's scale-up costs 100

D Detailed economic results 101

D.1 Capital and operating cost breakdown 101

D.2 Profitability analysis results 103

Glossary 107

List of symbols..... *109*

References *113*

List of Figures

Figure 1.1. Production line for market milk.
Figure 1.2. Production line for cheese.
Figure 1.3. Application opportunities for whey processing.
Figure 1.4. Photosynthesis rate against light irradiance curve.
Figure 1.5. Temperature effect on microalgae growth rates.
Figure 1.6. Illustration of (a) bubble column, (b) airlift, (c) horizontal tubular, (d) flat-plate, and (e) stirred tank photobioreactors.

Figure 2.1. Microscopic picture of *Galdieria sulphuraria*.
Figure 2.2. Scheme of the laboratory-scale continuous cultivation system.
Figure 2.3. Isometric and front view of the PBR used for the continuous cultivation of *G. sulphuraria*.
Figure 2.4. Experimental set-up for mixotrophic cultivation.
Figure 2.5. Experimental set-up for heterotrophic cultivation.
Figure 2.6. Orthophosphate calibration curve.
Figure 2.7. Schematic representation of the streams considered for yield calculations.
Figure 2.8. Process flow diagram of the large-scale heterotrophic permeate valorisation process.
Figure 2.9. Schematic representation of a disc-stack centrifuge bowl and phase separation mechanism.
Figure 2.10. First section of the process flow diagram for the proposed small-scale SCW valorisation process.
Figure 2.11. Second section of the process flow diagram for the sequential heterotrophic and mixotrophic small-scale SCW valorisation process.
Figure 2.12. PBR size and main characteristics.

Figure 3.1. Evolution of optical density at 680 and 750 nm during continuous heterotrophic cultivation.
Figure 3.2. Evolution of optical density at 750 nm during continuous heterotrophic cultivation, with the corresponding biomass productivity values measured under steady-state conditions.
Figure 3.3. Average biomass productivity under heterotrophic and mixotrophic conditions.

Figure 4.1. Discounted cash-flow profile over the project lifetime for the heterotrophic large-scale scenario.
Figure 4.2. Discounted cash-flow profile over the project lifetime for the heterotrophic small-scale scenario.
Figure 4.3. Discounted cash-flow profile over the project lifetime for the sequential heterotrophic and mixotrophic small-scale scenario.
Figure 4.4. Cumulative discounted cash-flow profiles for different electricity price scenarios considered in the sensitivity analysis.
Figure 4.5. Cumulative discounted cash-flow profiles for the different C-phycocyanin content scenarios considered in the sensitivity analysis.

Figure D.1. Annual cash-flow components for the heterotrophic large-scale scenario.
Figure D.2. Annual cash-flow components for the heterotrophic small-scale scenario.
Figure D.3. Annual cash-flow components for the sequential heterotrophic and mixotrophic small-scale scenario.

List of Tables

Table 1.1. Typical composition of selected dairy by-products and dairy processing streams.
Table 1.2. Regulatory pollution limits for dairy wastewater discharges to receiving waters.
Table 1.3. Typical wastewater discharge volumes in dairy processing according to product type.
Table 1.4. Bioactive compounds produced by *G. sulphuraria*.

Table 2.1. Formulation of the enriched MAM medium.
Table 2.2. Experimental matrix for continuous mixotrophic cultivation under different organic carbon concentrations and light intensities.
Table 2.3. Chemical Engineering Plant Cost Index (CEPCI) values for the last five years.
Table 2.4. Prices used for economic analysis.

Table 3.1. Experimental characterisation of milk permeate.
Table 3.2. Experimental characterisation of SCW.
Table 3.3. Representative inlet compositions adopted for the process calculations.
Table 3.4. TOC and TN concentrations measured under steady-state conditions during continuous heterotrophic cultivation.
Table 3.5. Yield coefficients obtained from the heterotrophic experiment under steady-state conditions.
Table 3.6. Average optical density, biomass concentration, and productivity values measured under steady-state conditions during continuous mixotrophic cultivation under different influent carbon concentrations and light intensities.
Table 3.7. TOC concentrations in the different streams under the tested conditions.
Table 3.8. TN concentrations in the different streams under the tested conditions.
Table 3.9. Yield coefficients obtained from the mixotrophic experiments under steady-state conditions.
Table 3.10. Productivity values adopted for the different process configurations.
Table 3.11. Yield coefficients adopted for the heterotrophic process design.
Table 3.12. Conversion and yield coefficients adopted for the mixotrophic process design based on SCW experiments.

Table 4.1. Volumetric flow rates, elemental concentrations, and biomass flow rates of the streams in the large-scale heterotrophic cultivation process.

Table 4.2. Volumetric flow rates, elemental concentrations, and biomass flow rates of the streams in the small-scale heterotrophic cultivation process.
Table 4.3. Volumetric flow rates, elemental concentrations, biomass flow rates, and C-phycocyanin flow rates of the streams in the sequential heterotrophic and mixotrophic small-scale cultivation process.
Table 4.4. Estimated CAPEX and OPEX of the analysed process scenarios.
Table 4.5. Comparison of the main profitability indicators for the analysed scenarios.

Table A.1. Survey carried out by the University of Bologna on the quantities of by-products produced by different dairy industries.

Table D.1. Installed cost of the main equipment items for the analysed process scenarios.
Table D.2. Total capital investment for the analysed process scenarios.
Table D.3. Annual revenues and main operating cost items for the analysed process scenarios.
Table D.4. Annual profitability and cash-flow results for the analysed scenarios.

Introduction

The dairy industry is one of the most important sectors of the food system, but it also generates large quantities of side-streams and by-products that still contain recoverable organic matter and nutrients. In particular, whey and related dairy residues are characterised by high concentrations of lactose, residual proteins, minerals, and other soluble compounds, which make them both an environmental burden and a potential resource for valorisation (Sar et al., 2022). Owing to their high organic load, these streams may exhibit elevated chemical oxygen demand (COD) and biochemical oxygen demand (BOD), so their disposal or inadequate management can create significant environmental and economic challenges for dairy producers. While some by-products, such as whey, are already widely utilised, others, including milk permeate and second cheese whey (SCW), remain comparatively underexploited despite their potential value. As a result, the disposal or treatment of these streams continues to represent an environmental and economic burden for dairy companies. Direct global production data for milk permeate and SCW are not readily available in public international dairy statistics. As contextual information, global whey production has been estimated at approximately 200 million tonnes per year, while SCW accounts for about 90% or more of the original whey in whey-cheese production (Barba, 2021).

In this context, increasing attention has been devoted, at both the scientific and industrial levels, to the development of alternative strategies capable of converting dairy by-products into value-added products rather than treating them solely as waste streams. Among the available approaches, microalgae are particularly attractive because they represent versatile biological platforms capable of transforming residual streams into valuable biomass and bio-based products. Within this framework, *Galdieria sulphuraria* is especially interesting because of its metabolic flexibility and its ability to grow under acidic conditions, which may reduce contamination issues and facilitate the use of organic-rich by-products. Therefore, investigating the cultivation of *G. sulphuraria* on dairy side-streams is relevant from both an environmental and a biotechnological-economic perspective.

However, the feasibility of these valorisation routes remains uncertain and strongly depends on the selected process configuration, cultivation strategy, and final product portfolio. For this reason, it is important not only to assess microalgal growth at laboratory scale, but also to connect the experimental results with process design and techno-economic analysis. From an industrial perspective, this issue is particularly relevant because dairy industries must manage these streams

while complying with environmental regulations and controlling wastewater-treatment costs. Although large companies generally manage these side-streams within established treatment systems, smaller dairies may have fewer options for proper handling and may still direct them to low-value uses, such as animal feed, or manage them less efficiently.

This work is motivated by the need to identify feasible valorisation routes for dairy by-products that are still underused. To support this investigation, data and samples were collected from dairy industries in the Bologna area. The study focuses on two specific streams, milk permeate and SCW, as potential substrates for the cultivation of *Galdieria sulphuraria*. Particular interest is given to the possibility of exploiting this microalga under both heterotrophic and mixotrophic conditions. While heterotrophic cultivation may favour higher biomass productivity, mixotrophic cultivation may enable not only biomass production but also the synthesis of higher-value compounds, such as pigments, including C-phycocyanin. Accordingly, the work compares not only different substrates, but also different cultivation and valorisation strategies.

The overall objective of this thesis is to assess the potential valorisation of selected dairy by-products through the cultivation of *Galdieria sulphuraria*, combining experimental investigation with a preliminary techno-economic evaluation. More specifically, the study aims to evaluate the suitability of milk permeate and SCW as substrates for the cultivation of *G. sulphuraria* and to investigate the growth performance of the microalga under both heterotrophic and mixotrophic conditions using dairy-derived media. In addition, the work aims to determine key experimental parameters, including biomass productivity and elemental yield coefficients, and to use these results as the basis for process simulation, conceptual plant design, and techno-economic assessment. Finally, the study compares different process scenarios at different scales in order to evaluate whether the valorisation of these dairy by-products through microalgal cultivation can be considered technically feasible and economically promising.

Following this Introduction, Chapter 1 will deal with the theoretical background, state of the art, and literature review related to the topic. More specifically, it will discuss the dairy sector, highlighting the by-products generated in this industry, namely milk permeate and SCW, and the most important aspects concerning microalgal cultivation, paying special attention to *Galdieria sulphuraria* and its biological and biotechnological features. The experimental procedures, material, and methodologies used in the study will be discussed in Chapter 2. In this chapter, the materials employed and used in the experiments as well as the laboratory scale cultivation will be described. Further, the methodology used for characterisation of dairy by-products, process simulation, and evaluation of productivity and yields will also be mentioned. The experimental results obtained, including the characterisation of the dairy by-products, as well as the productivity and yield coefficients determined will then be presented in Chapter 3, allowing further discussions

on the results obtained in Chapter 4, where the techno-economic results will be shown. Finally, the main conclusions are drawn, the limitations of the study are discussed, and possible avenues for future research are proposed.

Chapter 1

Theorical Background and State of Art

1.1 The dairy industry and its by-products

1.1.1 Overview of dairy processing

The dairy industry encompasses all activities involved in the production, processing, and distribution of milk and dairy products. These activities rely on the combined efforts of scientists, agricultural specialists, and industry professionals working to ensure product safety, quality, and efficiency throughout the production chain.

Raw milk is the primary raw material used in the dairy industry. Its composition, particularly the proportions of fat, proteins, lactose, and minerals, determines the processing conditions required for different dairy products. Before reaching consumers, it undergoes several treatment stages carried out in specialized processing equipment. Through these processes, raw milk is transformed into a wide variety of dairy products such as pasteurized milk, cheese, butter, and other derivatives. Each product requires specific processing conditions, although many of the initial treatment steps are common across different dairy manufacturing processes.

In a typical milk processing line (Figure 1.1), raw milk is first pumped into a balance tank, where it is temporarily stored and maintained at a constant level and at a temperature below 4 °C to limit microbial growth before entering the rest of the processing system (SPX Flow, 2019). From there, the milk is directed to a plate heat exchanger, where it is preheated through regenerative heat exchange with outgoing pasteurized milk. This step improves the overall energy efficiency of the process by recovering heat from the already processed milk.

Following preheating, the milk enters a centrifugal separator, where it is separated into two streams: cream and skim milk. In industrial dairy separators, the cream stream typically contains about 35–40% fat, while the skim milk contains only 0.01–0.05% residual fat, depending on the efficiency and operating conditions of the separator (Trucent, 2021).

The operating conditions of the separator therefore determine the fat distribution between the two streams. To obtain a final product with a fixed fat content, a controlled amount of cream is blended back with skim milk. This adjustment of the fat concentration, known as standardization, allows the production of milk with defined fat levels such as approximately 3.25–3.5% for whole milk, 1–2% for reduced-fat milk, and <0.5% for skim milk (McCarthy et al., 2017).

After standardization, the milk may undergo homogenization, a mechanical process that reduces the size of fat globules by forcing the milk through a narrow valve at high pressure. This treatment prevents the separation of cream during storage and improves the physical stability and texture of the product. In many industrial processes, partial homogenization is applied, meaning that only a portion of the milk stream is homogenized before being recombined with the remaining milk (Kiełczewska et al., 2022). This strategy allows the use of a smaller homogenizer while still achieving the desired product characteristics, making the process more economically efficient.

One of the most fundamental operations in the dairy industry is milk pasteurization, which constitutes the core process in the production of market milk. Pasteurization is a heat treatment designed to destroy pathogenic microorganisms and reduce the microbial load present in raw milk. This process is essential for ensuring the safety of dairy products and extending their shelf life. In most countries, heat treatment of milk intended for human consumption is required by law to protect public health by inactivating harmful microorganisms (Bylund, 1995).

Two main pasteurization methods are commonly used. Low-temperature long-time (LTLT) pasteurization is typically applied to small milk volumes (≤1000 L) using relatively simple equipment. In contrast, high-temperature short-time (HTST) pasteurization is used in continuous industrial processes, where milk is heated to at least 72 °C for 15 s and then rapidly cooled to 4 °C, allowing large-scale processing capacities of 5000 L h^{-1} or higher (Fox & McSweeney, 2002). In addition to being essential for the production of fluid milk, pasteurization also acts as an important preliminary step in the manufacture of many other dairy products, including cheese. To guarantee proper treatment, the system is equipped with a flow diversion valve that automatically redirects the milk back to the balance tank if the pasteurization temperature falls below the required level (Bylund, 1995).

After pasteurization, the milk is cooled in the heat exchanger. First, heat is transferred to the incoming raw milk through regenerative heat exchange, improving energy efficiency, and the milk is subsequently cooled using chilled or ice water to about 4–5 °C before packaging (Fox & McSweeney, 2002). Such processing technologies are essential given the scale of the dairy sector. Global per-capita milk supply in 2023 was approximately 110–120 kg per person per year (Ritchie & Roser, 2023).

Figure 1.1 illustrates the main stages involved in market milk production.

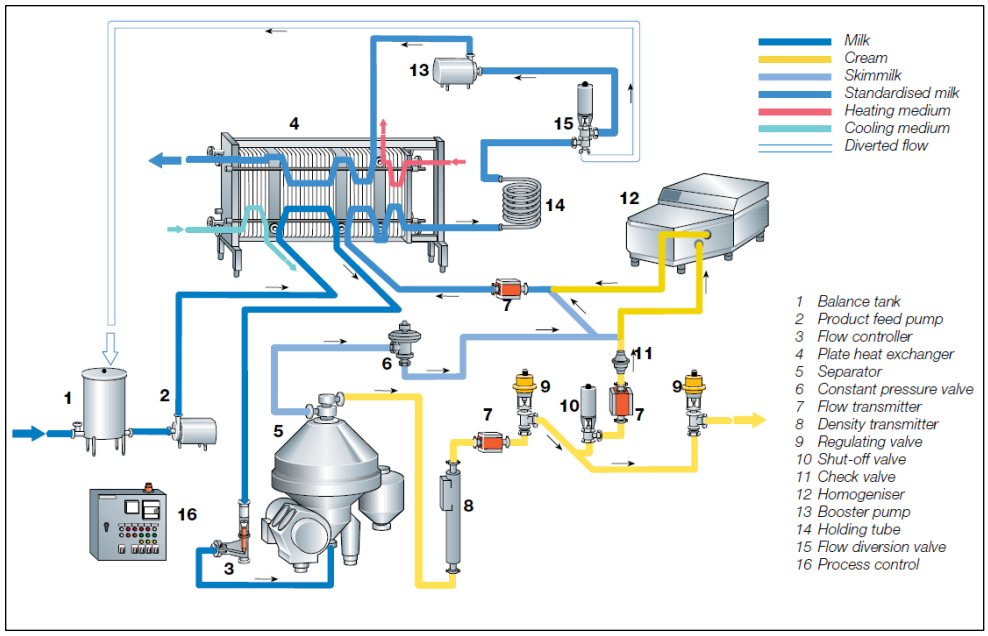

Figure 1.1. *Production line for market milk (Bylund, 1995).*

While pasteurized milk is one of the most common dairy products, many other dairy products require additional processing steps. Cheese production, for example, involves several biochemical and physical transformations that convert milk into a solid fermented product.

The initial stages of cheese production are similar to those used in market milk processing. Raw milk typically undergoes pasteurization, fat standardization, and filtration to ensure consistent composition and microbiological safety. Once the milk has been treated, starter cultures, mainly composed of lactic acid bacteria such as *Lactococcus*, *Lactobacillus*, and *Streptococcus* species, are added. These microorganisms ferment lactose, the primary sugar in milk, converting it into lactic acid (Coelho et al., 2022).

The production of lactic acid gradually lowers the pH of the milk, creating the conditions necessary for the next step of the process: coagulation. When the pH reaches the appropriate level, an enzyme is added to initiate the coagulation of milk proteins. This enzyme acts primarily on casein proteins, causing them to aggregate and form a gel-like structure known as the coagulum (Encyclopaedia Britannica, Inc., 2014).

Two main mechanisms of coagulation are commonly used in cheese production. In rennet coagulation, the rennet enzyme, which contains the protease chymosin, is added to milk. This process typically occurs at a relatively high pH and produces a firm curd that contributes to the characteristic texture and flavour development of many cheeses. On the other hand, acid coagulation occurs when acid is directly added to the milk, for example in the form of vinegar or

lemon juice. This process takes place at a lower pH and results in softer curds with a more delicate texture (Santiago-López et al., 2021).

Once coagulation has occurred, the gel structure is cut into small pieces known as curds. At this stage, curds and liquid whey coexist in the same vessel. Stirring and gentle heating promote the contraction of the curd particles, facilitating the separation of whey. The whey is subsequently removed as a by-product of the process.

In the final stages of cheese production, the curds are milled and salted before being placed into molds. The molded curds are then pressed at pressures typically ranging from 50 to 200 kPa, which removes additional whey and helps consolidate the cheese structure (Walstra et al., 2006). Finally, the cheese is transferred to a ripening stage, during which biochemical and microbial transformations develop the final texture, aroma, and flavour characteristics of the product. The ripening period can vary significantly depending on the type of cheese, ranging from a few weeks to several years (Encyclopaedia Britannica, Inc., 2014). An overview of cheese production process is reported in Figure 1.2.

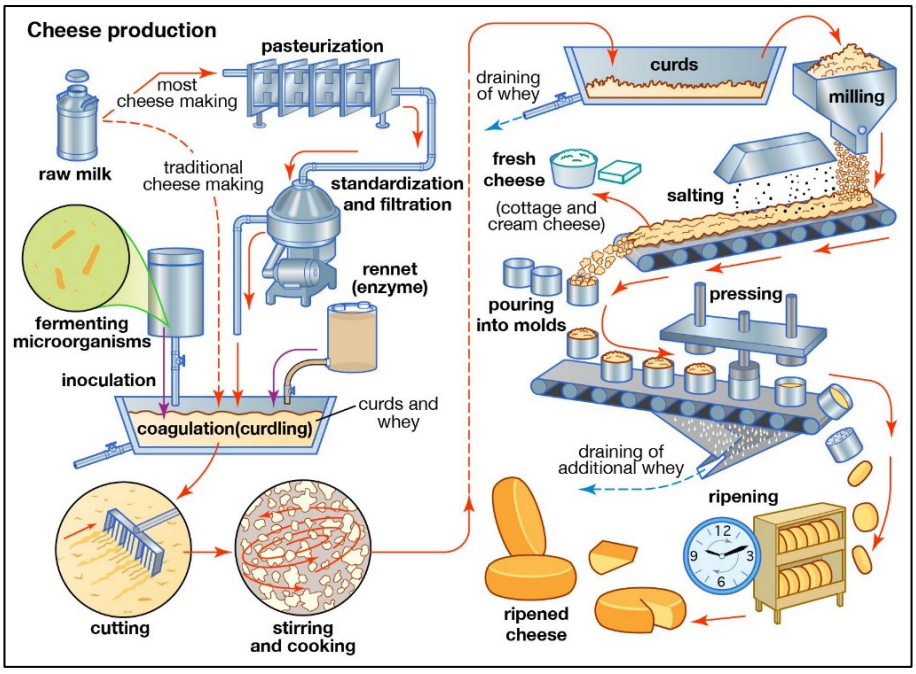

Figure 1.2. *Production line for cheese (Encyclopaedia Britannica, Inc., 2014).*

1.1.2 By-products of dairy industry

The dairy industry is a significant sector in global food production, as mentioned previously. However, dairy processing also generates large quantities of by-products. These materials were traditionally considered waste, but they are now increasingly recognized as valuable resources or as streams that must be properly treated before discharge in order to prevent environmental pollution. Major dairy by-products include buttermilk, cheese whey, ghee residue, and permeate.

Each of these by-products contains important nutritional components such as proteins, lactose, minerals, and vitamins, which provide opportunities for further processing and utilisation.

The most abundantly produced by-product is whey, which is generated during the production of cheese, casein, and yogurt. Roughly 80–90% of the milk processed in cheese production is converted into whey. Globally, this results in an estimated 180–190 million tonnes of whey produced each year, of which approximately 100 million tonnes originate from cheese manufacturing (Buchanan et al., 2023).

Whey is a diluted, pale greenish-yellow liquid that retains roughly half of the original milk solids and therefore represents a valuable source of nutrients such as lactose, whey proteins, minerals, and vitamins (Patel & Sakhale). It is the most abundant by-product generated in the dairy industry during the production of milk-derived products such as cheese. As described previously, whey is obtained during the coagulation stage, when the liquid fraction is separated from the curd.

Two main types of whey can be distinguished: sweet whey and acid (or sour) whey. The difference between these two types is mainly related to the production method and the resulting pH. Sweet whey, often referred to as cheese whey, is produced as a by-product of enzymatic coagulation using rennet during cheese production and typically has a pH around 5.6. In contrast, acid whey is produced during acid coagulation processes and generally has a pH of approximately 5.1 (Minj & Anand, 2020).

Although whey is one of the largest by-products of the dairy industry, it is also one of the most widely utilised and commercially valuable. The global market for whey products is estimated to reach approximately 6.5 billion USD in annual sales in 2023 (MarkNtel Advisors, 2024). Whey is mainly used in nutritional products, particularly within the sports nutrition market (Patel & Sakhale). In addition, it is used in the production of whey derivatives and whey protein concentrates. Another important application is the production of Ricotta cheese, a traditional Italian cheese made from cheese whey (Albenzio & Santillo, 2025). In smaller dairies, whey may also be used as fertilizer or animal feed, sometimes without clear separation from other waste streams.

As previously mentioned, other dairy by-products include permeate and SCW. Although they are produced in smaller quantities globally, they are also less widely utilised.

1.1.3 Permeate and second cheese whey (SCW)

Building on the previously mentioned dairy by-products, permeate streams and SCW represent secondary dairy processing residues with increasing potential for valorisation. These streams are generated during membrane separation processes or during the production of whey cheeses such

as ricotta. Although they are produced in smaller quantities than primary cheese whey, their relatively high lactose content and low protein and fat concentrations make them attractive substrates for further processing and biotechnological applications.

The chemical composition of these dairy by-products varies depending on the processing method and the origin of the raw material; however, lactose generally constitutes the major component of most permeate streams, while protein and fat contents are significantly lower than in the original milk. Table 1.1 summarises the typical composition of several relevant dairy by-products.

Table 1.1. *Typical composition of selected dairy by-products and dairy processing streams.*

By-product	*Lactose (%)*	*Protein (%)*	*Minerals/Ash (%)*	*Fat (%)*	*Reference*
Cheese whey (sweet) (dry basis)	56.9-74.6	11.1-16.6	7.1-10.7	0.37-1.52	Glass & Hedrick, 1977
Acid whey (dry basis)	58.8-71.7	8-12.6	7.3-12.2	0.34-0.74	Glass & Hedrick, 1977
Whey permeate (dry basis)	65-85	3-8	8-20	<1.5	Foegeding et al., 2011
Milk permeate (dry basis)	80	3	8.5	-	Tsermoula et al., 2024
Second cheese whey (dry basis, estimated)	69-71	2.1-3.1	14-16	7	Figueroa Pires et al., 2021
Skim milk powder	54.7	34.2	7.9	0.7	Pugliese et al., 2017
Buttermilk powder	43.7-63.4	-	6.2-7.6	~12	Sodini et al., 2006

Among these streams, milk permeate and whey permeate are the main by-products generated during membrane separation processes. Milk permeate is a by-product obtained through membrane-based separation processes used to fractionate milk components. Advances in membrane separation technologies have made it possible to efficiently separate and concentrate specific components of milk (Otari et al., 2024). More specifically, this by-product is generated during skim milk filtration in the production of milk concentrates. Milk permeate typically consists of approximately 80% lactose, 3% protein, 8.5% ash, and small amounts of fat and moisture (Tsermoula et al., 2024). Milk permeate is widely used for milk solids standardisation, lactose recovery, food formulation, and as a fermentation substrate (Tsermoula et al., 2024; Oliveira et al., 2019).

Another closely related stream is cheese whey permeate, which is generated during cheese manufacturing when whey undergoes ultrafiltration to concentrate proteins for cheese or whey protein products, leaving the permeate as the remaining fraction. Although its composition may

vary depending on the milk source, cheese type, and processing conditions, lactose remains the predominant component. Typical whey permeate contains 65–85% lactose, 3–8% protein, 8–20% ash, less than 1.5% fat content, and 3–5% moisture, giving it a composition similar to that of milk permeate.

Due to this composition, whey permeate has traditionally been utilised in several industrial applications. A large proportion of ultrafiltration (UF) permeate is currently processed into whey permeate powder, which is widely used in food and bakery applications (Foegeding et al., 2011) and marketed as a bulk commodity. However, alternative value-added applications are increasingly attracting interest. As early as 1976, Carbery Group Ltd. became one of the pioneering Irish dairy companies to utilise whey permeate derived from cheese production for ethanol manufacturing. This ethanol has been applied in various sectors, including the production of alcoholic beverages such as cream liqueurs. Furthermore, over recent decades, lactose recovered from whey permeate has been widely exploited for bioethanol production in several countries, including Ireland, New Zealand, Denmark, and United States of America (Oliveira et al., 2019).

In addition to permeate streams generated through membrane processes, another secondary by-product derived from whey processing is SCW. SCW is a dairy industry by-product obtained during ricotta cheese production. In Italy, only approximately 15% of the cheese whey produced annually is utilised for ricotta manufacturing, resulting in the generation of nearly 1 million tonnes of SCW (Figueroa Pires et al., 2021). SCW is also produced in other countries such as Spain, Greece, Turkey, and Romania during the production of similar whey cheeses.

This by-product is produced after the recovery of whey proteins through the thermal coagulation of cheese whey. The remaining liquid fraction after this step constitutes SCW (Figueroa Pires et al., 2021). Although it is not considered a high-value product, SCW still contains significant amounts of lactose, minerals, and nitrogenous compounds. More specifically, SCW contains approximately 50% of the original dry matter of whey, making it a substrate of growing interest for valorisation strategies.

The specific composition of SCW depends on the origin of the milk and the technological conditions applied during whey cheese manufacture. According to the study carried out by Pires et al. (2021), SCW derived from bovine whey typically contains lactose in the range of approximately 4.8–5.0%, proteins around 0.15–0.22%, and salts in the range of approximately 1.0–1.13% (w/w), with residual fat also present. Ovine SCW generally presents slightly higher protein and mineral contents compared to bovine SCW, although the overall compositions remain relatively similar. Overall, lactose and minerals constitute the major components of its dry matter,

while protein and fat levels are markedly reduced compared to primary cheese whey due to the recovery of whey proteins during whey cheese production.

The high lactose concentration in SCW makes it an attractive substrate for microbial fermentation processes, similarly to whey permeate. This compositional characteristic gives SCW considerable potential for use in biotechnological applications. However, despite this potential, SCW has traditionally been underutilised and is often disposed as animal feed or waste. Such disposal practices create environmental concerns due to the high biochemical oxygen demand (BOD) and chemical oxygen demand (COD) associated with this by-product (Figueroa Pires et al., 2021). In recent years, increasing environmental regulations and the transition toward circular bioeconomy models have stimulated growing interest in the revalorisation of SCW.

1.1.4 Regulations and environmental compliance for dairy by-products

Direct disposal of dairy by-products such as permeate or SCW is generally prohibited in most developed countries. In general terms, waste streams generated by dairy industries must undergo a series of treatment processes in order to reduce their environmental impact before discharge (Prazeres et al., 2012). This is due to their high BOD and COD, which can severely pollute water and soil.

BOD represents the amount of oxygen required by aerobic microorganisms to degrade organic matter in a water sample over a specified period and temperature. COD, on the other hand, measures the amount of oxygen required to chemically oxidize both biodegradable and non-biodegradable organic and inorganic substances present in water (Penn et al., 2006). Therefore, BOD and COD are commonly used metrics to express the amount of organic matter contained in liquid substrates and wastewater streams. These values vary depending on the specific dairy by-product. For example, SCW derived from cow's milk can present COD values of approximately 60 g/L and BOD values of around 45 g/L (BOD_5 measured over five days) (Sciuto et al., 2025).

As mentioned previously, strict regulations govern the disposal of dairy wastewater and by-products in developed countries. Within the European Union, the main legal framework regulating industrial emissions from dairy industries is the Industrial Emissions Directive (IED, 2010/75/EU) (European Parliament and Council, 2010).

Since 2019, the European Union has also established Best Available Techniques (BAT) conclusions for food, drink and milk industries through the Commission Implementing Decision (EU) 2019/203 (European Commission, 2019). BAT refers to the most advanced and effective stage in the development of processes, facilities, or operational methods capable of preventing or reducing waste generation and environmental pollution. These conclusions were prepared within the framework of Article 13 (1) of the IED. BAT take into account technological, economic, and

environmental factors and therefore represent a benchmark for environmental regulation and management in industrial sectors.

In practice, the implementation of BAT involves adopting operational and monitoring measures aimed at reducing environmental pollution. In dairy processing plants, these measures typically include monitoring of wastewaters flow rate, pH, and temperature, as well as regular sampling for analytical control (European Commission, 2019). For example, daily analyses are commonly performed for parameters such as COD, total nitrogen (TN), total organic carbon (TOC), total phosphorus (TP), and total suspended solids (TSS), while parameters such as BOD and chloride are typically monitored on a monthly basis.

More specifically within the dairy industry, wastewater streams from different processing stages are often treated together through co-treatment systems due to the large volumes generated during production. As a result, treatment strategies generally do not differentiate between individual wastewater streams but rather focus on the combined treatment of the total effluent. Typical treatment processes for dairy wastewater include preliminary treatments such as equalisation, neutralisation, and physical separation, followed by biological treatments (aerobic and anaerobic digestion). Additional processes may include nutrient removal through nitrification–denitrification for nitrogen removal and phosphorus recovery, as well as final solids removal through coagulation, flocculation, and filtration (Stasinakis et al., 2022).

Regulatory frameworks also define acceptable pollutant concentrations for wastewater discharged from dairy industries into receiving water bodies. Table 1.2 summarises the typical pollution limits for key wastewater parameters established by environmental regulations.

Table 1.2. *Regulatory pollution limits for dairy wastewater discharges to receiving waters (Stasinakis et al., 2022).*

Parameter	***Limit value***	***Unit of measurement***	***Averaging period***
Chemical Oxygen Demand (COD)	25-125	mg/L	Daily average
Total Suspended Solids (TSS)	450	mg/L	Daily average
Total Nitrogen (TN)	230	mg/L	Daily average
Total Phosphorus (TP)	0.24	mg/L	Daily average

In addition to pollutant concentration limits, regulatory guidelines also establish typical wastewater discharge volumes associated with different dairy processing operations. These limits

depend on the type of dairy product manufactured and the corresponding water usage during processing. Table 1.3 presents typical wastewater discharge volumes for several dairy products.

Table 1.3. *Typical wastewater discharge volumes in dairy processing according to product type (Stasinakis et al., 2022).*

Dairy product	*Limit value*	*Unit of measurement*
Market milk	0.3-3	m^3/ton of product
Cheese	0.75-2.5	m^3/ton of product
Milk powder	1.2-2.7	m^3/ton of product

In conclusion, European Union regulations require dairy industries to responsibly manage by-products such as permeate and SCW through appropriate treatment, valorisation strategies, or tightly regulated land application, thereby preventing their uncontrolled release into the environment. As a result, these environmental constraints have stimulated significant research efforts aimed at developing sustainable strategies for the treatment and valorisation of dairy by-products.

1.1.5 Valorisation of dairy by-products

The valorisation of dairy by-products refers to their transformation into higher-value products such as functional food ingredients, bioactive compounds, bioplastics, and biofuels. This approach supports the development of a circular bioeconomy while reducing the environmental impact associated with the disposal of large volumes of dairy side-streams. Given the substantial quantities generated worldwide, the effective utilisation of these streams represents both an environmental necessity and an economic opportunity.

Among dairy by-products, whey is the most abundant stream generated by the industry. Although historically regarded as a waste material, it is now widely recognised as a valuable resource due to its nutritional and functional properties. Whey contains significant amounts of proteins and other nitrogen-containing compounds with an excellent amino acid profile, including all essential amino acids and a relatively high cysteine-to-methionine ratio compared with many other protein sources. These characteristics contribute to its high biological value and to important functional properties such as solubility, foaming capacity, emulsifying ability, and water-binding capacity, which support its use in food and nutraceutical applications (Poonia & Trajkovska Petkoska, 2023).

The processing of whey into valuable products generally involves a combination of concentration, fractionation, and conversion strategies (Buchanan et al., 2023). Concentration processes increase the relative amount of solids by removing water, commonly through evaporation or membrane filtration. Fractionation then enables the separation of key components such as proteins, lactose, and minerals using techniques including membrane separation, crystallisation, electrodialysis, and drying. These fractions can subsequently undergo conversion processes that transform them into products with enhanced functional, nutritional, or industrial value. Such transformations may occur through biotechnological routes, including microbial fermentation and enzymatic reactions, or through chemical modifications such as lactose hydrolysis or isomerisation. In addition, streams with high organic content can be subjected to anaerobic digestion to recover energy in the form of biogas (Buchanan et al., 2023).

The main opportunities associated with whey processing are illustrated in Figure 1.3.

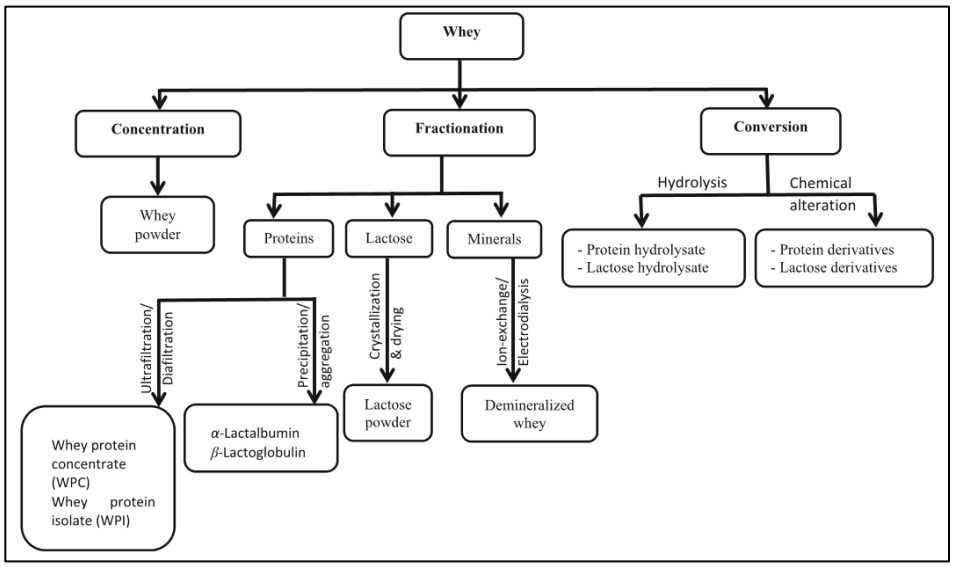

Figure 1.3. *Application opportunities for whey processing (Buchanan et al., 2023).*

Despite the extensive utilisation of whey, other dairy by-products such as permeate streams and SCW remain comparatively underutilised, even though they are produced in considerable quantities and still offer significant potential for further processing. Developing efficient strategies to exploit these streams therefore represents an important opportunity to improve the sustainability of dairy processing systems.

Milk permeate and whey permeate have gained increasing attention as substrates for food and biotechnological applications. In food systems, permeate can be incorporated into products such as baked goods, soups, and beverages, where it may partially replace sucrose or sodium while contributing to flavour development, browning reactions, and mineral enrichment. Its carbohydrate and electrolyte composition also make it suitable for functional beverages and sports

drinks. Beyond direct food applications, permeate can be used in microbial fermentation and enzymatic processes to produce compounds such as organic acids, prebiotic carbohydrates, microbial biomass, and alcoholic beverages. It may also serve as a growth medium for microorganisms, including fungi and microalgae, or as a feedstock for anaerobic digestion processes aimed at biogas production (O'Donoghue & Murphy, 2023; Azkarahman et al., 2025).
Similarly, SCW represents another promising dairy by-product for further utilisation. This stream has been investigated as a substrate for microbial and biotechnological processes, including the production of functional foods and beverages, microbial starter cultures, single-cell proteins and oils, bioactive compounds, and ingredients for animal feed or infant nutrition (Fancello et al., 2024). In addition, SCW can be used for the synthesis of bioplastic precursors such as lactic acid and polyhydroxyalkanoates (PHA), as well as for the production of biofuels including bioethanol, hydrogen, biogas, and biobutanol through fermentation and anaerobic digestion processes. These applications illustrate how SCW can generate value across the food, feed, chemical, and energy sectors while reducing the environmental burden associated with dairy waste streams.
In addition to these uses, dairy by-products can also serve as nutrient sources for microalgal cultivation. Dairy side-streams have increasingly been investigated as substrates for microalgal growth because they contain organic carbon, nitrogen, phosphorus, and minerals. Various dairy by-products have been evaluated as alternative culture media (Gramegna et al., 2020). Studies have demonstrated that microalgae species such as *Chlorella*, *Scenedesmus*, and *Spirulina* are capable of growing in these substrates while simultaneously removing nutrients and organic compounds from the medium. Consequently, the use of dairy side-streams for microalgal cultivation represents a promising strategy that combines biomass production with the treatment and valorisation of dairy industry residues (Ozcelik et al., 2024).

1.2 Microalgae and their industrial potential

Microalgae are a diverse group of predominantly unicellular photosynthetic microorganisms that inhabit a wide range of aquatic environments (Thoré et al., 2023). They include both prokaryotic organisms, such as cyanobacteria, and eukaryotic microalgae (Sarıtaş et al., 2025). Through photosynthesis, these microorganisms convert light energy, carbon dioxide, and inorganic nutrients into biomass. Microalgae are characterized by rapid growth rates, high photosynthetic efficiency, and the ability to adapt to different environmental conditions and metabolic modes, including photoautotrophic, heterotrophic, and mixotrophic growth (Sarıtaş et al., 2025).
From a biotechnological and industrial perspective, microalgae have attracted significant attention due to their ability to produce a wide range of valuable compounds. Depending on the species and

cultivation conditions, microalgal biomass can contain high levels of proteins, lipids, carbohydrates, pigments, vitamins, and other bioactive molecules (Silva et al., 2025). These characteristics make microalgae promising platforms for the production of compounds used in the food, feed, cosmetic, pharmaceutical, and energy sectors. Furthermore, microalgae cultivation can be integrated with environmental applications such as carbon dioxide capture and wastewater treatment, supporting the development of sustainable biotechnological processes and circular bioeconomy strategies (Omokaro et al., 2025).

Microalgae are currently used in a wide range of industrial applications, including food and feed production, cosmetics, pigment extraction, biofuel production, and environmental remediation.

1.2.1 Nutrition and feed applications

One of the most established applications of microalgae is their use in human and animal nutrition. The growing interest in alternative protein sources is partly driven by the increasing global demand for food, which is expected to nearly double by 2050 in order to support a projected population of around 9.8 billion people (Caporgno & Mathys, 2018). As conventional protein sources may become insufficient and concerns related to environmental sustainability, human health, and animal welfare continue to rise, sustainable protein sources such as microalgae are gaining increasing attention.

For human consumption, microalgae are commercially available in various forms, including tablets, capsules, powders, and liquid extracts. In addition to dietary supplements, microalgal biomass can be incorporated into food products such as pasta, snack foods, energy bars, and other functional foods (Caporgno & Mathys, 2018). The most widely cultivated species for this purpose include *Arthrospira* sp. (commonly known as Spirulina), *Chlorella* sp., *Dunaliella salina*, and *Aphanizomenon flos-aquae* (Spolaore et al., 2006). Among these, *Arthrospira* sp. is particularly valued due to its high protein content and favourable nutritional profile. Large-scale production systems have been developed worldwide to meet the growing demand for microalgal biomass. For example, one of the largest producers of *Chlorella* sp. operates photobioreactors with a total cultivation volume of approximately 700 m^3, producing up to 400 tonnes of dried biomass annually (Spolaore et al., 2006).

In addition to human nutrition, microalgae are also widely used in animal feed, including aquaculture, livestock, and pet nutrition. Approximately 30% of global algal production is dedicated to feed applications.

1.2.2 Cosmetics

Another important industrial application of microalgae is in the cosmetics industry (Guillerme et al., 2017). Microalgal extracts are widely incorporated into skincare formulations due to their antioxidant, moisturizing, and anti-aging properties. They are commonly found in products such as facial creams, sunscreens, and hair care products. The growing demand for natural ingredients has led several cosmetic companies to invest in microalgae cultivation technologies. For example, companies such as LVMH have explored the development of proprietary microalgae cultivation systems. In this sector, species such as *Arthrospira* and *Chlorella* are among the most frequently used (Spolaore et al., 2006).

1.2.3 Pigment production

Microalgae are also an important source of natural pigments. Different species produce various pigments in different concentrations, many of which have high commercial value. Consequently, pigment extraction from microalgal biomass represents a significant industrial application (Del Campo et al., 2007).

Microalgae are an important source of natural pigments with significant commercial value. Among the most relevant pigment groups are carotenoids and phycobiliproteins. Carotenoids include compounds such as β-carotene, astaxanthin, lutein, and zeaxanthin, which are widely used as natural colorants in food products and as additives in animal feed and cosmetic formulations (Spolaore et al., 2006). In addition, some microalgae produce phycobiliproteins such as phycocyanin, a water-soluble pigment with strong antioxidant properties that is commonly used as a natural blue colorant in food, cosmetics, and biotechnology applications. Owing to their functional and commercial value, these pigments represent some of the most important high-value products derived from microalgal biomass (Tounsi et al., 2023; Yu et al., 2024).

1.2.4 Biofuel technologies

Microalgae are increasingly being investigated as sustainable and innovative sources for biofuel production. The growing recognition that reliance on fossil fuels is environmentally and economically unsustainable has stimulated extensive research into renewable and potentially carbon-neutral bioenergy sources (Brennan & Owende, 2010; Chisti, 2007).

Biofuels are generally classified into three main categories depending on the origin of the raw materials used for their production. First-generation biofuels are produced from edible crops such as corn, wheat, and sugarcane. Second-generation biofuels are derived from non-edible biomass,

including agricultural residues, wood waste, and other lignocellulosic materials (Naik et al., 2010). Third-generation biofuels are mainly produced from algae and other microorganisms.

Among these alternatives, microalgae have attracted particular attention because they can grow rapidly, efficiently fix CO_2 through photosynthesis, and accumulate significant amounts of lipids, carbohydrates, and other energy-rich compounds that can be converted into different types of biofuels such as biodiesel, bioethanol, and biogas. However, despite their potential, the large-scale implementation of microalgae-based biofuels remains limited due to economic constraints and the relatively high production costs compared with conventional fuels (Davis et al., 2011). Consequently, current research efforts are mainly focused on improving cultivation efficiency, biomass productivity, and downstream processing technologies.

1.2.5 Environmental remediation technologies

In addition to their industrial applications, microalgae are increasingly being investigated for environmental remediation technologies. These applications take advantage of the metabolic capacity of microalgae to absorb nutrients and capture carbon dioxide while producing biomass.

One of the most promising environmental applications is carbon sequestration (Lam & Lee, 2012). Microalgae are capable of fixing carbon dioxide through photosynthesis with high efficiency, often exceeding that of terrestrial plants. During this process, microalgae can also capture other pollutants present in industrial emissions, such as nitrogen oxides (NO_X) and sulphur oxides (SO_X) (Omokaro et al., 2025). As a result, microalgae-based systems have significant potential for reducing greenhouse gas emissions.

Another important environmental application is wastewater treatment. In this approach, wastewater streams are used as nutrient sources for microalgal cultivation. Microalgae can remove nitrogen, phosphorus, and organic pollutants from wastewater while simultaneously producing valuable biomass. This strategy supports circular bioeconomy principles by combining wastewater treatment with biomass production and reducing the energy requirements associated with conventional wastewater treatment processes (McGinn et al., 2011).

Finally, microalgae are also being explored for the production of biodegradable materials. Microalgal biomass can be converted into biopolymers such as PHAs, which can serve as precursors for biodegradable plastics. These emerging applications further highlight the potential of microalgae as versatile biological platforms capable of contributing to sustainable industrial systems (Omokaro et al., 2025).

1.3 Microalgae cultivation

1.3.1 Cultivation regimes: autotrophic, heterotrophic and mixotrophic

To support these various industrial and environmental applications, microalgae must be cultivated under appropriate conditions that allow efficient biomass production. Depending on their source of energy and carbon, microalgae can grow under three main metabolic regimes: autotrophic, heterotrophic, and mixotrophic cultivation.

In autotrophic cultivation, microalgae use light as their primary energy source and inorganic carbon sources as their carbon source (Chisti, 2007). Through photosynthesis, solar energy is converted into chemical energy that supports cellular metabolism. In addition to carbon, microalgae require other essential nutrients such as nitrogen and phosphorus to sustain growth and biomass production.

Using chlorophyll and accessory pigments, microalgae capture light energy and convert it into biochemical energy that drives cellular processes. This energy is subsequently used to synthesize organic molecules such as sugars and lipids, which function as structural components and energy reserves for growth. Beyond biomass production, autotrophic microalgae also play an ecological role by releasing oxygen as a by-product of photosynthesis and contributing to atmospheric carbon dioxide regulation (Kurniawan et al., 2025). Since light represents the primary energy source in this cultivation regime, parameters such as light intensity, photoperiod (light duration), and spectral quality strongly influence photosynthetic efficiency and biomass productivity (Kurniawan et al., 2025; Carvalho et al., 2011).

In contrast to autotrophic metabolism, heterotrophic cultivation relies on the use of organic carbon as both a carbon and energy source. In this regime, microalgae utilise organic compounds such as glucose, glycerol, or acetate, which are metabolized through cellular respiration to generate energy. Heterotrophic growth occurs in the absence of light, as photosynthesis is not required (Liang et al., 2009). The culture medium used in heterotrophic systems is generally similar to autotrophic media, with the main difference being the addition of organic carbon sources.

Heterotrophic cultivation is considered particularly advantageous because it can overcome limitations associated with autotrophic systems. In autotrophic cultures, light penetration often limits biomass density due to self-shading effects. Moreover, large-scale production typically requires photobioreactors or open ponds, which may depend strongly on environmental conditions such as sunlight availability or require high energy inputs when artificial lighting is used. In contrast, heterotrophic cultivation eliminates the need for light and allows the use of conventional industrial fermenters, which can reduce infrastructure requirements and operational costs (Perez-Garcia et al., 2011; Bumbak et al., 2011).

However, not all microalgae species are capable of heterotrophic growth, as this metabolic strategy is limited to specific species. For a microalga to be suitable for heterotrophic cultivation, several characteristics are required. First, it must be able to undergo cell division in complete darkness while maintaining active metabolism. Second, it should efficiently utilise organic substrates as sources of carbon and energy. Finally, the organism must be sufficiently robust to tolerate the mechanical stress associated with mixing in industrial fermenters (Perez-Garcia et al., 2011).

Mixotrophic cultivation represents a metabolic strategy that combines the characteristics of autotrophic and heterotrophic growth. Under mixotrophic conditions, microalgae simultaneously utilise light and organic carbon sources, such as glucose, for biomass production. In this regime, cells are able to perform photosynthesis while also oxidizing organic carbon through respiratory metabolism (Wang et al., 2014).

Consequently, energy can be generated both through light-driven reactions and oxidative phosphorylation, producing adenosine triphosphate (ATP), the primary energy carrier of the cell (Verma et al., 2020). Although these metabolic regimes define the fundamental pathways through which microalgae obtain energy and carbon, their growth and productivity are also strongly influenced by several environmental and nutritional conditions.

1.3.2 Growth factors affecting microalgae

Growth and productivity of microalgae are strongly influenced by various environmental and nutritional factors. Understanding these parameters is essential for optimizing cultivation conditions. The following factors play a critical role in regulating microalgal growth and metabolic activity.

1.3.2.1 Nutrients availability

Microalgae require a variety of nutrients to sustain their metabolism and support biomass production. These nutrients are generally classified into macronutrients and micronutrients. Macronutrients are required in large quantities for cellular growth and biomass formation, whereas micronutrients are needed only in trace amounts and mainly act as enzymatic and metabolic cofactors (Markou et al., 2014). Among the macronutrients, carbon, nitrogen, and phosphorus are considered the most essential elements for microalgal development (Geider & La Roche, 2002).

Carbon plays a central role in microalgal metabolism because it constitutes the main structural component of cellular biomass. In cultivation systems, carbon can be supplied in either inorganic or organic forms. Inorganic carbon is typically provided as carbon dioxide (CO_2), which dissolves in water and forms a carbonate buffering system composed of dissolved CO_2, bicarbonate

(HCO_3^-), and carbonate (CO_3^{2-}), depending on the pH of the medium (Raven et al., 2014). This inorganic carbon may be introduced through aeration with air, concentrated CO_2, flue gas, or bicarbonate salts. Once it is introduced, it is fixed within the growing microalgal biomass through the photosynthetic metabolism, which is the main actor in autotrophic growth. However, some microalgal species are also capable of utilizing organic carbon sources such as glucose, acetate, glycerol, etc (Perez-Garcia et al., 2011). These compounds can enter the cell through diffusion or active transport mechanisms and serve as carbon and energy sources (Markou et al., 2014). Along with this, the combined absence or presence of light constitutes different trophic regimes, namely heterotrophic and mixotrophic respectively.

Alongside carbon, nitrogen represents another fundamental nutrient required for microalgal growth, representing the second most abundant element in cellular biomass. Nitrogen is essential for the synthesis of proteins, nucleic acids, and other nitrogen-containing biomolecules. Microalgae are able to assimilate nitrogen from several inorganic sources, including nitrate (NO_3^-), nitrite (NO_2^-), ammonium (NH_4^+), ammonia (NH_3), and nitric oxide (NO) (Wang et al., 2014). Among these forms, nitrate is the most commonly used nitrogen source in synthetic culture media, although ammonium is often metabolically preferred because it requires less energy for cellular assimilation. In addition to inorganic sources, some species can also utilise organic nitrogen compounds such as urea or certain amino acids, which are metabolized intracellularly (Markou et al., 2014).

Phosphorus also plays a crucial role in cellular metabolism. It forms part of essential molecules such as nucleic acids, ATP, and membrane phospholipids, making it indispensable for energy transfer and cell structure (Geider & La Roche, 2002). Microalgae generally assimilate phosphorus in the form of orthophosphate, although other inorganic and organic phosphorus compounds may also be utilised after enzymatic conversion by phosphatases (Markou et al., 2014). In aquatic environments such as natural waters or wastewater streams, phosphorus can occur in multiple forms, including dissolved organic phosphorus and polyphosphates. An additional physiological feature of many microalgae is their capacity to store excess phosphorus intracellularly as polyphosphate granules. This mechanism, known as luxury uptake, allows microalgae to accumulate phosphorus reserves and continue growing even when external phosphorus concentrations become limited (Powell et al., 2008).

1.3.2.2 Light

Light is a fundamental factor for microalgal growth. Photoautotrophic microalgae depend on light as their primary energy source, converting it into chemical energy through photosynthesis.

Mixotrophic microalgae rely on both light and organic carbon. Therefore, light availability and intensity strongly influence growth and biomass production (Parveen et al., 2023).

Light can be natural or artificial, and each type presents different characteristics. The main parameters that influence microalgal growth are light intensity, light spectrum, and photoperiod. The optimal combination of these parameters varies depending on the species being cultivated (Maltsev et al., 2021). Among them, light intensity plays a particularly critical role, as the photosynthetic response of microalgae varies according to the amount of irradiance received. This relationship between light intensity and photosynthetic rate is commonly described by the photosynthesis–irradiance (P–I) curve.

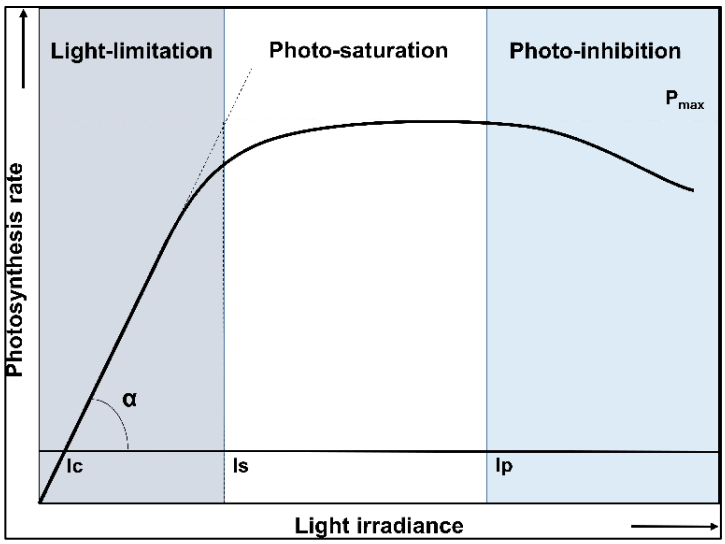

Figure 1.4. *Photosynthesis rate against light irradiance curve (Ferro, 2019).*

At low light intensities, photosynthesis occurs in the light-limited region, where the photosynthetic rate increases almost linearly with irradiance because light is the limiting factor. As light intensity increases, the curve reaches a light-saturated region in which photosynthesis approaches its maximum rate and biochemical processes become the limiting factor. At very high light intensities, excessive irradiance may damage the photosynthetic apparatus, leading to a decrease in photosynthetic efficiency. This phase is known as photoinhibition (Maltsev et al., 2021).

1.3.2.3 pH

Microalgal growth is also strongly influenced by pH. Depending on the species, different pH levels may positively or negatively affect growth. Most commonly studied microalgae, particularly freshwater and marine green algae, grow best under neutral to slightly alkaline conditions (pH 7–10). However, certain extremophilic species, such as *Galdieria sulphuraria*, can thrive under highly acidic conditions (pH 1–4) (Retta et al., 2024).

The distribution of inorganic carbon species in water (CO_2, HCO_3^- and CO_3^{2-}) is directly determined by pH. Since microalgae primarily assimilate CO_2 and HCO_3^-, pH strongly influences carbon availability. This distribution follows bicarbonate equilibrium chemistry and can be described by the Henderson–Hasselbalch Equation 1.1 (Keymer et al., 2013):

$$pH = pKa + \log_{10} \frac{[A^-]}{[HA]} \quad (1.1)$$

where [HA] represents the molar concentration of the undissociated acid, $[A^-]$ represents the molar concentration of the conjugate base, and pKa is defined as $-\log_{10}(Ka)$, where Ka is the acid dissociation constant.

Variations in pH can alter microalgal physiological responses and specific growth rates, ultimately affecting biomass accumulation and culture productivity (Goldman et al., 1982).

1.3.2.4 Temperature

Temperature is one of the most influential environmental factors regulating microalgal growth because it directly controls metabolic and physiological processes that determine the specific growth rate. Temperature affects enzyme kinetics, photosynthetic efficiency, respiration, membrane fluidity, nutrient assimilation, and ultimately biomass productivity (Singh & Singh, 2015).

The optimal temperature for growth is species-specific. Most mesophilic microalgae grow optimally between 20 °C and 25 °C, whereas thermophilic species may grow at temperatures up to 40 °C (Ras et al., 2013). As illustrated in Figure 1.5, each microalgal species exhibits a distinct optimal growth temperature.

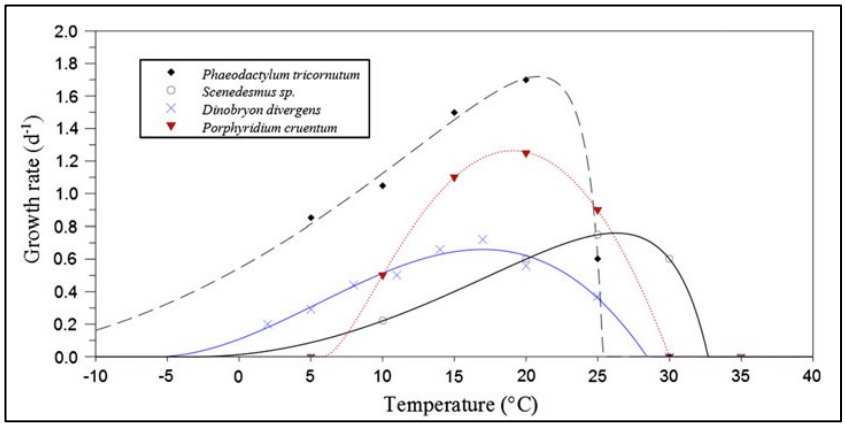

Figure. 1.5. *Temperature effect on microalgae growth rates (Ras et al., 2013).*

At temperatures below the optimal range, increasing temperature generally stimulates metabolic activity. Enzymatic reactions accelerate, resulting in enhanced photosynthetic rates and faster cell division. In this range, growth often follows an Arrhenius-type relationship, where the growth rate

approximately doubles for every 10 °C increase until the optimal temperature is reached (Ras et al., 2013).

In contrast, when temperatures exceed the optimal range, growth rate decreases due to heat stress. Elevated temperatures can cause enzyme inactivation and inhibit photosystem activity. Heat stress may also lead to the dissociation of essential components of the oxygen-evolving complex and promote the formation of reactive oxygen species, which damage cellular structures. As a result, the balance between photosynthesis and respiration becomes disrupted and net biomass accumulation decreases (Allakhverdiev et al., 2008; Ras et al., 2013).

1.3.3 Cultivation strategies

While the metabolic regimes and environmental factors described above determine how microalgae grow and metabolize nutrients, successful large-scale production also depends on the operational strategy used to manage the cultivation system. The operational mode determines how nutrients are supplied, how growth conditions are maintained, and how biomass is harvested, which ultimately influences system stability, scalability, and economic viability. Among the different approaches, batch and continuous cultivation are the most widely applied operational modes.

1.3.3.1 Batch

Batch cultivation is an operational mode in which microorganisms are grown in a fixed volume of culture medium that is inoculated at the start of the process, with no inflow or outflow of material during cultivation. Consequently, no additional nutrients or fresh medium are supplied until the end of the growth phase, when the biomass is harvested (Quiroz et al., 2025). Consequently, the system has an inlet only at the start of the cultivation process and no outlet during operation. Microalgae grow until nutrients become limiting or the desired biomass concentration is reached. At the end of the cultivation cycle, the entire culture is harvested. The system is then cleaned, sterilized if necessary, and restarted with fresh medium and inoculum.

Batch operation is commonly used in both open and closed cultivation systems. It is characterized by operational simplicity and relatively low technical complexity.

However, because nutrients are not replenished during cultivation, growth occurs only for a limited period. In addition, batch processes require intermediate phases between cultivation cycles, such as reactor cleaning, sterilization, and preparation, during which no biomass is produced. As a result, these operational interruptions and the discontinuous nature of the process may lead to lower overall productivity compared with continuous systems (Vuppaladadiyam et al., 2018).

Despite these limitations, batch cultivation remains widely used in microalgae production, particularly in laboratory studies and certain industrial applications (Quiroz et al., 2025).

1.3.3.2 Continuous

In continuous cultivation systems, fresh nutrient medium is continuously supplied to the reactor while an equivalent volume of culture containing biomass is simultaneously removed. After an initial start-up phase, the system reaches a steady state in which growth conditions and biomass concentration remain relatively constant.

Compared with batch cultivation, continuous systems offer several advantages. Since the culture operates without repeated start-up and shutdown phases, time is saved in the preparation of new cultures between production cycles. Furthermore, steady state conditions allow the maintenance of optimal growth parameters, often resulting in higher volumetric biomass productivity (Chisti, 2007). Continuous cultivation systems also enable higher overall productivity, can be integrated with wastewater treatment processes, and are generally well suited for scale-up and automation. These characteristics make continuous systems particularly attractive for industrial applications (Razzak et al., 2017).

Nevertheless, continuous cultivation also presents several challenges. The installation and operation of these systems are technically more complex than batch systems, and certain processes are difficult to operate continuously (Kim et al., 2013). In addition, the nutrient composition of the incoming medium must be carefully controlled, since variations may affect both microalgal growth and the composition of the produced biomass. Maintaining stable operating conditions over long periods can also be difficult, which may compromise long-term productivity. Furthermore, continuous systems are more susceptible to contamination by other microorganisms. Finally, the initial installation costs of continuous systems are typically higher, which may limit their industrial implementation (Zhu, 2015).

1.3.4 Cultivation systems

Microalgae can be cultivated using different technological approaches. Based on the degree of environmental control and system configuration, cultivation systems are commonly classified into open systems and closed systems.

1.3.4.1 Open systems

Open systems refer to cultivation systems that are exposed to the surrounding environment, such as open ponds, tanks, or raceway ponds (Udayan et al., 2021). These systems offer several

advantages, including relatively low capital and operational costs, reduced energy requirements for mixing compared with closed systems, and simpler infrastructure.
However, open systems also present important limitations. Large land areas are often required to achieve industrial-scale production, and the exposure to environmental conditions increases the risk of contamination by other microorganisms. Environmental factors such as temperature fluctuations, evaporation, and varying light conditions may also affect culture stability and productivity (Narala et al., 2016).

1.3.4.2 Closed systems

Closed systems consist of enclosed cultivation systems in which microalgae are grown under controlled conditions using different types of bioreactors. One of the main advantages of closed systems is the ability to maintain precise control over cultivation parameters such as temperature, pH, and nutrient supply. This controlled environment significantly reduces the risk of contamination and allows the production of biomass with more consistent quality (Udayan et al., 2021).
In addition, closed systems generally require less physical space and can provide improved light distribution for microalgal growth. Despite these advantages, closed systems also have several drawbacks. They typically require higher capital investment and operational costs compared with open systems. Moreover, technical challenges such as overheating and the accumulation of dissolved oxygen may limit microalgal growth. Maintenance and cleaning procedures can also be more complex in enclosed systems (Narala et al., 2016).
Overall, although closed systems provide better environmental control and product consistency, they are generally more expensive to construct and operate than open cultivation systems.

1.3.5 Cultivation equipment and scale-up considerations

The type of reactor used for microalgae cultivation is closely related to the cultivation system and its operating conditions. In outdoor systems such as open ponds and raceways, cultures are directly exposed to environmental factors, including daily and seasonal temperature fluctuations (Ras et al., 2013). These variations can significantly influence growth conditions and overall production efficiency. Consequently, different types of reactors have been developed depending on whether the cultivation system is open or closed.
In open cultivation systems, microalgae are typically grown in shallow ponds or channels that allow exposure to natural sunlight. Among the available configurations, open ponds and raceway ponds represent the most common industrial designs. Open ponds consist of shallow reservoirs

containing nutrient-supplemented water where microalgae grow under natural illumination (Razzak et al., 2017). Mixing is generally achieved using paddle wheels, which keep the culture in motion and prevent cell sedimentation. Raceway ponds operate on a similar principle but are designed as oval or race-track-shaped channels that enable continuous circulation of the culture medium. The paddle wheel circulates the culture along the channel, ensuring that microalgal cells periodically reach the surface and receive sufficient light for photosynthesis (Vuppaladadiyam et al., 2018). Owing to their relatively simple design and low operational costs, these systems are widely used in industrial cultivation, although they remain subject to the limitations associated with open environments.

In contrast, closed cultivation systems employ enclosed reactors known as photobioreactors (PBRs), which allow greater control over environmental conditions (Benner et al., 2022). PBRs are typically constructed from transparent materials to enable light penetration for photosynthesis while allowing a controlled supply of carbon dioxide and regulation of parameters such as temperature and pH. Because the culture is maintained within an enclosed environment, the risk of contamination is significantly reduced compared with open systems (Kumar et al., 2025). Furthermore, the compact design of PBRs generally requires less physical space than open pond systems (Udayan et al., 2021).

Several photobioreactor configurations have been developed to optimize light utilization, gas exchange, and mixing efficiency. These include bubble column, airlift, tubular, flat-plate, and stirred tank reactors, as illustrated in Figure 1.6.

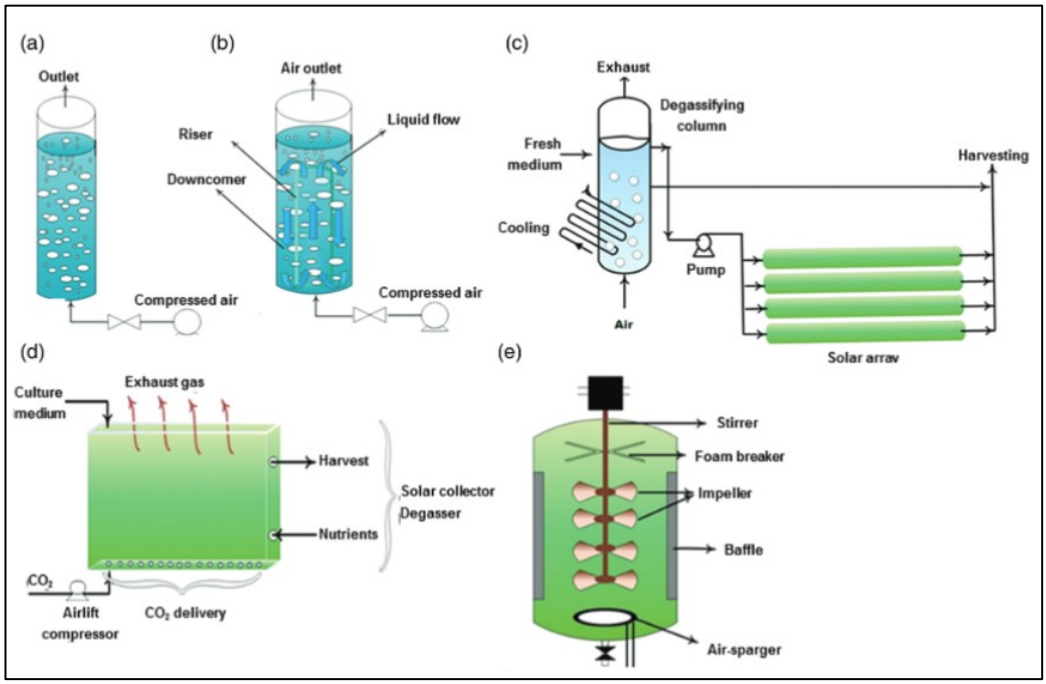

Figure 1.6. *Illustration of (a) bubble column, (b) airlift, (c) horizontal tubular, (d) flat-plate, and (e) stirred tank photobioreactors (Narala et al., 2016).*

Among these designs, bubble column and airlift reactors rely primarily on gas-driven circulation to maintain mixing and supply carbon dioxide. In bubble column reactors, air or carbon dioxide is introduced through a sparger located at the bottom of a vertical cylindrical vessel. When external light is required, the reactor is typically constructed from transparent materials to allow light penetration (Benner et al., 2022). As the gas bubbles rise through the culture medium, they simultaneously promote mixing and deliver the carbon dioxide required for photosynthesis. Airlift PBRs operate under a similar principle; however, circulation is enhanced through an internal loop created by air injection, which improves mixing and gas exchange without the need for mechanical agitation (Narala et al., 2016).

Other photobioreactor designs focus primarily on maximizing light exposure through their geometry. Tubular photobioreactors consist of long transparent tubes, usually made of glass or plastic, through which the microalgal culture circulates while being exposed to natural or artificial illumination along the length of the reactor (Legrand et al., 2021). Flat-plate photobioreactors, on the other hand, employ thin transparent panels that create a high surface to volume ratio, thereby improving light penetration and photosynthetic efficiency. Mixing in these systems is commonly achieved through air bubbling or mechanical circulation, and they are frequently applied in laboratory and pilot-scale studies (Sierra et al., 2008).

Another configuration used in microalgae cultivation is the stirred tank photobioreactor. In these systems, the culture is contained within a transparent cylindrical vessel equipped with mechanical mixing devices such as impellers, baffles, or stirrers. These components ensure adequate circulation and mass transfer within the reactor (Uyar et al., 2024).

Microalgae cultivation systems can also be classified according to their operational scale, which typically ranges from laboratory to pilot and industrial levels. Each scale serves a distinct role in the development and implementation of microalgae cultivation processes.

At the early stages of process development, cultivation is generally carried out in laboratory-scale PBRs, where small and highly controlled systems allow researchers to investigate the effects of environmental and operational parameters on microalgal growth. These reactors commonly operate under artificial lighting conditions to ensure reproducibility of experimental results (Legrand et al., 2021; Benner et al., 2022). Once optimal cultivation conditions have been identified, the process is typically transferred to pilot-scale systems, which represent an intermediate step between laboratory experiments and industrial implementation. At this stage, reactors are larger and are often operated under natural sunlight, although their configuration depends on the intended industrial application (Penloglou et al., 2024). The objective of pilot-scale cultivation is to evaluate whether the results obtained under controlled laboratory conditions can

be reproduced under more realistic operating environments (Legrand et al., 2021). Ultimately, successful processes are implemented at the industrial scale, where cultivation systems must be capable of producing large quantities of biomass while remaining technically efficient and economically viable. Large-scale microalgae production commonly relies on open pond systems or large PBRs, depending on the specific requirements of the process and the target products (Legrand et al., 2021).

Despite technological advances in reactor design, scaling up microalgae cultivation systems remains a significant challenge. Transitioning from laboratory-scale reactors to larger systems often introduces several technical and operational constraints (Razzak et al., 2017). Among the most critical challenges are light distribution, mass transfer, mixing efficiency, and overall energy consumption (Legrand et al., 2021).

One of the main difficulties during scale-up is maintaining effective light penetration throughout the reactor volume. As system size increases, the surface-to-volume ratio typically decreases, which reduces light availability within the culture. In addition, limitations in gas transfer, oxygen accumulation, and hydrodynamic mixing may further restrict productivity in large systems. Temperature control can also become problematic, particularly in large outdoor PBRs such as tubular systems exposed to direct sunlight, where overheating may occur (Chanquia et al., 2021).

Ultimately, the greatest challenge in scaling up microalgae cultivation systems lies in maintaining high productivity at larger scales, as the various physical and operational limitations described above can significantly influence overall process performance.

1.4 *Galdieria sulphuraria*

The selection of a suitable microalgal species is a key factor in designing an efficient cultivation system. As discussed in the previous sections, the choice of reactor configuration, operational strategy, and cultivation regime depends strongly on the physiological characteristics and metabolic capabilities of the organism being cultivated. In this thesis, the microalga *Galdieria sulphuraria* is selected due to its exceptional metabolic flexibility and its ability to grow under extreme environmental conditions (Gross & Schnarrenberger, 1995). In particular, its capacity to thrive at low pH provides a significant advantage when using dairy by-product streams, where contamination by heterotrophic bacteria represents a major challenge due to the high organic content. Under such acidic conditions, the growth of most contaminating microorganisms is inhibited, allowing for more stable and controlled cultivation.

1.4.1 Taxonomy and physiology

Galdieria sulphuraria is a unicellular red alga classified within the class *Cyanidiophyceae* (SAG, 1992), a group known for its remarkable capacity to survive and proliferate in extreme environments (Curien et al., 2021). This species is particularly notable for its ability to grow under highly acidic conditions, typically within a pH range of 1–4, and at elevated temperatures of up to approximately 56 °C (Pleissner & Händel, 2023; Curien et al., 2021). In addition, it demonstrates a high tolerance to significant concentrations of heavy metals and salts. In natural environments, *G. sulphuraria* is commonly found in volcanic hot springs, fumaroles, calderas, acidic soils, and acid mine drainage sites (Cozzolino et al., 2000; Curien et al., 2021).

1.4.2 Growth conditions and nutrient requirements

One of the most distinctive features of *G. sulphuraria* is its high metabolic flexibility. This microalga is capable of growing under autotrophic, heterotrophic, or mixotrophic conditions, allowing it to adapt to a wide range of environmental and cultivation scenarios (Retta et al., 2024). In natural acidic habitats, however, photosynthetic growth can be limited by the availability of inorganic carbon, as bicarbonate is almost absent under such low pH conditions (Salbitani & Carfagna, 2020).

Like other microalgae, *G. sulphuraria* requires essential nutrients such as nitrogen, phosphorus, and carbon to sustain growth. Nitrogen is commonly supplied in the form of nitrate, while phosphorus is typically provided as inorganic phosphate. Carbon can be assimilated either through photosynthesis, using light as an energy source, or through the metabolism of organic carbon compounds such as sugars and polyols during heterotrophic or mixotrophic growth (Curien et al., 2021). This metabolic versatility contributes to the organism’s adaptability and facilitates its cultivation under different operational regimes.

1.4.3 Biotechnological relevance

Beyond its physiological adaptability, *G. sulphuraria* has attracted increasing interest due to its ability to produce a variety of bioactive compounds with potential industrial applications. Among these compounds, phycobiliproteins represent one of the most important groups. Phycobiliproteins are light harvesting pigments known for their strong antioxidant, antibacterial, and antitumor properties, and they comprise several specific proteins including phycocyanin, phycoerythrin, and allophycocyanin (Retta et al., 2024). In addition to these pigments, *G. sulphuraria* is also capable of synthesizing other valuable biomolecules such as lipids, carbohydrates, and secondary

metabolites. All these compounds have been investigated for applications in sectors such as pharmaceuticals, nutraceuticals, cosmetics, the food industry, and biotechnology research. Table 1.4 summarizes several relevant compounds produced by *G. sulphuraria* and their associated applications.

Table 1.4. *Bioactive compounds produced by G. sulphuraria (Retta et al., 2024).*

Bioactive compound	***Uses***
C-phycocyanin	Used as natural colouring agent in food industries Demonstrates strong antioxidant activity Anti-inflammatory and neuroprotective effects
Phycoerythrin	Utilised in fluorescence-based techniques
Allophycocyanin	Used as a fluorescent marker
Glutathione	Antioxidant

In addition to these bioactive molecules, the biomass of *G. sulphuraria* can also be used for the production of single cell protein, owing to its relatively high protein content (Salbitani & Carfagna, 2020). This characteristic makes it a potential nutritional ingredient for human consumption, while also offering applications in animal feed and aquaculture (Retta et al., 2024).

The species also shows significant potential in wastewater remediation processes (Rahman et al., 2021). *G. sulphuraria* can remove various pollutants, including nitrogen (ammonia), phosphates, and organic contaminants measured as BOD. It has demonstrated effectiveness in treating contaminants present in urban and industrial wastewater as well as produced water from oil and gas industries. During these processes, the microalga contributes to nutrient removal while simultaneously generating valuable biomass (Rahman et al., 2021). Moreover, it is capable of adsorbing and recovering heavy metals such as gold, platinum, and copper, as well as rare earth elements (REEs) including cerium, from contaminated water (Retta et al., 2024).

Finally, the biochemical composition and efficient photosynthetic machinery of *G. sulphuraria* suggest promising applications in the bioenergy sector. Its biomass is rich in organic compounds such as carbohydrates and lipids and lacks lignin, which makes it particularly suitable for thermochemical conversion processes**.** For this reason, the microalga has been investigated as a potential renewable energy resource, as its biomass can be converted into bio-oil and hydrogen-rich syngas through processes such as pyrolysis and gasification (Banihashemi et al., 2023). These products can subsequently be used as fuels or energy carriers. Consequently, the metabolic characteristics of *G. sulphuraria* make it a promising organism for future research aimed at

developing sustainable bioenergy technologies and improving photosynthetic efficiency in biotechnological applications.

1.5 Objective of the thesis

The increasing environmental pressure associated with industrial waste generation highlights the need for more sustainable production systems. In the dairy industry, large volumes of by-products such as milk permeate and SCW are generated each year, creating challenges for their management and disposal. At the same time, the transition towards a circular economy encourages the valorisation of these by-products as alternative raw materials for new biotechnological processes, thereby reducing waste while creating added value.

In this context, microalgae cultivation emerges as a promising approach for the bioconversion of industrial residues into valuable biomass. Among the different microalgal species, *Galdieria sulphuraria* is particularly attractive because of its metabolic versatility and its ability to grow under extreme conditions, including heterotrophic and mixotrophic regimes that allow the utilisation of various organic carbon sources.

The main objective of this thesis is to evaluate the feasibility of using two dairy industry by-products, milk permeate and SCW, as feedstocks for the cultivation of *Galdieria sulphuraria*. This work builds on laboratory-scale experimental evidence, in which the growth performance of the microalga is investigated under heterotrophic and mixotrophic conditions using dairy-derived substrates. The mixotrophic cultivation experiments are performed as part of the present thesis, whereas the heterotrophic experimental data are obtained from complementary laboratory studies carried out within the same research group. These results provide the basis for assessing the potential of these by-products as alternative culture media for microalgal biomass production.

The study is then extended to the industrial level through conceptual plant design, process simulation, and preliminary techno-economic assessment. Two different process scales are considered in order to analyse how production scale influences feasibility. In the large-scale scenario, milk permeate is selected as the main feedstock, whereas the small-scale configuration is based on SCW. This comparative approach makes it possible to examine the advantages and limitations associated with each substrate and process scale, and to evaluate the technical and economic potential of their valorisation through the cultivation of *Galdieria sulphuraria*.

Chapter 2

Materials and Methods

This chapter describes the experimental methods for *Galdieria sulphuraria* cultivation on dairy by-products, together with the methodology adopted for process simulation, conceptual plant design, and techno-economic assessment.

2.1 Algal strain and acclimation conditions

The algal strain used in this study was *Galdieria sulphuraria* (SAG 21.92), obtained from the Culture Collection of Algae at the University of Göttingen (Figure 2.1). As discussed in Chapter 1, *G. sulphuraria* is a particularly suitable organism for this work because of its ability to grow under highly acidic conditions and under different trophic regimes, including heterotrophic and mixotrophic cultivation. For this reason, an acclimation step is carried out before each cultivation campaign in order to adapt the inoculum to the operating conditions of the selected regime.

During acclimation, the strain is cultivated in 250 mL Quickfit Drechsel® bottles at 30 °C, using 6 g_C L^{-1} of organic carbon, equivalent to 15 g L^{-1} of glucose. In both mixotrophic and heterotrophic regimes, culture mixing is provided by atmospheric air sparging combined with magnetic stirring at the bottom of the bottles. The two acclimation strategies differ only in the light conditions: continuous illumination at 75 µmol m^{-2} s^{-1} is applied for mixotrophic acclimation, while heterotrophic acclimation is performed in the absence of light.

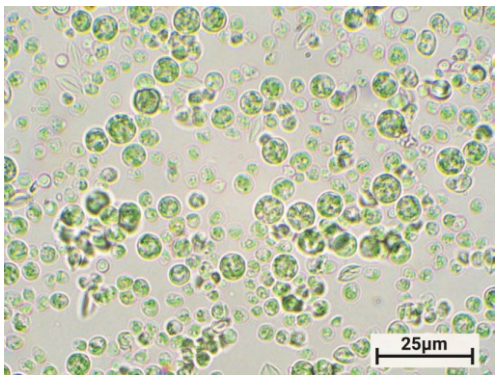

Figure 2.1. *Microscopic picture of Galdieria Sulphuraria (Van Etten, 2020).*

Regarding the nutrient medium, MAM (Modified Allen Medium) is used for strain acclimation prior to cultivation under the selected operating conditions. The medium is supplemented with glucose at 15 g L^{-1}, corresponding to an equivalent organic carbon concentration of 6 g_C L^{-1}. These cultures are subsequently used as pre-inocula in the different experimental campaigns and are regularly diluted with the respective sterile media to maintain exponential growth.
The detailed composition of the medium, which is acidified to pH 2 using 95–98% sulfuric acid after sterilization by autoclaving at 120°C, is presented in Table 2.1 (Allen, 1968).

Table 2.1. *Formulation of the enriched MAM medium.*

Component	***Concentration [g L^{-1}]***
NaCl	0.02
$(NH_4)_2SO_4$	5.6
$MgSO_4 \cdot 7H_2O$	0.6
K_2HPO_4	0.5
$CaCl_2 \cdot 2H_2O$	0.02
$C_6H_8O_7 \cdot xFe^{3+} \cdot yNH_3$	0.02
$CuSO_4 \cdot 5H_2O$	$1.37 \cdot 10^{-3}$
$(NH_4)_6Mo_7O_{24} \cdot 4H_2O$	$4.2 \cdot 10^{-3}$
$ZnSO_4 \cdot 7H_2O$	18
$CoCl_2 \cdot 6H_2O$	$8.6 \cdot 10^{-5}$
$MnCl_2 \cdot 4H_2O$	$4.6 \cdot 10^{-3}$

2.2 Continuous cultivation

Following the acclimation of *G. sulphuraria*, continuous cultivation is investigated under heterotrophic and mixotrophic regimes to assess the growth performance of the strain using milk permeate as the organic carbon source. The aim is to evaluate the potential valorisation of this dairy industry by-product. For these experimental campaigns, the culture medium is prepared based on the standard medium described in Section 2.1. Depending on the required equivalent organic carbon concentration, permeate is added to the sterilised medium under axenic conditions.

The laboratory-scale continuous cultivation system is illustrated in Figure 2.2.

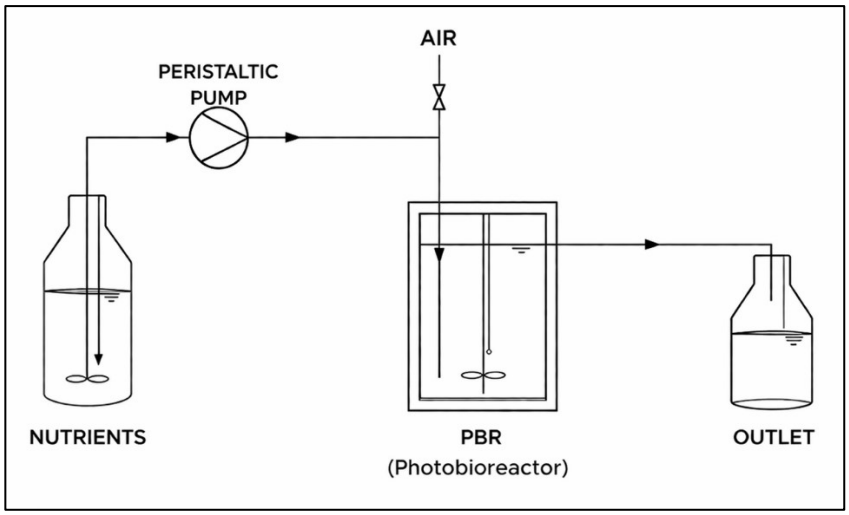

Figure 2.2. *Scheme of the laboratory-scale continuous cultivation system.*

The cultivation medium is fed continuously into the reactor by means of a multichannel peristaltic pump (205S/CA, Watson-Marlow Fluid Technology Group), which allows the inlet flow rate to be adjusted according to the desired residence time (τ) by setting the pump speed. Residence time (Equation 2.1) represents the average time that the culture medium remains inside the reactor before leaving the system. The excess culture leaves the system through an overflow outlet. Since the outlet flow rate equals the inlet flow rate, the working volume remains constant throughout the experiment.

$$\tau\ [d] = \frac{V}{Q} \tag{2.1}$$

Where V is the reactor volume in L and Q is the volumetric flow rate in L/d.

Owing to the efficient mixing provided by the magnetic stirrer placed at the bottom of the reactor and by the aeration system, the reactor is assumed to operate under conditions approximating those of a continuous stirred-tank reactor (CSTR). Accordingly, perfect mixing is assumed within the reactor volume. The reactors are maintained at approximately the optimum growth temperature of 45 °C, using a thermostatically controlled incubator (Frigomeccanica Andreaus s.r.l.) for the mixotrophic experiments and a Witeg® thermostatic bath chiller for the heterotrophic experiments. Under mixotrophic conditions, continuous illumination is provided by a white LED lamp set to the desired light intensity. Constant aeration is supplied by an air pump (Oase Living Water), and the air stream is sterilised by means of a 0.22 μm filter installed along the aeration line.

2.2.1 Mixotrophic experiments

This first part of the continuous cultivation study focuses on mixotrophic cultivation. The experiments are carried out in polycarbonate flat-panel PBRs with a working volume of 0.2 L, a thickness of 0.035 m, and an illuminated surface area of approximately 80 cm². The flat-panel PBR used in the experiments is shown in Figure 2.3.

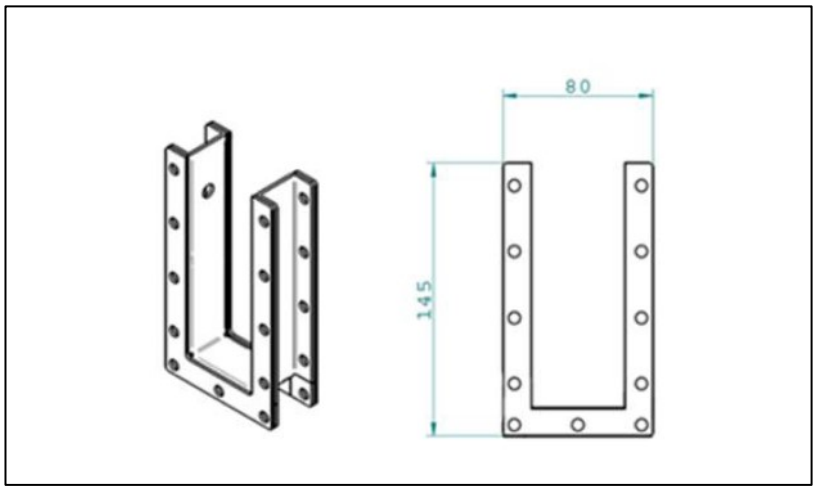

Figure 2.3. *Isometric and front view of the PBR used for the continuous cultivation of* G. sulphuraria *(Ostardo, 2024).*

In this set of experiments, the combined effect of influent organic carbon concentration and light intensity on culture performance is investigated, while all other operating variables are kept constant. In particular, the residence time is set at 1.5 d, the temperature is maintained at 45 °C, and the cultivation medium consists of Modified Allen Medium (MAM) acidified to pH 2 with sulphuric acid. The experimental conditions considered are summarised in Table 2.2.

Table 2.2. *Experimental matrix for continuous mixotrophic cultivation under different organic carbon concentrations and light intensities.*

	75 µmol m^{-2} s^{-1}	***150 µmol m^{-2} s^{-1}***	***215 µmol m^{-2} s^{-1}***
1.3 g_C L^{-1}			
6 g_C L^{-1}			

As shown in Table 2.2, the experimental space defined by different levels of organic carbon concentration and light intensity is sampled in order to obtain an overall view of the system response under mixotrophic conditions. Therefore, only a selection of the possible combinations is experimentally assessed, with the aim of identifying general trends in culture performance under different levels of carbon and light availability.

Figure 2.4 shows the laboratory-scale set-up used for the continuous mixotrophic cultivation experiments.

Figure 2.4. *Experimental set-up for mixotrophic cultivation.*

2.2.2 Heterotrophic cultivation

The second part of the continuous cultivation study focuses on heterotrophic cultivation. A continuous heterotrophic experiment is performed as a preliminary step to obtain the experimental data required for the process simulation developed in the following chapters. Accordingly, one representative operating condition is selected for this experimental campaign.

The cultivation is carried out at an influent organic carbon concentration of 6 g_C L^{-1}, in the absence of light, at 45 °C and pH 2, with a residence time of 2 d. Under these conditions, biomass growth relies exclusively on the assimilation of the supplied organic carbon source. The reactor is cylindrical and has a working volume of 0.235 L. Thermal control is ensured by means of a Witeg® thermostatic bath chiller.

The complete experimental set-up adopted for these runs is shown in Figure 2.5.

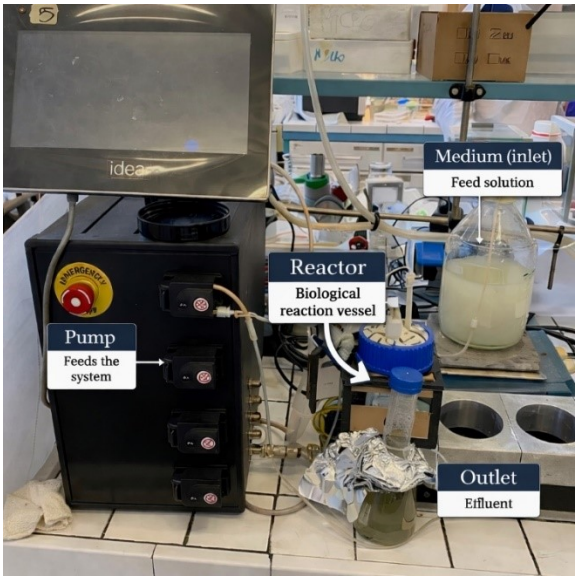

Figure 2.5. *Experimental set-up for heterotrophic cultivation.*

Once the culture medium is prepared, the set-up is assembled and the reactor is placed in the thermal bath. The feeding line is connected to the medium reservoir and to the peristaltic pump, which is set to deliver the desired flow rate. Samples are periodically collected from the reactor in order to monitor the cultivation performance over time.

2.3 Monitoring, analytical methods and measurements

Several analyses were carried out on both the dairy by-products used as inlet medium and on the different experimental samples, including the filtrate and biomass-containing fractions, in order to characterise their composition and to better understand microalgal growth and biomass formation.

2.3.1 Optical density

Optical density (OD) measurements are performed routinely to monitor culture growth and to obtain a rapid indication of biomass concentration during cultivation. This method is based on the Beer–Lambert law, which relates absorbance to sample concentration according to Equation 2.2.

$$A = \varepsilon \cdot C \cdot l \tag{2.2}$$

where A is the absorbance, C is the sample concentration, l is the optical path length, and ε is the attenuation coefficient. This relationship is valid within the linear measurement range of the instrument.

In this study, OD is measured using a Shimadzu® UV-1900 spectrophotometer at 680 and 750 nm, employing cuvettes with an optical path length of 1 cm and using the corresponding culture

medium as blank. Before analysis, samples are diluted when necessary to maintain absorbance values within the reliable operating range of the instrument. These measurements are performed routinely during cultivation in order to follow biomass growth and to determine when the process reaches stationary conditions. Once stationary conditions are achieved, dry weight measurements are carried out for a more accurate quantification of biomass concentration.

2.3.2 Dry weight

Dry weight (DW) determination represents one of the main methods used in this work to quantify biomass concentration in the culture, expressed as g L^{-1}. Whereas OD provides a rapid estimate of cell growth, DW gives a more accurate and quantitative measurement of the actual biomass concentration. In continuous experiments, this method is applied after the culture reaches steady state conditions. At least four consecutive DW measurements showing stable values are collected in order to confirm that steady state has been achieved.

The procedure for DW determination involves several steps. First, filters with a pore size of 0.22 µm are dried in an oven at approximately 110 °C for at least 10 min in order to remove residual moisture. The filters are then weighed using a high-precision analytical balance to determine the tare weight. Each filter is placed on a stainless-steel Büchner funnel connected to a vacuum flask, through which a known volume of culture is filtered. 10 mL of sample are used for each measurement. After filtration, the filter retaining the biomass is dried again in the oven for at least 2 h at the same temperature and then weighed to determine the gross weight.

The biomass concentration (C_x) is calculated using the following Equation 2.3.

$$C_x = DW\ [g\ L^{-1}] = \frac{Gross\ weight - Tare\ weight}{Filtrated\ volume} \quad (2.3)$$

The filtrate not retained by the filter is stored at -18 °C for subsequent analyses, such as total organic carbon.

Biomass productivity (P_x) (Equation 2.4) is defined as the rate at which biomass is formed per unit volume of culture and per unit time. It therefore describes how efficiently the system produces biomass during cultivation and is usually expressed in g L^{-1} d^{-1}.

$$P_x\ [g\ L^{-1}\ d^{-1}] = \frac{C_x}{\tau} \quad (2.4)$$

2.3.3 Total organic carbon and total nitrogen

The determination of total organic carbon (TOC) and total nitrogen (TN) constitutes one of the main analytical methods employed in this study to characterise the composition of the different streams involved in the cultivation process. These parameters provide essential information on the

carbon and nitrogen content of the samples and are therefore used to evaluate substrate composition, nutrient consumption, and the distribution of components between the liquid phase and the produced biomass.

TOC and TN analyses are performed on SCW and permeate for substrate characterisation, as well as on the corresponding prepared culture media to verify that the desired organic carbon concentration is effectively supplied to the culture. In addition, these analyses are also carried out on the filtrate and biomass-containing fractions obtained from the culture samples after filtration, in order to develop the carbon and nitrogen material balances and to derive the corresponding elemental yields. Carbon and nitrogen concentrations are measured using a TOC-L CPH Shimadzu® analyser equipped with a TNM-L module for TN determination. This instrument enables the accurate and reproducible measurement of total carbon (TC), total organic carbon (TOC), inorganic carbon (IC), and total nitrogen (TN) in liquid samples.

Before analysis, the samples are prepared according to the expected concentration range. When necessary, they are diluted with Milli-Q water in order to ensure that the measured values fall within the sensitivity limits of the instrument, which is calibrated in the range from 5 μg L^{-1} to 100 mg L^{-1}. The analyser provides the results as peak areas, which are then converted into concentration values (mg L^{-1}) by means of the corresponding calibration curves for each type of analysis.

The results obtained are used to identify the composition of the by-products and culture media and to quantify the variation in carbon and nitrogen concentrations during cultivation. These values are subsequently used in the material balance calculations and in the estimation of elemental yields, as described in the following sections.

2.3.4 Phosphates analysis

The protocol followed for the determination of the concentration of orthophosphate (PO_4^{3-}) in the samples is based on the colorimetric method, as described by Innamorati et al. (1990). Orthophosphate analysis is carried out on the prepared culture media to verify the phosphorus concentration supplied to the culture, as well as on the filtered samples collected under the different experimental conditions in order to quantify phosphate consumption during cultivation. These measurements are also used for the development of phosphorus material balances and for the derivation of the corresponding elemental yields.

In this method, the reaction of 2 mL of a diluted sample with 400 μL of a particular reagent mixture results in a coloured product, whose concentration of PO_4^{3-} is related to the absorbance at a particular wavelength. The reagent mixture consists of the following: for 1 mL of reagent, 500 μL of a solution of 5 N sulphuric acid, 100 μL of a solution of antimony potassium tartrate at a

concentration of 1.36 g L^{-1}, 200 µL of a solution of ammonium heptamolybdate at a concentration of 30 g L^{-1}, and 200 µL of a solution of ascorbic acid at a concentration of 54 g L^{-1}. Due to the instability of the reagent, it must be used within one hour of its preparation.

The colour change, which is related to the reaction between PO_4^{3-} and molybdenum, results in a blue-coloured product, which is formed through a reaction that takes place within a period of 10 min. The reaction product is then analysed spectrophotometrically at a wavelength of 705 nm, followed by the calculation of the concentrations of orthophosphate through the calibration curve in Equation 2.5:

$$PO_4^{3-}\ [mg\ L^{-1}] = 7.905 \cdot abs_{705} - 0.12 \qquad R^2 = 0.997 \qquad (2.5)$$

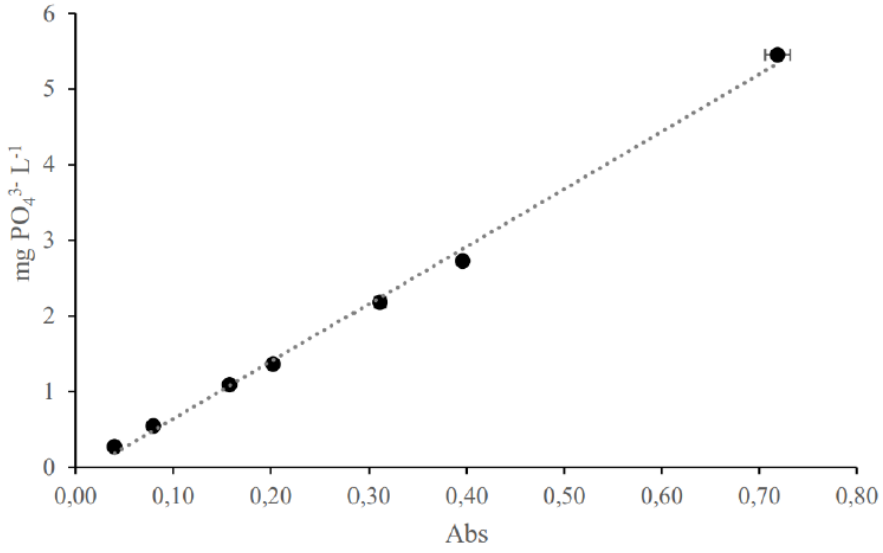

Figure 2.6. *Orthophosphate calibration curve.*

2.4 Material balances

Mass balances are fundamental tools in process design, they are carried out to determine the flow rates and compositions of all streams involved in the process, as well as the yield coefficients of the main components incorporated into the biomass. These calculations form the basis for estimating biomass production, substrate consumption, nutrient requirements, recycle flows, and residual effluents, and support the scale-up, process simulation, and conceptual design of the industrial-scale system.

Before performing the material balances, the biomass productivity under the selected experimental conditions must be determined. However, productivity alone is not sufficient for process scale-up. The laboratory experiments are conducted using diluted media, whereas the industrial scenarios evaluated in this work consider the direct use of permeate and SCW without prior dilution.

Consequently, in addition to productivity, elemental consumption and distribution yields must be established in order to relate biomass formation to the composition of the inlet by-product streams. In this context, the experimental determination of carbon, nitrogen, and phosphorus yields is essential, since the elemental concentrations used at laboratory scale differ from those of the undiluted by-products considered at industrial scale.

Once productivity and the corresponding elemental yield coefficients are established, mass balances are performed under steady state conditions. Following to the assumption that the reactor operates as a CSTR, steady state operation implies that no mass accumulation occurs within the system. Therefore, the accumulation term is neglected in all unit operations, and the general mass balance is expressed as Equation 2.6.

$$0 = Input - Output + Generation - Consumption \quad (2.6)$$

Component balances are then applied to the main species considered in the simulation, namely carbon, nitrogen, and phosphorus, while biomass formation and substrate conversion are represented through the experimentally determined yield coefficients.

All calculations are implemented in Microsoft Excel or with the Excel Solver, where the corresponding set of mass balance equations is solved for each process scenario. This modelling framework provides a consistent basis for process simulation and for estimating the main stream flow rates and compositions required for the conceptual plant design.

2.4.1 Carbon balances

Among the elemental balances, carbon is of primary importance because it constitutes the main limiting substrate for biomass production in the selected by-products. In order to determine the carbon-based yield coefficients, the carbon concentrations of the relevant streams shown in Figure 2.7 are first measured by TOC/TN analysis.

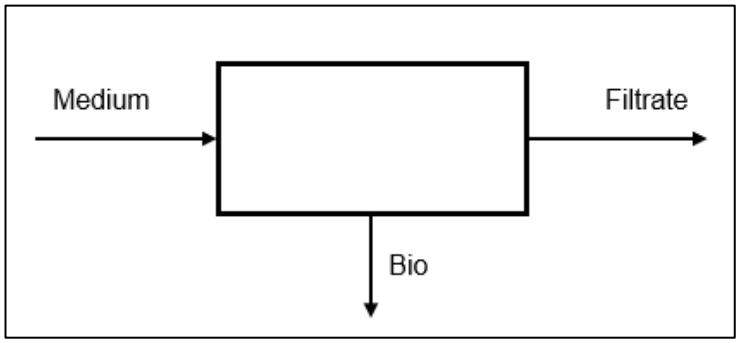

Figure 2.7. *Schematic representation of the streams considered for yield calculations.*

According to Figure 2.7, three carbon concentrations are considered for the development of the carbon balance. The first is the carbon concentration in the culture medium or entering the reactor,

C_{IN}, which represents the total organic carbon initially supplied to the culture. The second is the carbon concentration measured in the reactor sample, C_{BIO}, which includes both the organic carbon associated with the biomass and the residual organic carbon still present in the medium. This value is generally lower than C_{IN}, since part of the inlet carbon is consumed by the biomass and converted into CO_2, which is no longer detected as organic carbon by the TOC analyser. The third is the carbon concentration in the filtrate, C_{FIL}, which represents the residual organic carbon remaining in the liquid phase after biomass removal and therefore corresponds to the fraction not consumed by the microalgal metabolism. The reactor sample used to determine C_{BIO} is collected directly from inside the reactor by means of a syringe.

On the basis of these measurements, the carbon mass balance is expressed by Equation 2.7, which takes into account both the yield coefficient $Y_{C/X}$, representing the carbon incorporated into biomass, and $Y_{CO_2/X}$, representing the carbon converted into CO_2 per unit of biomass produced.

$$0 = C_{IN} - C_{FIL} + C_X \cdot (-Y_{C/X} - Y_{CO_2/X}) \tag{2.7}$$

The overall carbon conversion X_C is then calculated according to Equation 2.8:

$$X_C = \frac{C_{IN} - C_{FIL}}{C_{IN}} \tag{2.8}$$

where $[C]_{IN}$ and $[C]_{FIL}$ are both expressed in g L^{-1}.

To determine the fraction of carbon associated with the biomass, the difference between the carbon concentration measured in the reactor sample and that measured in the filtrate is calculated. This difference represents the organic carbon associated with the biomass. The corresponding carbon-based yield coefficient is then related to the biomass concentration through Equation 2.9:

$$Y_{C/X} = \frac{C_{BIO} - C_{FIL}}{C_x} \tag{2.9}$$

where C_x is the biomass concentration (g L^{-1}).

2.4.2 Nitrogen balances

The same methodological approach described for carbon is also applied to nitrogen. In this case, the nitrogen concentrations in the relevant streams are determined by TOC/TN analysis and used to evaluate the distribution of nitrogen between the liquid phase and the biomass. As for carbon, the nitrogen balance is developed on the basis of the inlet medium, the reactor sample, and the filtrate. Since the procedure and the derivation of the corresponding equations are analogous to those presented for carbon, they are not reported again in full here. The same relationships are used, replacing carbon concentrations with the corresponding nitrogen concentrations.

Accordingly, the nitrogen mass balance is expressed by Equation 2.10:

$$0 = N_{IN} - N_{FIL} - C_X \cdot Y_{N/X} \quad (2.10)$$

where $Y_{N/X}$ represents the yield coefficient of nitrogen in biomass.

In the same way as for carbon, the nitrogen associated with the biomass is determined from the difference between the nitrogen concentration measured in the reactor sample and that measured in the filtrate. The corresponding nitrogen-based yield coefficient is therefore calculated according to Equation 2.11:

$$Y_{N/X} = \frac{N_{BIO} - N_{FIL}}{C_X} \quad (2.11)$$

These experimentally determined coefficients allow the estimation of the fraction of inlet nitrogen that remains dissolved in the liquid phase and the fraction assimilated into the biomass during cultivation. The nitrogen balance is particularly relevant for assessing nutrient supplementation requirements and for verifying that sufficient nitrogen is available to sustain the biomass productivity predicted from the carbon-based calculations.

2.4.3 Phosphorus balances

An analogous procedure is adopted for phosphorus. Instead of TOC/TN analysis, phosphate measurements are carried out, followed by the corresponding calculations.

Equation 2.12 presents the phosphorus mass balance, taking into account $Y_{P/X}$, which represents the phosphorus in biomass yield.

$$0 = P_{IN} - P_{OUT} - C_X \cdot Y_{P/X} \quad (2.12)$$

After the phosphorus concentrations in the inlet, filtered, and biomass-associated fractions have been experimentally determined following the procedure described in Section 2.3.4, the relevant yield coefficient is calculated to characterize the partitioning of phosphorus within the system.

Once the carbon, nitrogen, and phosphorus balances are established, the stream compositions and flow rates required for the conceptual design of the industrial-scale process can be defined.

2.5 Process simulation and conceptual plant design

In the conceptual design and process simulation, biomass production is calculated from the flow rate and composition of the inlet feed, particularly its carbon content, through the application of the experimentally determined yield coefficients. Accordingly, for each process scenario, the amount of biomass obtained is derived from the available substrate in the feed and the corresponding yields measured in the laboratory experiments. Consequently, for each process, the

productivity is a known value based on the experiments. Therefore, the first objective is to determine the inlet flow rate of dairy by-products based on data from real factories, in order to quantify the biomass production obtainable and assess whether these by-products can be profitably valorised. Two scenarios were considered, namely representative of large- and small-scale dairy factories.

In both scenarios, the plants are assumed to operate for 8,150 h per year, since the process is continuous and algal growth is expected to occur continuously throughout the year, the rest is needed for maintenance operations.

Permeate is selected as the by-product for the large-scale case because it is generated in large and industrially relevant volumes in membrane-based dairy processing, whereas SCW is a secondary by-product formed only after whey-cheese production from cheese whey and is therefore associated with a more specific and less widely available production route.

2.5.1 Large-scale process design

2.5.1.1 Process flow diagram and process description

In line with the objective defined in Section 1.5, the large-scale scenario investigates the valorisation of permeate through heterotrophic cultivation of *G. sulphuraria*.

The selection of the permeate inlet flow rate for the large-scale process is based on literature. Industrial ultrafiltration (UF) systems provide relevant benchmarks. A single large UF line in a dairy plant can produce approximately 10^3–10^4 kg/h of permeate. Specifically, Tetra Pak reports processing capacities ranging from 32,900 to 81,100 L/h for skim milk and from 26,550 to 55,320 L/h for sweet whey processing (Tetra Pak International S.A., 2026). In addition, a conceptual design study reports an inlet flow of 32,348 kg/h of milk permeate (Quispe-Chávez, 2004). Based on these references, an inlet flow rate of 30,000 L/h of permeate is selected for the large-scale process, as it represents a realistic and industrially relevant scenario.

The process simulation is developed in Microsoft Excel by means of material and energy balances. The large-scale process is designed under the following assumptions. The system operates at steady state, and the heterotrophic cultivation step is modelled at a fixed residence time of 2 d. Biomass production is calculated from the composition of the inlet feed, with particular emphasis on its carbon content, by applying the experimentally determined carbon-to-biomass yield coefficient. The components explicitly considered in the simulation are water, permeate, ammonium sulphate, carbon dioxide, and microalgal biomass. In addition, the carbon, nitrogen, and phosphorus content of the substrate are taken into account in order to ensure consistent

elemental balances throughout the process. Trace compounds present in the real permeate stream are neglected, since their contribution is assumed to be negligible at the conceptual design stage, while the nutrients considered in the model are assumed to be sufficient to sustain adequate biomass growth. All feed streams are assumed to enter the system at 20 °C and 1 atm. Heat exchange requirements are included in the calculations, although the corresponding auxiliary units are not represented in the process flow diagram in order to keep the conceptual scheme simple.

As shown in Figure 2.8, the permeate feed is evenly distributed among six parallel cultivation lines. This configuration is adopted to handle the high inlet flow rate while maintaining reactor sizes within a feasible industrial range. Although bioreactors with volumes of up to 600 m^3 can be constructed (Meyer et al., 2017), microalgae applications generally employ smaller units, typically up to around 250 m^3, while somewhat larger reactors, such as 300 m^3, remain feasible and are occasionally reported (Eilertsen et al., 2022). On this basis, the large-scale process is arranged as six parallel reactors. Each reactor is operated under heterotrophic conditions and receives the corresponding share of the inlet feed.

Each reactor is supplemented with ammonium sulphate in order to provide the nitrogen required for biomass growth at a suitable C/N ratio. Based on the mass balance calculations, the required ammonium sulphate concentration is 4.91 g L^{-1}. This addition is necessary because, as discussed in Chapter 1, permeate does not contain sufficient nitrogen to sustain the desired biomass growth. Although this addition is simplified in the process flow diagram, ammonium sulphate is fed directly to each reactor. Air is also supplied to satisfy the oxygen demand of heterotrophic metabolism.

After cultivation, the outlet streams from all reactors are combined and sent to a solid-liquid separation step, where the biomass is recovered as the final product and the clarified liquid stream is discharged to wastewater treatment. For this purpose, a centrifugal disc-stack separator is selected, in accordance with the technology assessment reported by Fasaei et al. (2018).

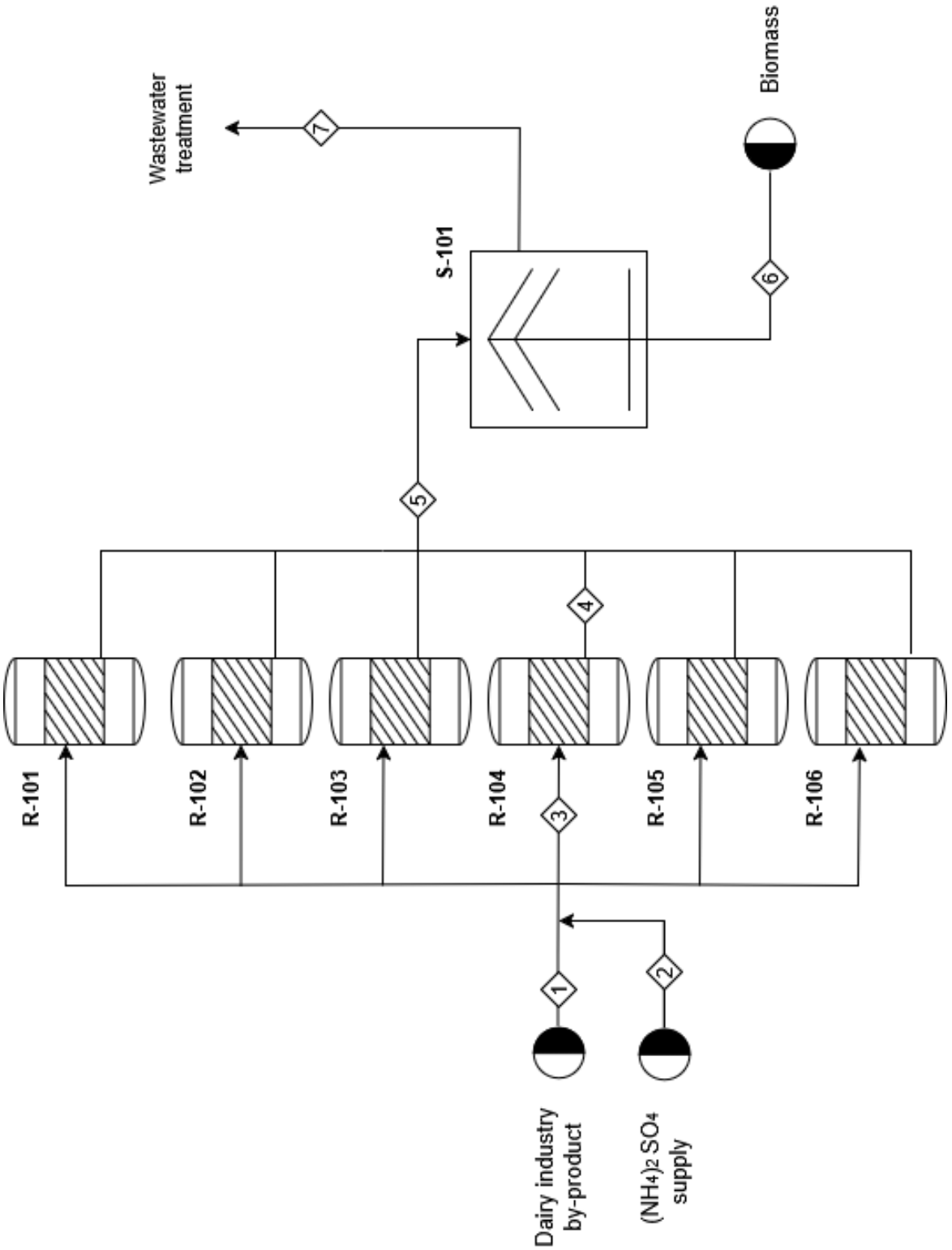

Figure 2.8. *Large scale heterotrophic cultivation process flow diagram.*

2.5.1.2 Main equipment and operating conditions

The cultivation system consists of six stirred-tank bioreactors (R-101 to R-106) operating in parallel under heterotrophic conditions. This configuration distributes the total process volume flow among multiple units, thereby providing greater operational flexibility and scalability than a single large reactor. Each reactor has a total volume of 300 m^3 and an operating volume corresponding to 80% of the total capacity, leaving sufficient headspace for gas handling and safe operation.

The reactors operate at 45 °C, atmospheric pressure, and approximately pH 2, in accordance with the laboratory conditions selected for *G. sulphuraria* cultivation. This acidification is reached by addition of sulfuric acid to the reactor, the amount of sulfuric acid needed to be added is small compared to the inlet streams. Each bioreactor is equipped with two Rushton turbine impellers with a diameter of 1.83 m. Agitation is set at 50 rpm, a low stirring rate is commonly used in microalgae cultivation to maintain biomass in suspension and improve mixing and mass transfer, while limiting the risk of excessive shear stress (Huang et al., 2017; Mediboina et al., 2022). A height-to-diameter ratio of 4 is adopted, as recommended in the literature for this type of system (Mediboina et al., 2022).

Due to the strongly acidic operating conditions, the reactors and associated equipment are decided to be constructed in stainless steel 316L, which provides high corrosion resistance. Its molybdenum content improves resistance to pitting and crevice corrosion, while its low carbon content reduces the risk of intergranular corrosion (Rahman et al., 2018).

Temperature control is achieved by means of spiral plate heat exchangers associated with each reactor (Gaber et al., 2022). These units operate with hot water at 90 °C supplied by an industrial boiler. The final recovery step is carried out in a solid-liquid separation unit (S-101), modelled as a disc-stack centrifugal separator (Figure 2.9). This technology is commonly used in microalgae processing because of its high separation efficiency and its ability to operate continuously (Fasaei et al., 2018). In this unit, the feed enters a rotating bowl containing a stack of conical discs that increases the effective settling area. Under centrifugal force, the denser biomass particles migrate outward and are collected, while the clarified liquid phase is discharged separately (Najjar & Abu-Shamleh, 2020). In the simulation, the solid–liquid separation step is described by assuming a separation efficiency of 1, corresponding to complete biomass recovery in the solid stream. The parameter F_{ds} is introduced to represent the mass fraction of dry biomass in the recovered wet paste. In the present work, a value of F_{ds}=0.2 is assumed (Lohrey & Kochergin, 2012). This assumption is required to define the composition of the outlet stream and to perform the subsequent mass balance calculations. The separated biomass stream constitutes the final product of the

process and is considered ready for subsequent commercialisation, whereas the liquid effluent is sent to wastewater treatment.

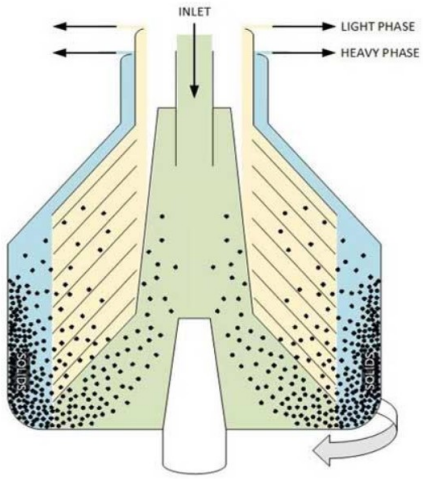

Figure 2.9. *Schematic representation of a disc-stack centrifuge bowl and phase separation mechanism (Prabhu).*

2.5.2 Small-scale process design

2.5.2.1 Process flow diagram and process description

The small-scale case study focuses on SCW. As discussed in Section 1.1, this stream remains comparatively underutilized despite its residual lactose and nutrient content. The inlet flow rate selected for SCW was determined on the basis of both industrial data and literature sources. To support this selection, a survey was conducted among dairy factories to gather information on whey and SCW production (Appendix A). Literature data further indicate that approximately 8–10 L of cheese whey are generated per kilogram of cheese produced, while around 18 L of SCW are generated per kilogram of whey cheese produced (Figueroa Pires et al., 2021). Nevertheless, not all the cheese whey produced is used for ricotta manufacture; consequently, the amount of SCW generated depends on the fraction of whey effectively allocated to whey cheese production. According to Pontonio et al. (2021), the ricotta yield from cheese whey is usually below 4%, meaning that less than 4% of the whey volume is converted into ricotta cheese. In addition, Tuson and Coffey (1976) reported a cheese whey production of 3,000 kg per day for a small dairy company. Assuming these average production conditions, together with 250 working days per year and 12 h of operation per day, the corresponding average SCW flow rate is estimated to be approximately 180 L h^{-1}. This value is consistent with the quantities reported in the survey for small factories (Appendix A). For this reason, the inlet stream selected for the project corresponds to Dairy Factory 3, which generates 9,000 L a week of SCW. This value is assumed to correspond to an average inlet flow rate of 150 L h^{-1}.

The first section of the small-scale process (Figure 2.10) describes the heterotrophic cultivation of *G. sulphuraria* using SCW as the main substrate. SCW is employed as the principal carbon source and enters the system through Stream 1. Since the nitrogen naturally present in SCW is not sufficient to satisfy the nutritional requirements for optimal biomass growth, granular ammonium sulphate is supplied directly to the reactor, as in the large-scale case. For modelling purposes, only carbon, nitrogen, and phosphorus are taken into account in SCW, whereas trace components are neglected in order to simplify the mass balance calculations.

The resulting feed stream enters reactor R-101, where *G. sulphuraria* is cultivated under the same operating conditions adopted in the large-scale case. During this stage, the organic fraction of SCW is consumed as carbon source for biomass production. The cultivation broth leaving the reactor is then sent to the solid-liquid separation unit S-101, where the biomass is separated from the liquid phase. The concentrated biomass is recovered as the main product of this first stage, whereas the clarified liquid stream is divided into two fractions. One fraction is recycled because it still contains residual nutrients, while the other is sent to the second part of the small-scale process, namely the mixotrophic section. This configuration improves the overall valorisation of SCW by enabling the further use of the liquid fraction after biomass recovery. Such a recycle strategy is feasible in the small-scale plant, where the bioreactor volume remains acceptable, but it is not retained in the large-scale case because the inlet flow rate is already very high, thus requiring multiple large reactors.

This configuration improves the overall valorisation of SCW by enabling further use of the liquid fraction after biomass recovery.

Figure 2.10 illustrates the initial section of the process flow diagram for the proposed small-scale SCW valorisation process.

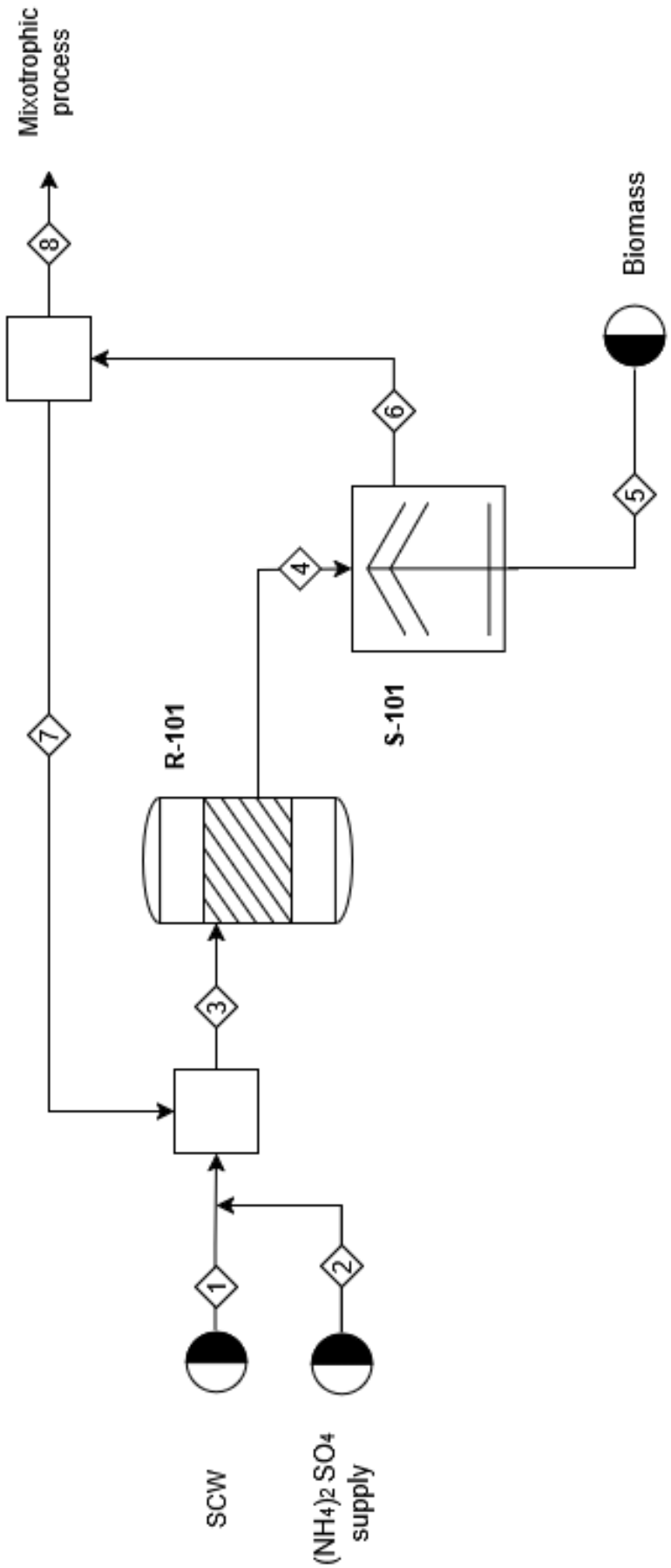

Figure 2.10. *Small scale heterotrophic cultivation, first part of process flow.*

The second stage of the process (Figure 2.11) corresponds to the mixotrophic cultivation section, which is introduced to further valorise the outlet stream from the heterotrophic system. Since this stream still contains residual nutrients and organic matter, it is considered suitable for further processing through an additional cultivation step. Nevertheless, ammonium sulphate supplementation is still required in order to match the nitrogen concentration adopted in the experimental conditions. Accordingly, a second mixotrophic stage is introduced to enable the production of not only additional biomass, but also C-phycocyanin as a value-added pigment. In the present work, the C-phycocyanin content in *Galdieria sulphuraria* biomass is assumed to be 10.1 ± 0.5% on a dry-weight basis (Abiusi et al., 2022). This additional stage therefore improves the overall valorisation of the initial by-product by allowing the recovery of a further high-value product.

The mixotrophic section is developed under steady state conditions, and cultivation in the photobioreactor is carried out at a fixed residence time of 1.5 d. Before entering the photobioreactor, the outlet stream from the heterotrophic section is diluted with water in order to adjust the substrate concentration; for the energy balance, this make-up water is assumed to be heated in a natural-gas-fired boiler to the operating temperature before entering the process. This dilution is necessary because an excessively high organic carbon concentration would favour predominantly heterotrophic metabolism, thereby limiting photosynthetic activity and, consequently, pigment formation. By reducing the inlet carbon concentration, the process is shifted towards mixotrophic conditions, in which photosynthesis is promoted and C-phycocyanin accumulation can occur. For this reason, an inlet carbon concentration of 2.5 $g_C\ L^{-1}$ is selected as a compromise between two competing objectives: providing sufficient carbon to sustain biomass production while limiting the organic load enough to stimulate photosynthetic metabolism and pigment synthesis.

However, the nitrogen and phosphorus contents of the outlet stream are not sufficient to reach the desired concentrations before entering the reactor; therefore, nutrient supplementation is required. For nitrogen, ammonium sulphate is added in order to match the target concentration adopted in the experimental conditions. For phosphorus, monoammonium phosphate (MAP, $NH_4H_2PO_4$) is selected as the phosphorus source because of its high water solubility and its moderately acidic behaviour in solution, which make it suitable for acidic process conditions and it has relatively low bulk prices compared with specialty water-soluble phosphate products (Haifa Group, 2026; U.S. Department of Agriculture, 2026).

After dilution and nutrient adjustment, the resulting stream is fed to photobioreactor PBR-101, where mixotrophic cultivation takes place. The outlet stream from the photobioreactor is subsequently sent to centrifugal separator S-102, where the biomass is separated from the liquid

phase. As in the large-scale case, all separator units are assumed to operate with a separation efficiency equal to 1. In addition, the parameter F_{ds}, representing the mass fraction of dry biomass in the recovered wet paste, is assumed to be equal to 0.2.

The clarified liquid stream leaving separator S-102 is then divided into two fractions: one fraction is recycled, while the remaining fraction is discharged to wastewater treatment. The recycle is introduced in order to reduce the freshwater requirement in Stream 15 and thus improve the overall water efficiency of the process. A recycle ratio of 0.7 is adopted, defined as the ratio between the recycle stream and the sum of the recycle stream and the additional freshwater stream.

The concentrated biomass recovered in separator S-102 is subsequently sent to the high-pressure homogeniser H-101, whose purpose is to disrupt the cells and release the intracellular compounds. This cell disruption step is necessary to enable the subsequent extraction of C-phycocyanin. The disrupted biomass stream is then fed to the solid–liquid extraction vessel V-101, where water is used as the extraction solvent. The use of water is suitable for the extraction of C-phycocyanin because this pigment is water-soluble. According to the literature, the extraction step requires approximately 4 h (Jaeschke et al., 2021). Therefore, although the overall process is represented as continuous, this stage must be appropriately controlled, for example by means of a valve and a suitable residence time strategy, in order to ensure the required extraction time. An option could be serpentine pipes.

The mixture leaving the extraction vessel is then sent to a second centrifugal separator, S-103, where the remaining residual biomass is separated from the liquid extract. Since the cells have already been disrupted, this residual biomass may be considered for valorisation as a biofertilizer. The liquid stream containing the extracted C-phycocyanin is subsequently processed by microfiltration (MF-101) followed by ultrafiltration (UF-101). These membrane steps are included to improve the purity of the pigment extract. According to Chiklakhan et al. (2018), after these purification steps the C-phycocyanin is pure enough to be sold in food-grade applications. Finally, the purified product stream is sent to the freeze-drying unit FD-101, where water is removed and the final C-phycocyanin product is obtained in dry form. This final step improves product stability and facilitates storage and commercialisation.

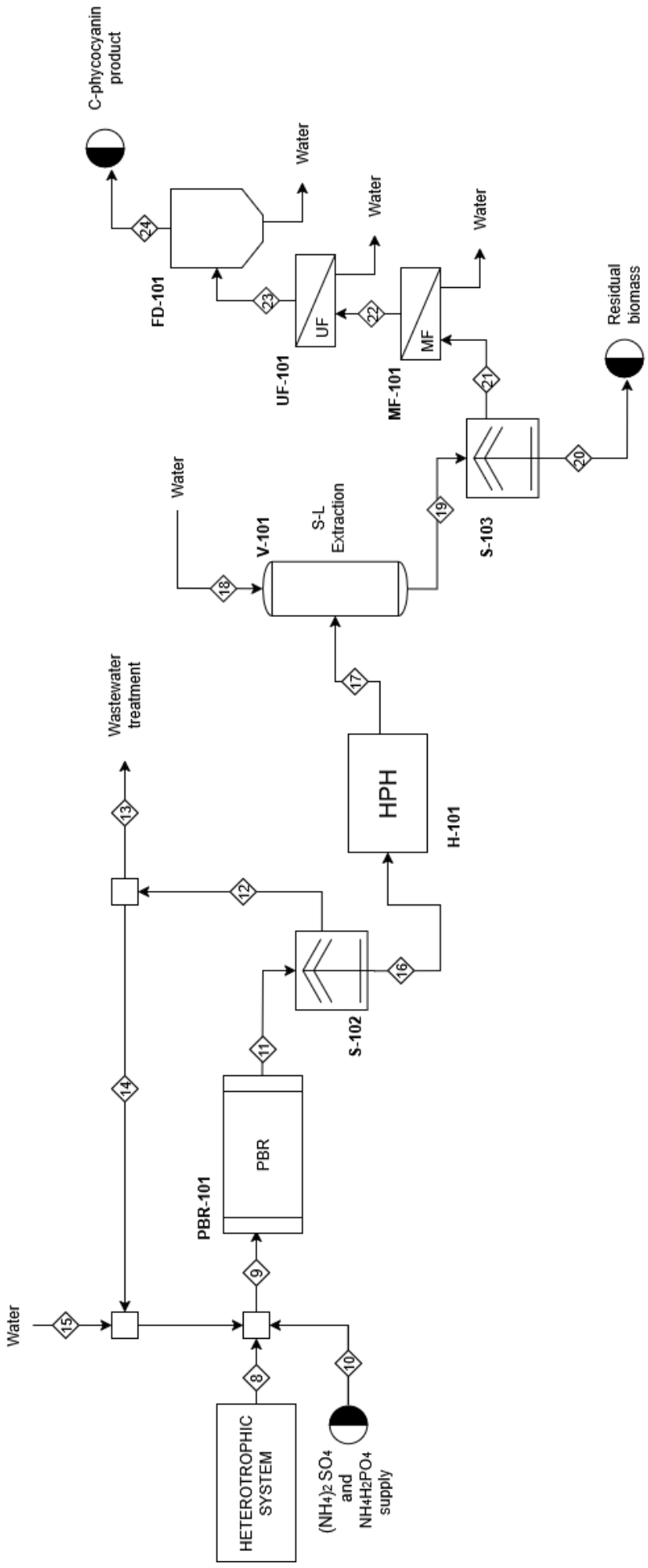

Figure 2.11. *Small scale mixotrophic cultivation, second part of process flow*

2.5.2.2 Main equipment and operating conditions

The first section of the small-scale process corresponds to the heterotrophic cultivation system. The reactor operates at atmospheric pressure and 45 °C, in accordance with the conditions selected for *G. sulphuraria* cultivation. A stainless steel 316L stirred-tank reactor with a total volume of 15.3 m³ is selected. The reactor type and general design criteria are kept consistent with those adopted for the large-scale case in order to preserve comparability between the two process configurations.

Because of the smaller reactor size, temperature control is provided by means of a double-pipe heat exchanger rather than the spiral plate heat exchanger used in the large-scale design. Heating is achieved using hot water supplied at 90 °C from an industrial boiler fired with natural gas.

The reactor is equipped with two Rushton turbine impellers of 0.678 m diameter, operating at 50 rpm. As in the large-scale configuration, this arrangement provides an adequate balance between mixing efficiency and shear stress, thereby ensuring suitable mass transfer conditions for microalgal cultivation (Mediboina et al., 2022). A height-to-diameter ratio of 4 is also maintained, following the same design basis adopted previously.

After cultivation, the broth is directed to a solid-liquid separation step carried out in a disc-stack centrifugal separator. The selected unit is a smaller version of that considered in the large-scale process, with a treatment capacity of 0.255 m^3 h^{-1} instead of 30 m^3 h^{-1}, in accordance with the lower system throughput. The separated biomass constitutes the main product of this first stage, whereas the liquid effluent, which still contains residual nutrients and dissolved compounds, is directed to the subsequent mixotrophic section.

The second section of the process requires a larger cultivation volume than the first one because the outlet from the heterotrophic system is diluted before entering the mixotrophic unit. This dilution is necessary to adjust the carbon concentration of the inlet stream to the value selected from laboratory experiments and, consequently, increases the total volumetric flow to be treated in the PBR system.

For this stage, a horizontal tubular photobioreactor (Figure 2.12), designated PBR-101, is selected (Chandola et al., 2026). Culture circulation is maintained by means of a centrifugal pump, thereby ensuring continuous movement of the suspension through the tubular loop and adequate exposure of the cells to light. Based on the design calculations, the system is composed of nine modules with a total installed volume of 36 m^3 and an effective working volume of 30.6 m^3. Each module has a volume of approximatehoy 4 m^3, corresponding to an effective operating volume of 3.4 m^3 (Chandola et al., 2026).

The PBR is designed on the basis of the productivity extrapolated from the experiments. At laboratory scale, a photobioreactor volume of 0.2 L, a flat-panel illuminated area of 0.00594 m², and a biomass productivity of 1.43 g L^{-1} d^{-1} are considered. From these data, an areal productivity of 48.15 g m^{-2} d^{-1} is determined and used as the basis for scale-up.

The light intensity profile is also taken into account in the reactor design. The geometrical characteristics of the tubular photobioreactor are selected according to Chandola et al. (2026), including a tube diameter of 0.052 m. In order to reproduce, at process scale, light conditions comparable to those identified experimentally, the light perceived by the culture is considered. Since the selected inlet carbon concentration for the mixotrophic stage is 2.5 g_C L^{-1}, the corresponding central light intensity is derived by interpolation (Appendix B) from the experimental results obtained at different carbon concentrations.

Based on this target value at the centre of the tube, the required incident light intensity at the reactor surface is calculated by applying the Lambert–Beer law for light attenuation in a microalgal culture, as reported in Equation 2.13. From this relationship, an average incident light intensity of 164.31 µmol m^{-2} s^{-1} is obtained.

$$I_{center} = I_0 \cdot exp(-K_a \cdot C_x \cdot \frac{D_t}{2}) \quad (2.13)$$

Where I_0 represents the incident light intensity at the reactor surface, while I_{center} is the light intensity at the centre of the reactor after attenuation through the culture medium. The term K_a is the biomass absorption, coefficient, which describes the capacity of the cells to absorb light, and C_x is the biomass concentration in the medium. The term $\frac{D_t}{2}$ is the distance travelled by light from the reactor wall to its centre (being D_t the tube diameter).

The required illuminated area is calculated by first determining the area that must be exposed to light. The tubular layout is based on modules 100 m in length and 1.33 m in width, resulting in approximately 19 tubes per module, with a centre-to-centre spacing of 0.07 m (Chandola et al., 2026).

On this basis, the total tube length required is 1883.5 m, corresponding to a total illuminated area of 133 m².

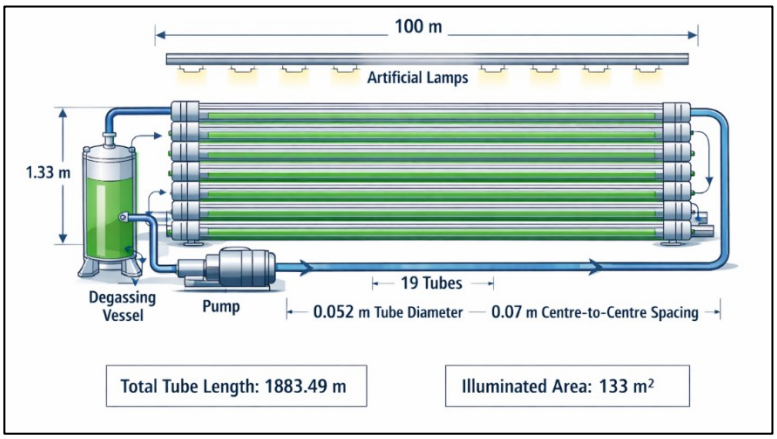

Figure 2.12. *PBR size and main characteristics (AI-generated image).*

Artificial illumination is provided to satisfy the photosynthetic requirements of the culture. For each module, the total light demand is estimated from the selected photon flux and illuminated area, resulting in a power requirement that can be met using 600 W lamps with a photon efficiency of 2.5 μmol J^{-1} (Shenzhen Igrow Bio-Tech Co., Ltd., 2026). On this basis, 15 lamps per module are selected in the final design in order to provide a sufficient safety margin.

Downstream of the PBR, the biomass is first concentrated in centrifugal separator S-102. A second, smaller centrifugal separator, S-103, is then used after extraction to remove the residual disrupted biomass from the liquid phase. Cell disruption is carried out in the high-pressure homogeniser H-101 in order to release intracellular compounds before extraction. The homogenised stream is then sent to the extraction vessel V-101, a small solid-liquid extraction tank with a volume of approximately 0.054 m³. In this unit, water is used as extraction solvent because of the water solubility of C-phycocyanin. The liquid extract is then purified through a membrane sequence consisting of MF-101 followed by UF-101. These units are included to remove remaining suspended material and to improve the concentration and purity of the pigment extract. Finally, the purified stream is sent to the freeze-drying unit FD-101, where the product is dehydrated to obtain a stable final powder.

All streams and units, with the exception of the high-pressure homogeniser, operate at atmospheric pressure. The high-pressure homogeniser operates at 700 bar (Chen et al., 2022). The process temperature in this stage is also assumed to be 45 °C. In addition, no heat losses from the first part of the process are considered; consequently, the inlet stream to the PBR is also assumed to be at 45 °C. On the basis of these process configurations and operating assumptions, energy balances are then carried out to determine the thermal requirements of the proposed systems.

2.6 Energy balances

After defining the process flow sheets and the main operating conditions of each scenario, energy balances are carried out to determine the thermal requirements of the proposed systems. Their main purpose is to estimate the heat duty required to maintain the cultivation units at the selected operating conditions. In this work, the analysis focuses mainly on the reactor units, since these are the process sections in which temperature control is required to maintain the culture medium at the operating temperature selected for *G. sulphuraria* cultivation.

As in the case of the mass balances, the energy balances are developed under steady state conditions. Therefore, no energy accumulation is considered. Under these assumptions, the heat duty required from the heat exchanger is determined from three main contributions: heating of the inlet stream, heat exchange with the surroundings through the reactor wall, and mechanical energy provided by agitation. Accordingly, the reactor energy balance is expressed as Equation 2.14:

$$\dot{Q}_{HX} = \rho\dot{V}\ C_p(T - T_{IN}) + \dot{Q}_{wall} - \dot{Q}_{shaft} \tag{2.14}$$

where $\dot{Q}_{HX}$ is the heat supplied by the heat exchanger, $\rho\dot{V}\ C_p(T - T_{IN})$ represents the sensible heat required to raise the inlet stream from its feed temperature to the reactor operating temperature, $\dot{Q}_{wall}$ corresponds to the heat dissipated through the reactor walls, and $\dot{Q}_{shaft}$ represents the mechanical energy introduced into the system by agitation.

Heat transfer through the reactor wall is estimated by an overall heat transfer approach according to Equation 2.15.

$$\dot{Q}_{wall} = U_w A_w (T - T_{amb}) \tag{2.15}$$

where U_w is the overall heat transfer coefficient through the reactor wall, A_w is the heat transfer area, T is the reactor temperature, and T_{amb} is the ambient temperature.

The overall heat transfer coefficient through the wall is determined by considering the internal convective resistance in the liquid phase, the conductive resistance of the wall, and the external convective resistance. This is expressed as Equation 2.16.

$$\frac{1}{U_w} = \frac{1}{h_i} + \frac{\delta}{k_{316L}} + \frac{1}{h_0} \tag{2.16}$$

where h_i is the internal heat transfer coefficient, h_0 is the external heat transfer coefficient, δ is the wall thickness, and k_{316L} is the thermal conductivity of the material used.

The mechanical contribution associated with agitation is also included in the energy balance. In this work, the power transmitted by the impellers is treated as shaft work input to the reactor and is therefore considered as an energy generation term within the system. This contribution reduces the external heat duty required from the heat exchanger, since part of the energy needed to maintain the operating temperature is supplied by agitation.

Once the thermal demand of the reactor is determined, the heat supplied by the heating system is related to the performance of the corresponding heat exchanger. The exchanger duty is calculated using Equation 2.17:

$$\dot{Q}_{HX} = U_{HX} A_{HX} \, \Delta T_{lm,HX} \tag{2.17}$$

where U_{HX} is the overall heat transfer coefficient of the heat exchanger, A_{HX} is the heat transfer area, and $\Delta T_{lm,HX}$ is the logarithmic mean temperature difference between the heating fluid and the process stream.

This formulation makes it possible to determine the heating requirements of the reactor system and to size the associated heat exchange equipment on the basis of the selected operating conditions. In both large-scale and small-scale reactors, the energy balance is used to estimate the heat that must be supplied to compensate for feed heating requirements and thermal losses while accounting for the contribution of agitation. All calculations are implemented in Microsoft Excel, where the energy balance equations are solved for each reactor configuration and process scenario. These results are subsequently incorporated into the economic analysis, as the estimated thermal duties affect both equipment design and utility costs.

2.7 Methodology for economic analysis

In this study, a relevant assumption is made regarding the inlet stream of dairy by-products. This stream is considered as having an indirect economic value, as it no longer requires wastewater treatment by the producing companies. Although it does not generate direct revenue, its utilisation results in cost savings, which are accounted for in the overall economic assessment.

Additionally, pumping costs are neglected in this analysis. Since this work focuses on a preliminary techno-economic evaluation and no significant pressure changes occur within the process, these costs are assumed to be negligible. Furthermore, the by-product streams are already being pumped to wastewater treatment facilities in the current industrial scenario; therefore, any associated pumping costs are considered to be already borne by the company.

In cost estimation studies, it is recommended to use recent cost index values, typically within the last five years, as construction costs, labour productivity, and technological factors may vary over time. The Chemical Engineering Plant Cost Index (CEPCI) is widely used to update equipment and plant costs.

The most recent CEPCI values are reported in Table 2.3 (Towering Skills, 2025; Chemical Engineering, 2025).

Table 2.3. *Chemical Engineering Plant Cost Index (CEPCI) values for the last five years*

Year	*2021*	*2022*	*2023*	*2024*	*2025*
CEPCI	708.8	816	797.9	800.7	~805

As shown in Table 2.3, the CEPCI has remained relatively stable around values close to 800 in recent years. Based on this trend, a reference value of 800 is adopted in this study for the estimation of equipment purchase costs.

The economic performance of the proposed process is evaluated through a preliminary techno-economic analysis based on the estimation of capital expenditures (CAPEX) and operating expenditures (OPEX). Within the framework of conceptual design, the economic potential is defined as the difference between the revenues generated and the total annual costs, which include both variable production costs and annualised capital investment (Bezzo, 2024). Variable costs include raw materials, utilities, and wastewater treatment, while capital costs are associated with the main equipment required for cultivation and separation. Investment costs are annualised using simplified approaches commonly applied in conceptual design, enabling direct comparison with yearly operating costs (Bezzo, 2024).

The economic analysis assumes a discount rate of 10%, which is typical for this type of application (Turton et al., 2018), a taxation rate of 45%, and an equipment lifetime of 15 years (Turton et al., 2018). In addition, straight-line depreciation method and compound interest are assumed in the profitability analysis (Bezzo, 2024). These assumptions allow the estimation of annualised capital costs and ensure consistency in the evaluation of process feasibility. Revenues are assumed to originate from multiple potential products, including microalgal biomass, C-phycocyanin, and residual biomass, which can be valorised as a biofertilizer. All investment costs are assumed to occur within a single year, as the plant construction period is considered to be one year. The equations used for equipment cost estimation are reported in Appendix C. Unless otherwise specified, these correlations are taken from Turton et al., *Analysis, Synthesis and Design of Chemical Processes.*

Capital investment is estimated using the selected cost correlations. The purchase cost of each equipment item is first determined from the correlations reported in Appendix C (Turton et al., 2018), and these values are subsequently used to calculate the installed equipment cost, which accounts for additional contributions such as construction materials, piping, installation labour, and instrumentation and control. For conventional equipment, including reactors, heat exchangers,

and impellers, cost estimation is based on the procedure proposed by Turton et al. (2018), as reported in Appendix C. Whenever the design size lies outside the range of validity of the original correlations, appropriate scale-up relationships are applied (Appendix C.4).

For non-conventional equipment, namely centrifuges (Fasaei et al., 2018; Chaiklahan et al., 2018), membrane units (Chaiklahan et al., 2018), and the freeze-dryer (Rybak et al., 2021), the reference purchase cost and the corresponding processing capacity are obtained from literature and subsequently adjusted to the design capacity using the scaling relationship reported in Appendix C.4. In contrast, the associated specific energy consumption is taken directly from literature, as it is expressed per unit mass of processed material and therefore does not require scaling. The resulting purchase costs are then corrected by means of the corresponding bare module factors in order to estimate the installed equipment costs.

A different procedure is followed for the high-pressure homogeniser, owing to the more limited availability of directly applicable cost correlations. First, the reference purchase cost is obtained from a commercial source (New Life Scientific, 2024). The processing capacity of the equipment is then identified from the manufacturer's technical specifications (Microfluidics). On this basis, the cost is scaled to the required design capacity and corrected with the appropriate factors to estimate the installed cost. Finally, the specific energy consumption, expressed per unit mass of processed material, is taken from literature (Valdovinos-García et al., 2022).

All costs are expressed in euros using a currency conversion factor of 0.85 EUR per USD, based on the exchange rate of March 2026. The total installed cost is then adjusted using a location factor of 1.14, corresponding to Italy, and a module factor of 1.18. Subsequently, indirect costs are estimated as 18% of the direct costs, defined as the sum of the inside battery limits (ISBL) and outside battery limits (OSBL) costs (Bezzo, 2024). Working capital is assumed to be 15% of the total fixed capital cost, which is, the sum of direct and indirect costs, whereas start-up costs are estimated as 8% of the same quantity (Bezzo, 2024). The sum of ISBL, OSBL and indirect costs gives the total CAPEX.

OPEX is estimated by calculating the consumption of raw materials, utilities, such as cooling water, electricity, and natural gas, and wastewater treatment requirements, and by adding labour costs. Labour costs are estimated according to standard methodologies (Bezzo, 2024). In the small-scale configuration, labour costs are assumed to be lower than standard industrial estimates, reflecting the simplicity of the process, the limited scale of the equipment, and the absence of extensive installations. In addition, it is assumed that part of the operational activities may be carried out by existing company personnel.

Product prices represent a key parameter in the economic evaluation. In this study, the biomass selling price is estimated as 1.5 times the production cost, according to literature data (Pahmeyer et al., 2022). The value of C-phycocyanin is selected on the basis of the expected purity of the product obtained in this project, using reported market values (Romero-García et al., 2022), while the price of the residual biomass intended for use as biofertilizer is derived from literature sources (Chiklakhan et al., 2018). The values adopted for raw materials, utilities, and product prices are summarised in Table 2.4. When a range of values is available, the average value is selected in order to maintain a conservative approach.

Table 2.4. *Prices used for economic analysis.*

Utility/raw material	***Price***	***Source***
Microalgae Biomass	6.67 €/kg	Pahmeyer et al., 2022
C-Phycocyanin product	460 €/kg	Chiklakhan et al., 2018
Biomass biofertilizer	2.5 €/kg	(Romero-García et al., 2022)
$(NH_4)_2\ SO_4$	0.25 €/kg	(Chemanalyst, 2025)
$NH_4H_2PO_4$	0.97 €/kg	(U.S. Department of Agriculture, 2026)
Water	0.002 €/kg	(Arezzo Parcheggi, 2025; Utilitatis, 2025)
Natural Gas	0.10 €/kWh	(GlobalPetrolPrices.com, 2026)
Electricity	0.23 €/kWh	(Eurostat, 2025)
Wastewater management	1.21 €/m^3	(Stasinakis et al., 2022)

Chapter 3

Laboratory Results and Discussion

This chapter presents and discusses the experimental results obtained in this work. It first reports the characterisation of both dairy by-products, namely SCW and milk permeate, as their composition is relevant for evaluating their potential for microalgal cultivation and for supporting the subsequent process analysis. It then presents the results of the cultivation experiments, which in the present study are performed only with milk permeate as substrate.

3.1 Characterisation of the by-products and culture media

The first stage of the experimental work consists of the characterisation of the selected by-products and culture media in terms of the main components of interest for microalgal cultivation. In particular, carbon, nitrogen, and phosphorus concentrations are determined by means of the analytical methods described in Chapter 2, namely TOC, TN, and orthophosphate analyses. The resulting data are subsequently compared with literature values in order to assess their representativeness and to define the inlet compositions adopted in the process calculations.

3.1.1 Milk permeate

Milk permeate is first characterised in order to determine its carbon, nitrogen, and phosphorus contents. The experimental results obtained for this stream are summarised in Table 3.1.

Table 3.1. *Experimental characterisation of milk permeate.*

Component	***Experimental values (g L^{-1})***
C	18.81 ± 0.39
P	0.28 ± 0.01
N	0.22 ± 0.01

The experimentally determined concentrations are compared with literature values in order to assess both their consistency and the representativeness of the analysed stream. Literature data for liquid milk permeate report estimated carbon concentrations of approximately 17.7–22.3 g_C L^{-1} (Abd El-Khair, 2009; Hattem et al., 2011), estimated nitrogen concentrations of about 0.33–0.41 g_N L^{-1} (Abd El-Khair, 2009; Hattem et al., 2011), and phosphorus concentrations of about 0.34 g_P L^{-1} (Abd El-Khair, 2009). On this basis, the carbon concentration measured in this work is in line with the literature, while the nitrogen and phosphorus concentrations are of the same order of magnitude, although some deviations are observed. Such differences are not unexpected, as milk permeate composition is influenced by the characteristics of the original stream and by the processing conditions adopted in the dairy plant (Tsermoula et al., 2024).

3.1.2 Second cheese whey

The same characterisation procedure is also applied to SCW. Although SCW is not used in the cultivation experiments presented in this work, its composition is analysed because this by-product is considered in the conceptual design of the small-scale process. The experimental characterisation obtained for SCW is reported in Table 3.2.

Table 3.2. *Experimental characterisation of SCW.*

Component	***Experimental values (g L^{-1})***
C	20.25 ± 0.46
P	0.21 ± 0.01
N	0.44 ± 0.01

The experimentally determined concentrations are then compared with literature data in order to evaluate their representativeness and to support the definition of suitable inlet values for the process calculations. In particular, Russo et al. (2021) report a nitrogen concentration of approximately 0.59 g_N L^{-1}, while Fancello et al. (2024) describe SCW streams with carbon concentrations as high as 25.3 g_C L^{-1}. These differences confirm the variability in SCW composition reported in the literature, which may also depend on the origin of the stream and on the operating conditions of the dairy process.

3.1.3 Representative inlet compositions adopted for process calculations

On the basis of the comparison between the experimental results and the literature data, representative inlet compositions are defined for the subsequent process calculations. These values are not intended to represent direct experimental measurements only; rather, they are selected to provide realistic and consistent input data for the simulation of the process scenarios considered in this work.

For milk permeate, the experimentally measured carbon concentration is retained for the process calculations, since it is consistent with the values reported in the literature and because the carbon content of permeate is known to vary significantly depending on the specific production process. For this reason, the laboratory sample analysed in this work is considered representative of the stream to be simulated. By contrast, the phosphorus and nitrogen values adopted for the calculations are selected on the basis of both the experimental results and the literature data, assuming conservative values that remain close to the experimental measurements while being in line with the literature values.

In the case of SCW, the experimentally determined composition also falls within the ranges reported in the literature. However, for the small-scale process scenario, a relatively concentrated and sugar-rich SCW stream is assumed in order to evaluate the process under favourable, yet still literature-based, conditions. Since carbon concentrations as high as 25.3 $g_C\ L^{-1}$ have been reported in the literature (Fancello et al., 2024), a value of 24.5 $g_C\ L^{-1}$ is selected for the process calculations. For nitrogen and phosphorus, the adopted values are again obtained by averaging the experimental and literature values. The resulting composition therefore represents a concentrated SCW stream suitable for the conceptual design of the small-scale process.

The representative inlet compositions adopted for the two by-products in the process calculations are summarised in Table 3.3.

Table 3.3. *Representative inlet compositions adopted for the process calculations.*

Component	***Milk permeate (g L^{-1})***	***SCW (g L^{-1})***
C	18.81	24.5
P	0.30	0.22
N	0.22	0.54

Overall, the characterisation of the by-products provides the compositional basis required both to interpret the cultivation results and to define the inlet streams used in the process simulations. On

this basis, the following section presents the results of the continuous heterotrophic cultivation experiment performed with *G. sulphuraria* using milk permeate as carbon source.

3.2 Results of the continuous heterotrophic cultivation

This section presents the results obtained from the continuous heterotrophic cultivation experiment carried out under the operating conditions described in Chapter 2. In this case, only one operating condition is investigated, corresponding to an inlet organic carbon concentration of 6 g_C L^{-1}, a residence time of 2 d, a temperature of 45 °C, and pH 2.

The first parameter monitored during the cultivation is the optical density (OD). Figure 3.1 shows the evolution of optical density at 680 and 750 nm during the heterotrophic experiment. Both wavelengths are monitored as indirect indicators of biomass concentration, since the measured signal is mainly related to light scattering by the suspended cells. In particular, OD_{750} is widely used to estimate biomass because pigment absorption is negligible at this wavelength, whereas under heterotrophic conditions OD_{680} is also mainly influenced by scattering due to the low pigment content of the cells.

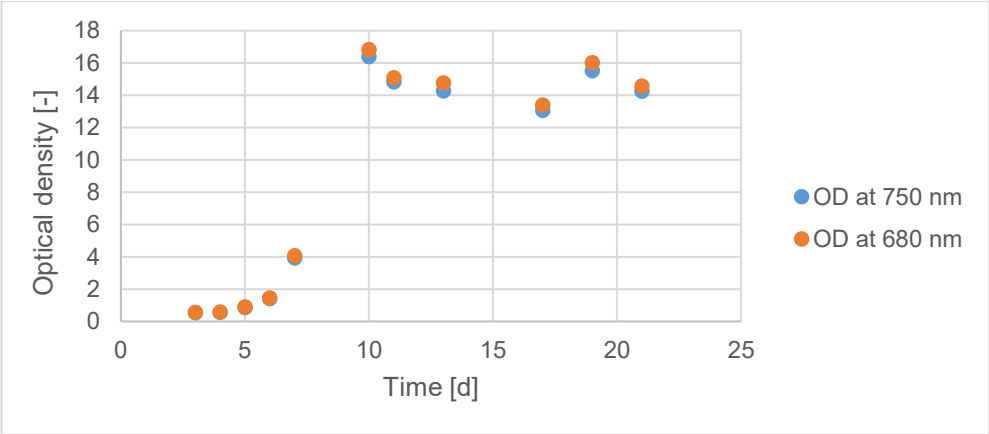

Figure 3.1. *Evolution of optical density at 680 and 750 nm during continuous heterotrophic cultivation.*

As shown in Figure 3.1, the optical density increases progressively during the first days of cultivation, indicating biomass growth and adaptation of the culture to the operating conditions. After approximately day 10, both OD_{680} and OD_{750} reach relatively stable values, with only limited fluctuations over time, suggesting that the system approaches steady state conditions. In addition, the similar trend observed at the two wavelengths indicates good consistency between the absorbance measurements.

Once this regime is reached, biomass concentration is quantified by dry weight analysis, as described in Chapter 2. Figure 3.2 presents the evolution of optical density at 750 nm during continuous heterotrophic cultivation, together with the biomass productivity values determined

from dry weight measurements under steady state conditions. The OD_{750} trend allows the attainment of apparent steady state to be identified, while the P_X values quantify culture performance under stable operation.

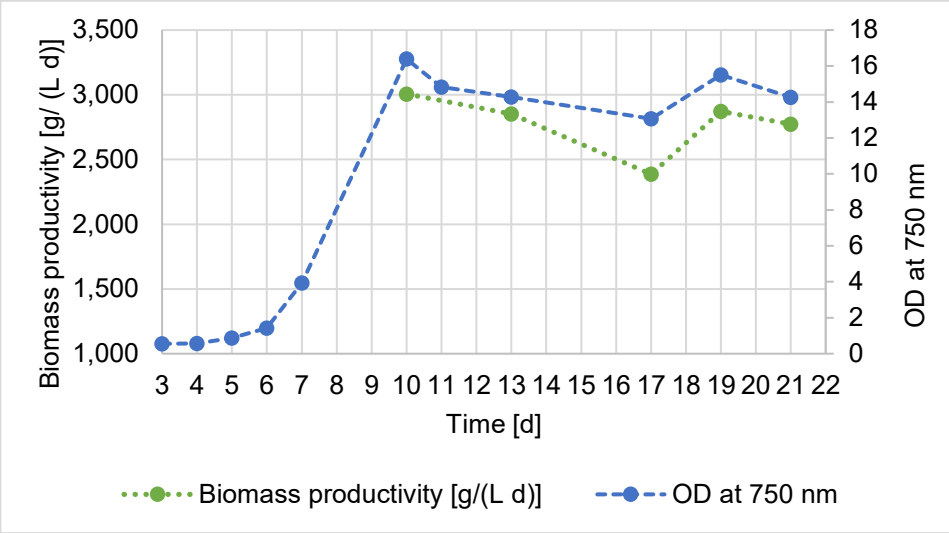

Figure 3.2. *Evolution of optical density at 750 nm during continuous heterotrophic cultivation, with the corresponding biomass productivity values measured under steady state conditions.*

Under steady state conditions, the biomass concentration is 5.71 ± 0.11 g L^{-1}, while the biomass productivity is 2.83 ± 0.05 g L^{-1} d^{-1}. Overall, these results confirm that *G. sulphuraria* is able to grow under continuous heterotrophic conditions on permeate and provide the experimental basis for the subsequent process simulation.

In comparison, Russo et al. (2021) report biomass dry weight values above 10 g L^{-1} for SCW-based media optimised by response surface methodology with nitrogen supplementation. In that study, the optimisation is carried out on SCW diluted to 2.0% reducing sugars, corresponding to approximately 20 g L^{-1} of reducing sugars. Therefore, the biomass concentration obtained in the present work is lower than that reported under those optimised SCW-based conditions. However, this comparison should be interpreted with caution, since the two systems differ in substrate composition, medium optimisation strategy, and cultivation conditions.

To complement biomass quantification, TOC and TN analyses are carried out on the culture medium, the reactor broth sample, and the filtrate in order to characterise substrate consumption and nutrient distribution. TOC analysis of the medium is used to verify that the prepared feed provides the expected organic carbon concentration, whereas the comparison between reactor sample and filtrate allows the partitioning of carbon and nitrogen between the biomass-associated fraction and the liquid phase to be assessed.

Table 3.4 summarises the TOC and TN concentrations measured in the culture medium, the reactor sample, and the filtrate under steady state conditions during the heterotrophic experiment. Based

on these values, the corresponding yield coefficients are calculated and reported in Table 3.5. These parameters represent the main outputs of the experimental work, since they describe carbon and nitrogen partitioning within the system and are subsequently used in the process design calculations.

Table 3.4. *TOC and TN concentrations measured under steady state conditions during continuous heterotrophic cultivation.*

Parameter	***Culture medium (g L^{-1})***	***Reactor sample (g L^{-1})***	***Filtrate (g L^{-1})***
TOC	7.11 ± 0.02	6.68 ± 0.47	4.16 ± 0.38
TN	1.20 ± 0.04	1.20 ± 0.04	0.77 ± 0.02

Table 3.5. *Yield coefficients obtained from the heterotrophic experiment under steady state conditions.*

Yield coefficient	***Value***
$Y_{C/X}$	0.44
$Y_{CO2/X}$	0.08
$Y_{N/X}$	0.07
$Y_{P/X}$	0.01

Since only one heterotrophic operating condition is investigated, the results do not allow a comparative analysis of the effect of individual operating variables. Nevertheless, they provide the experimental information required to characterise biomass growth and substrate consumption under continuous heterotrophic conditions, and they are therefore used as the basis for the simulation of the heterotrophic large-scale process.

3.3 Results of the continuous mixotrophic cultivation

This section presents the results obtained from the continuous mixotrophic cultivation experiments carried out under the operating conditions described in Chapter 2. In all experiments, the residence time is maintained at 1.5 d.

3.3.1 Biomass productivity

As in the heterotrophic experiment, culture evolution under mixotrophic conditions is initially monitored by optical density measurements in order to identify the attainment of steady state

conditions. Once this regime is reached, biomass concentration is determined by dry weight analysis, and the corresponding biomass productivity is calculated according to the procedure described in Chapter 2. Since the residence time is constant in all mixotrophic experiments, biomass productivity provides a direct basis for comparing the performance of the different operating conditions.

Table 3.6 summarises the average optical density, biomass concentration, and biomass productivity values obtained under steady state conditions for the tested combinations of influent carbon concentration and light intensity. Only the values measured after the attainment of steady state are considered; therefore, the reported results do not include all the sampling days of the cultivation period.

Table 3.6. *Average optical density, biomass concentration, and productivity values measured under steady state conditions during continuous mixotrophic cultivation under different influent carbon concentrations and light intensities.*

Parameter	***1.3 g L^{-1} (75 µmol m^{-2} s^{-1})***	***1.3 g L^{-1} (150 µmol m^{-2} s^{-1})***	***6 g L^{-1} (215 µmol m^{-2} s^{-1})***
OD 680 nm	4.19 ± 0.89	3.30 ± 0.19	4.79 ± 0.91
OD 750 nm	4.16 ± 0.98	3.97 ± 0.16	4.69 ± 0.91
C_X [g L^{-1}]	1.57 ± 0.16	1.71 ± 0.04	2.33 ± 0.24
P_X [g L^{-1} d^{-1}]	0.99 ± 0.10	1.10 ± 0.02	1.56 ± 0.16

As shown in Table 3.6, the highest biomass concentration and productivity are obtained under the condition combining the highest influent carbon concentration and light intensity. In particular, the experiment carried out at 6.0 g_C L^{-1} and 215 µmol m^{-2} s^{-1} reaches a biomass concentration of 2.33 ± 0.24 g L^{-1} and a productivity of 1.56 ± 0.16 g L^{-1} d^{-1}, indicating that these conditions are the most favourable among those tested for biomass production.

A comparison between the two experiments performed at the same influent carbon concentration of 1.3 g_C L^{-1} shows that increasing the light intensity from 75 to 150 µmol m^{-2} s^{-1} leads to a slight increase in both biomass concentration and productivity. This suggests a positive effect of light intensity within the investigated range, although the magnitude of the increase remains limited.

The optical density values reported in Table 3.6 are consistent with the overall cultivation trends and support the identification of steady state conditions. However, the comparison between operating conditions is more appropriately based on biomass concentration and productivity, which provide a more direct measure of process performance.

Overall, the available experiments allow only a partial assessment of the individual effects of the operating variables. In particular, the influence of light intensity can only be evaluated for the experiments performed at 1.3 g_C L^{-1}, whereas the effect of carbon concentration cannot be independently isolated, since no experiments are performed at constant light intensity and different influent carbon concentrations. This experimental choice is made because the conditions tested in this work are defined on the basis of previous experiments carried out with glucose, which already identify the most relevant operating conditions for further investigation with dairy-derived substrates. Therefore, the present results mainly support a comparative discussion of the tested operating conditions rather than a systematic evaluation of the individual effect of each variable.
The biomass productivity values obtained in the present work are higher than those reported in the literature for mixotrophic cultivation of *G. sulphuraria* under comparable conditions, using buttermilk instead of permeate as substrate. Specifically, Occhipinti et al. (2023) report a productivity of 0.55 g L^{-1} d^{-1} at an influent carbon concentration of 2 g_C L^{-1} and an incident light intensity in the range of 100–200 μmol m^{-2} s^{-1}, which is lower than the values achieved in this study.

3.3.2 TOC and TN

Tables 3.7 and 3.8 report the TOC and TN concentrations measured in the culture medium, the unfiltered reactor sample, and the filtrate under the tested mixotrophic conditions. TOC analysis of the medium is used to verify that the prepared feed provides the expected carbon concentration and, in particular, that the target organic carbon content is effectively supplied to the culture. The comparison between reactor sample and filtrate concentrations then allows substrate consumption and the partitioning of carbon and nitrogen between the biomass and the liquid phase to be evaluated.

Table 3.7. *TOC concentrations in the different streams under the tested conditions.*

Stream	***1.3 g L^{-1} (75 μmol m^{-2} s^{-1})***	***1.3 g L^{-1} (150 μmol m^{-2} s^{-1})***	***6 g L^{-1} (215 μmol m^{-2} s^{-1})***
Medium	1.25 ± 0.02	1.12 ± 0.13	6.10 ± 0.09
Reactor sample	1.04 ± 0.08	0.90 ± 0.09	6.09 ± 0.09
Filtrate	0.33 ± 0.11	0.39 ± 0.08	4.39 ± 0.34

Table 3.8 presents the TN concentrations measured in different parts of the experiment.

Table 3.8. *TN concentrations in the different streams under the tested conditions.*

Stream	***1.3 g L^{-1} (75 µmol m^{-2} s^{-1})***	***1.3 g L^{-1} (150 µmol m^{-2} s^{-1})***	***6 g L^{-1} (215 µmol m^{-2} s^{-1})***
Reactor sample	1.35 ± 0.02	1.23 ± 0.02	1.21 ± 0.05
Filtrate	0.91 ± 0.09	0.90 ± 0.12	0.92 ± 0.06

3.3.3 Phosphorus content

The phosphorus analysis is carried out through the determination of orthophosphate (PO_4^{3-}) concentration in the samples, since this is the form directly measured by the adopted colorimetric method, as described in Chapter 2. The experimental results are therefore first expressed as orthophosphate concentration and then converted into phosphorus content for the purpose of mass balance calculations.

In the present study, only one phosphorus analysis is performed, corresponding to the experiment conducted at 1.3 g_C L^{-1} and 150 µmol m^{-2} s^{-1}, which is reported here as a representative example. Under this condition, the phosphorus concentration measured in the biomass-containing fraction is 0.12 ± 0.02 g L^{-1}, whereas that measured in the filtrate is 0.11 ± 0.02 g L^{-1}. However, since a single experimental determination is available, the phosphorus value used for the derivation of the corresponding yield coefficient is selected on the basis of literature information and previous analyses conducted within the department.

3.3.4 Experimental yield coefficients

The yield coefficients derived from the experimental data collected under the different mixotrophic conditions are reported in Table 3.9. As phosphorus is not determined for all the experiments, the corresponding phosphorus yield coefficient is not reported here.

Table 3.9. *Yield coefficients obtained from the mixotrophic experiments under steady state conditions.*

Yield coefficient	***1.3 g L^{-1} (75 µmol m^{-2} s^{-1})***	***1.3 g L^{-1} (150 µmol m^{-2} s^{-1})***	***6 g L^{-1} (215 µmol m^{-2} s^{-1})***
$Y_{C/X}$	0.45 ± 0.02	0.30 ± 0.06	0.73 ± 0.05
$Y_{CO2/X}$	0.13 ± 0.05	0.14 ± 0.03	0.05 ± 0.01
$Y_{N/X}$	0.26 ± 0.04	0.19 ± 0.08	0.12 ± 0.03

3.4 Comparison between heterotrophic and mixotrophic cultivation

A comparison between the heterotrophic and mixotrophic experiments carried out at a nominal influent carbon concentration of 6 g_C L^{-1} shows that heterotrophic cultivation leads to higher biomass concentration and productivity under the tested conditions. The heterotrophic experiment reaches an average biomass concentration of 5.71 ± 0.11 g L^{-1}, compared with 2.33 ± 0.24 g L^{-1} for the mixotrophic case. Similarly, and as shown in Figure 3.3, biomass productivity is higher under heterotrophic conditions, with a value of 2.83 ± 0.05 g L^{-1}, whereas the corresponding value for the mixotrophic experiment is 1.56 ± 0.16 g L^{-1}. These results indicate that, under the operating conditions investigated in the present study, heterotrophic cultivation is more favourable for biomass production. Nevertheless, this trend should not be generalised, since the relative performance of heterotrophic and mixotrophic cultivation depends strongly on the strain, carbon source, and light regime considered.

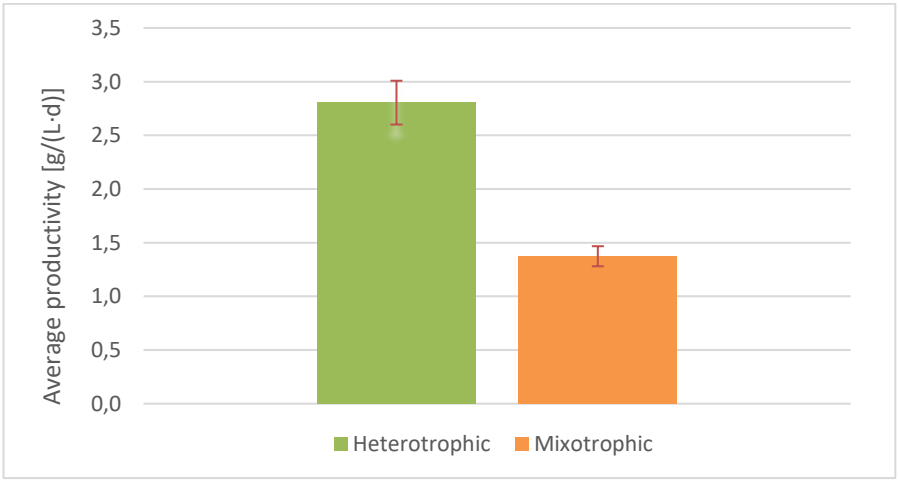

Figure 3.3. *Average biomass productivity under heterotrophic and mixotrophic conditions (error bars represent standard deviation).*

In addition, carbon conversion, calculated according to Equation 2.8 in Section 2.4.1, is approximately 41.5% for the heterotrophic case and 28.0% for the mixotrophic one. This indicates that, under the investigated conditions, the heterotrophic regime is more efficient in converting the supplied carbon into biomass-related products. However, mixotrophic cultivation remains relevant because it enables the production of value-added compounds such as C-phycocyanin, so its performance should not be assessed solely on the basis of biomass yield or carbon conversion.

3.5 Productivity and yield coefficients selected for process design

This section reports the productivity and yield coefficients adopted for the subsequent process design and techno-economic analysis. These values are selected on the basis of the experimental

results obtained in this work and, when necessary, integrated with literature data. Since the discussion of these parameters is presented in the corresponding results sections, only the final values used in the process calculations are summarised here.

The biomass productivity values adopted for the different process configurations are reported in Table 3.10. These values are obtained by extrapolating the laboratory productivities on the basis of the inlet carbon concentration of the corresponding by-product stream. For the heterotrophic cases, the inlet streams considered are permeate and SCW. In the mixotrophic SCW case, the stream entering the photobioreactor is adjusted to an organic carbon concentration of 2.5 $g_C\ L^{-1}$, as discussed previously. The procedure used to calculate the productivity values reported in the following table is described in Section 2.4. Briefly, for process simulation, the productivity is recalculated on the basis of the inlet carbon concentration of the industrial stream and the experimentally determined carbon yield coefficients. For clarity, the inlet carbon concentration considered in each case is also reported in the Table 3.10.

Table 3.10. *Productivity values adopted for the different process configurations.*

Process configuration	***P_X [g L^{-1} d^{-1}]***	***Inlet carbon concentration (g L^{-1})***
Heterotrophic permeate	7.55	18.81
Heterotrophic SCW	7.47	24.50
Mixotrophic SCW	1.43	2.50

For the heterotrophic case, the yield coefficients adopted for process design are based mainly on the experimental results obtained under continuous cultivation with permeate. Since this experimental campaign constitutes the basis for the simulation of the large-scale heterotrophic process, the corresponding coefficients are adopted as representative design parameters. At the time this work is carried out, no heterotrophic continuous cultivation experiments on SCW are yet available within the research group. However, since the yield coefficients obtained in this work are in agreement with literature data reported for heterotrophic *G. sulphuraria* cultivation on organic substrates, they are considered representative and are therefore also adopted for the SCW process (Occhipinti et al., 2023). For phosphorus, the value used in the design calculations is taken from previous work developed within the research group, as it is considered more reliable for process design purposes.

The final heterotrophic experiment coefficients are summarised in Table 3.11.

Table 3.11. *Yield coefficients adopted for the heterotrophic process design.*

Yield	***Value***
$Y_{C/X}$	0.443
$Y_{CO2/X}$	0.077
$Y_{N/X}$	0.076
$Y_{P/X}$	0.0075

For the mixotrophic case, the coefficients adopted in the process design are obtained from the available experimental dataset and subsequently interpolated to the operating conditions selected for the present study. More specifically, the coefficients for the SCW-based process are based on previous results generated within the laboratory research group for mixotrophic cultivation on SCW and are adjusted to the inlet carbon concentration of 2.5 g_C L^{-1} and the corresponding light intensity. For carbon, the available dataset reports the overall conversion X_C rather than the individual yield coefficients; therefore, X_C is used directly in the process calculations, as it already represents the total fraction of inlet carbon consumed. The final values used in the calculations are reported in Table 3.12.

Table 3.12. *Conversion and yield coefficients adopted for the mixotrophic process design based on SCW experiments.*

Yield	***Value***
X_C	0.92
$Y_{N/X}$	0.12
$Y_{P/X}$	0.0075

Chapter 4

Techno-Economic Results and Discussion

Chapter 4 presents and discusses the techno-economic results obtained for the process configurations developed in Chapter 2, based on the experimental findings reported in Chapter 3. Three scenarios are analysed: the large-scale heterotrophic scenario, the small-scale heterotrophic scenario, and the small-scale sequential heterotrophic and mixotrophic scenario. To improve the interpretation of the results, the discussion is organised scenario by scenario. For each configuration, the main technical results are first presented in terms of stream flow rates and compositions, production capacities, and utility requirements; the corresponding economic performance is then assessed through capital and operating costs and discounted cash-flow indicators. This structure makes it possible to directly relate process performance to economic feasibility and to highlight the effect of process scale, cultivation strategy, and product portfolio on the overall viability of the proposed systems. The chapter concludes with a comparative discussion of the three scenarios and a sensitivity analysis focused on the small-scale sequential heterotrophic and mixotrophic scenario.

4.1 Large-scale scenario: heterotrophic cultivation

This section presents and discusses the main technical and economic results obtained for the large-scale heterotrophic scenario. First, the results of the mass and energy balances are analysed in order to describe the process performance under the selected design assumptions, with particular attention to stream flow rates and compositions, biomass production, and utility requirements. The economic performance of the configuration is then assessed through capital and operating costs and through discounted cash-flow indicators, so as to evaluate its overall feasibility from a techno-economic perspective.

4.1.1 Process performance and stream compositions

The results of the large-scale heterotrophic permeate scenario confirm that milk permeate can be valorised through heterotrophic cultivation of *Galdieria sulphuraria* at industrial scale. The process treats an inlet permeate flow rate of 30 m^3 h^{-1}, which is distributed among six parallel reactors. Under these conditions, the cultivation system produces 453 kg h^{-1} of biomass, corresponding to 3691.95 t y^{-1}. Compared to the largest-scale experimental system reported by Pleissner et al. (2025), consisting of a 120 L heterotrophic reactor, the large-scale scenario developed in this work achieves a higher volumetric biomass productivity. Specifically, the proposed process reaches 7.55 g L^{-1} d^{-1}, while the productivities derived from the results of Pleissner et al. (2025) are approximately 3.00, 1.58, and 1.17 g L^{-1} $d^{-1}$for the different substrates tested. Therefore, the improved performance of the present configuration is not due solely to its larger scale, but also to a higher productivity per unit reactor volume, which may be partly explained by the higher inlet carbon concentration used in this work. Nevertheless, this comparison should be interpreted with caution, since the substrates investigated by Pleissner et al. (2025) differ from the dairy by-products considered in the present study.

After cultivation, the outlet streams from the six reactors are combined and sent to a disc-stack centrifuge, where the biomass is separated from the liquid phase. The clarified liquid stream, with a flow rate of 28.19 m^3 h^{-1}, is then discharged to wastewater treatment.

The mass balance also shows that ammonium sulphate must be added at a rate of 147.31 kg h^{-1} to each of the six reactors to satisfy nitrogen requirements for biomass growth, since permeate alone does not provide sufficient nitrogen under the selected operating conditions. In addition, the energy balance indicates a heating duty of 111.78 kW per reactor, mainly associated with heating the inlet streams to the operating temperature and compensating for thermal losses during operation.

Overall, the simulated results demonstrate that the proposed configuration is able to process a high flow rate of dairy by-product, recover biomass, and operate under technically consistent conditions. The mass balance shows that the process achieves only partial valorisation of the inlet stream, since approximately 41.5% of the inlet carbon is consumed during cultivation, while the remaining carbon leaves the system in the clarified liquid stream, which still requires downstream wastewater treatment. The clarified liquid stream is of 28.19 m^3 h^{-1}. Therefore, the process enables only partial valorisation of the by-product, although it contributes to reduce the pollutant load of the original stream.

The corresponding process flow diagram is shown in Chapter 2 (Figure 2.8), while Table 4.1 summarises the main stream flow rates and compositions obtained from the simulation.

Table 4.1. *Volumetric flow rates, elemental concentrations, and biomass flow rates of the streams in the large-scale heterotrophic cultivation process.*

Line no. stream component	***Volumetric flow [m^3/h]***	***Mass flow [kg/h]***	***C [kg/m^3]***	***N [kg/m^3]***	***P [kg/m^3]***	***Biomass [kg/h]***
1 Permeate feed stream	30	30,000	18.81	0.22	0.30	-
2 $(NH_4)_2SO_4$ supply stream	-	147.31	-	-	-	-
3 Reactor inlet stream	5	5,000	18.81	1.26	0.30	-
4 Reactor outlet stream	5	5,000	11.01	0.13	0.17	75.5
5 Total reactors outlet	30	30,000	11.01	0.13	0.17	453
6 Recovered biomass stream	1.81	-	11.01	0.13	0.17	453
7 Purge to wastewater treatment	28.19	28,190	11.01	0.13	0.17	-

4.1.2 Economic performance and feasibility

The economic performance of the large-scale heterotrophic scenario is first evaluated in terms of capital expenditure (CAPEX) and operating expenditure (OPEX), and then assessed through discounted cash-flow indicators. For this configuration, the estimated CAPEX is 12.77 M€, whereas the OPEX is 5.37 M€ y^{-1}. Based on the adopted economic assumptions, the process generates total annual revenues of 24.55 M€ y^{-1}. The detailed breakdown of the individual cost items is reported in Appendix D.1.

In addition to CAPEX and OPEX, profitability is evaluated through the net present value (NPV) and the discounted payback period (DPB), which make it possible to assess the ability of the process to recover the initial investment and generate economic returns over the project lifetime.

The detailed annual cash-flow components used in the calculation, including depreciation allowance, profit before tax, income tax, profit after tax, and net cash flow, are reported in Appendix D.2.

The profitability of the large-scale heterotrophic scenario is illustrated in Figure 4.1, which reports the cumulative discounted cash-flow profile over the project lifetime. As shown in the figure, the discounted cash flow is initially negative because of the capital investment required for plant construction and then increases progressively as positive annual cash flows are generated during operation. The curve crosses the zero line after a relatively short time, indicating that the initial investment can be recovered in the early years of operation.

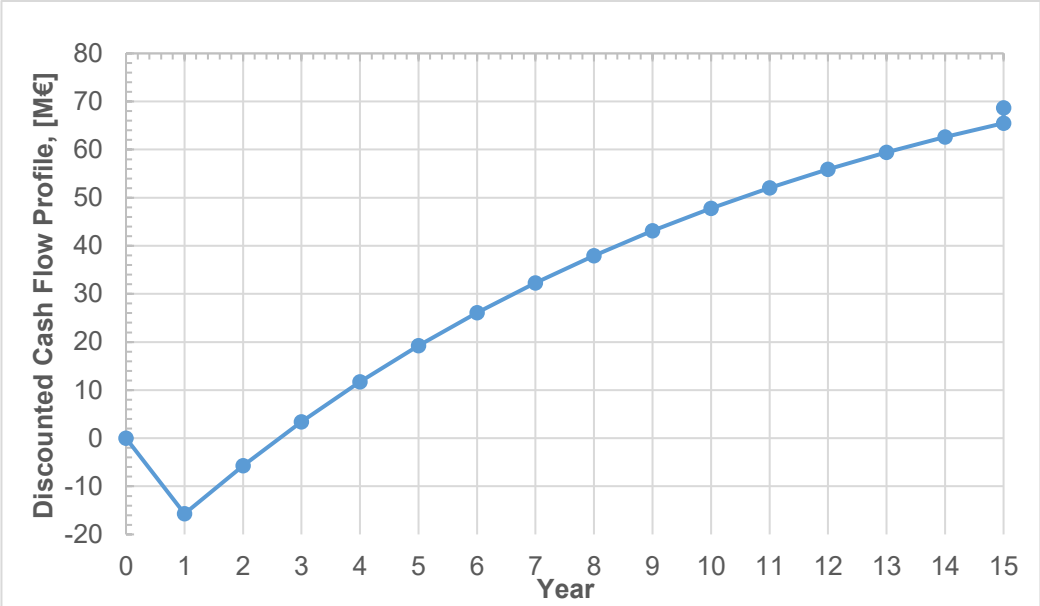

Figure 4.1. *Discounted cash-flow profile over the project lifetime for the heterotrophic large-scale scenario.*

The results show an NPV of 65.5 M€, which indicates that the process is economically attractive under the assumptions considered in this work. In addition, the DPB is equal to 2.62 years, meaning that the initial investment is recovered in less than three years on a discounted basis. Therefore, although the process achieves only partial valorisation of the inlet permeate from a technical point of view, the large treatment capacity and high biomass production make the scenario economically favourable overall. On this basis, the large-scale heterotrophic scenario can be regarded as techno-economically feasible under the selected assumptions.

Pleissner and Smetana (2020) reported that heterotrophic microalgal cultivation on food waste can be economically feasible when biomass is sold directly. Somers et al. (2021), in a *Galdieria sulphuraria* techno-economic study, highlighted the strong influence of substrate cost and cultivation capital on process economics. Therefore, the favourable profitability obtained in the present work appears coherent with literature suggesting that heterotrophic cultivation is more attractive when based on by-product valorisation and aimed at biomass.

4.2 Small-scale scenario: heterotrophic cultivation

This section discusses the results obtained for the small-scale heterotrophic scenario based on SCW. In contrast with the large-scale case, the analysis here concerns a more limited treatment capacity, for which the effects of scale are expected to play a more critical role in the overall techno-economic performance. The section first examines the main technical results of the process, including stream flow rates and compositions, biomass production, and utility requirements, and then evaluates the corresponding economic performance in order to assess whether the configuration is feasible as a standalone option.

4.2.1 Process performance and stream compositions

The small-scale heterotrophic scenario considers the valorisation of SCW through heterotrophic cultivation of *Galdieria sulphuraria*. The process treats an inlet SCW flow rate of 0.15 m^3 h^{-1}, which is fed to the heterotrophic reactor together with the required nitrogen supplementation. Under these conditions, the cultivation system produces 3.81 kg h^{-1} of biomass, corresponding to 31.05 t y^{-1}, showing that part of the organic load of SCW can be converted into valuable microalgal biomass.

After cultivation, the reactor outlet is sent to a disc-stack centrifuge, where complete biomass recovery is assumed. The clarified liquid stream, with a flow rate of 0.1347 m^3 h^{-1}, is split so that 70% is recycled to the heterotrophic section and the remaining 30% is either sent to the subsequent mixotrophic stage for the process configuration in section 4.1.3 or discharged to wastewater treatment. In addition, ammonium sulphate must be supplied at a rate of 1.06 kg h^{-1} to satisfy the nitrogen requirements for biomass growth. Finally, the energy balance shows that the heat exchanger is required to provide a total heating duty of approximately 16.62 kW.

Overall, the simulation results show that the small-scale heterotrophic configuration is technically consistent and capable of recovering biomass from SCW.

The corresponding process flow diagram is reported in Chapter 2 (Figure 2.10), while Table 4.2 summarises the main stream flow rates and compositions obtained from the simulation. However, the process still achieves only partial valorisation of the by-product stream, since a residual clarified liquid fraction remains after biomass separation.

Table 4.2. *Volumetric flow rates, elemental concentrations, and biomass flow rates of the streams in the small-scale heterotrophic cultivation process.*

Line no. stream component	***Volumetric flow [m^3/h]***	***Mass flow [kg/h]***	***C [kg/m^3]***	***N [kg/m^3]***	***P [kg/m^3]***	***Biomass [kg/h]***
1 SCW feed stream	0.15	150	24.5	2.045	0.22	-
2 $(NH_4)_2 SO_4$ supply stream	-	1.06	-	-	-	-
3 Reactor inlet stream	0.26	255	19.05	1.25	0.14	-
4 Reactor outlet stream	0.26	255	11.27	0.11	0.03	3.81
5 Biomass product stream	0.02	15	11.27	0.11	0.03	3.81
6 Separator clarified liquid stream	0.24	-	11.27	0.11	0.03	-
7 Recycle stream	0.11	105	11.27	0.11	0.03	-
8 Purge to wastewater treatment	0.13	134	11.27	0.11	0.03	-

4.2.2 Economic performance and feasibility

The estimated CAPEX and OPEX of the small-scale heterotrophic scenario are equal to 0.32 M€ and 0.16 M€ y^{-1}, respectively. Although these values are substantially lower than those of the large-scale scenario in absolute terms, the reduced plant capacity also limits biomass production and revenue generation (205,471.52 € y^{-1}). A detailed breakdown of the cost items is reported in Appendix D.1, while the corresponding annual cash-flow components are provided in Appendix D.2.

The discounted cash-flow profile of the scenario is shown in Figure 4.2. As can be observed, the cumulative discounted cash flow remains negative over the entire project lifetime, despite

increasing progressively during operation. This indicates that the economic returns generated by the process are not sufficient to recover the initial investment within the considered time horizon.

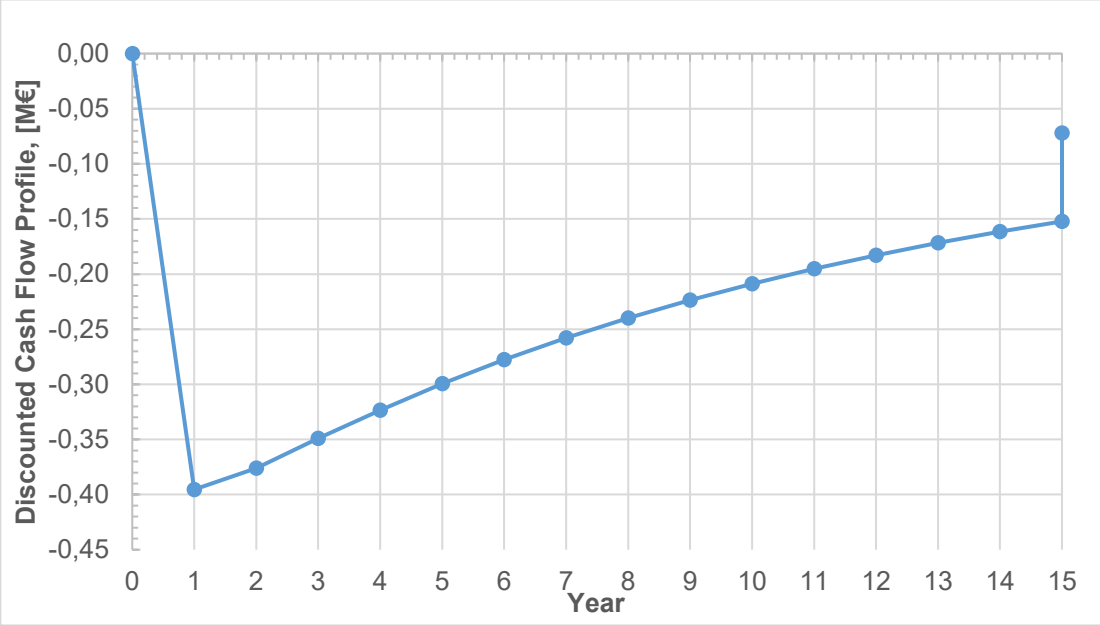

Figure 4.2. *Discounted cash-flow profile over the project lifetime for the heterotrophic small-scale scenario.*

The scenario yields an NPV of −0.15 M€, and the investment is not recovered within the project lifetime. Therefore, while the configuration is technically viable, it is not economically attractive under the selected assumptions. This result suggests that, at small scale, biomass production alone is insufficient to ensure profitability. Although the clarified liquid stream leaving the heterotrophic section still contains recoverable carbon and nutrients, their valorisation is not sufficient in the standalone configuration to generate an economically favourable outcome. For this reason, a subsequent mixotrophic stage is introduced in Section 4.3 in order to further exploit this residual stream and improve the overall profitability of the process.

4.3 Small-scale scenario: sequential heterotrophic and mixotrophic cultivation

Since the small-scale heterotrophic scenario is not economically attractive as a configuration, an additional mixotrophic stage is introduced in order to further valorise the clarified liquid stream leaving the heterotrophic section. As shown in Section 4.2, this stream still contains residual carbon and nutrients that can support further biomass production. In this way, the sequential configuration aims to increase the overall value recovered from SCW by coupling additional biomass generation with the extraction of C-phycocyanin as a higher-value product. The section first presents the main technical results of the added mixotrophic and downstream processing

stages, and then discusses the corresponding economic performance of the overall sequential configuration.

4.3.1 Process performance and stream compositions

In the small-scale sequential heterotrophic and mixotrophic scenario, the clarified liquid stream from the heterotrophic stage is used as the feed for a subsequent mixotrophic cultivation step. Before entering the photobioreactor, this stream is diluted with water in order to adjust the inlet carbon concentration to 2.5 g_C L^{-1}. In addition, ammonium sulphate and monoammonium phosphate are supplied to reach the desired nitrogen and phosphorus concentrations at the reactor inlet, adding 1.01 kg h^{-1} of ammonium sulphate and 0.05 kg h^{-1} of monoammonium phosphate. Under these conditions, the photobioreactor section produces 1.80 kg h^{-1} of biomass, corresponding to 14.6 t y^{-1}. This result confirms that the residual liquid stream from the heterotrophic stage still retains sufficient value to sustain further cultivation. The biomass productivity estimated for the mixotrophic stage in the present work (about 1.91 kg m^{-3} d^{-1}) [is] of the same order of magnitude, and slightly higher than, the value assumed by Somers et al. (2021) for mixotrophic *Galdieria sulphuraria* cultivation in a helical photobioreactor (1.575 kg m^{-3} d^{-1}). However, their techno-economic study shows that this level of productivity alone is not sufficient to ensure strong economic performance, because feasibility remained strongly dependent on the overall process configuration and, especially, on the final product. In the present case, the positive economic outcome is more plausible because the process is directed toward the recovery of C-phycocyanin, a higher-value product.

After cultivation, the outlet stream is sent to a separator, where biomass recovery is assumed to be complete. The clarified liquid stream leaving the separator, equal to 0.62 m^3 h^{-1}, is partially recycled in order to reduce freshwater consumption, while the remaining fraction is discharged to wastewater treatment.

The recovered biomass is subsequently sent to downstream processing for C-phycocyanin extraction. Under the selected assumptions, this section enables the recovery of 0.18 kg h^{-1} of C-phycocyanin, equivalent to 1.48 t y^{-1} while the residual treated biomass, equal to 1.62 kg h^{-1}, is further valorised as biofertilizer. Therefore, the addition of the mixotrophic and downstream processing stages broadens the valorisation pathway of the original SCW stream by enabling the recovery of both additional biomass and a higher-value product.

From an energy standpoint, the sequential configuration also introduces additional utility requirements associated with artificial illumination and downstream processing. In particular, the installed electrical demand of the lighting system is equal to 9 kW. Although this increases the

operating burden of the process, it also supports the production of C-phycocyanin, which plays a key role in the economic performance of the configuration.

Overall, the sequential configuration allows a more extensive valorisation of SCW than the standalone heterotrophic case, since the outlet stream from the first stage is no longer treated simply as a residual liquid stream but as an additional resource for product recovery.

The corresponding process flow diagram is presented in Chapter 2 (Figure 2.11), while Table 4.3 summarises the main stream flow rates and compositions obtained from the simulation.

Table 4.3. *Volumetric flow rates, elemental concentrations, and biomass flow rates of the streams in the sequential heterotrophic and mixotrophic small-scale cultivation process for the second part.*

Line no. stream component	***Volumetric flow [m^3/h]***	***Mass flow [kg/h]***	***C [kg/m^3]***	***N [kg/m^3]***	***P [kg/m^3]***	***Biomass [kg/h]***	***C-P (kg/h)***
8 Heterotrophic effluent	0.13	130	11.27	0.11	0.03	-	-
9 PBR feed stream	0.63	630	2.50	0.38	0.03	-	-
10 Nutrient supplementation stream	-	1.06	-	-	-	-	-
11 PBR outlet stream	0.63	630	0.20	0.04	0.01	1.80	-
12 S-102 clarified liquid stream	0.62	620	0.20	0.04	0.01	-	-
13 Purge stream to wastewater treatment	0.36	360	0.20	0.04	0.01	-	-
14 Recycle stream	0.26	260	0.20	0.04	0.01	-	-
15 Make-up water stream	0.23	230	-	-	-	-	-
16 S-102 concentrated biomass stream	0.007	7	0.20	0.04	0.01	1.80	
17 Homogenised biomass slurry	0.007	7	0.20	0.04	0.01	1.80	-
18 Extraction water stream	0.004	4	-	-	-	-	-
19 Post-extraction slurry	0.011	11	0.13	0.03	0.006	1.62	0.18
20 Residual biomass stream	0.007	7	0.13	0.03	0.006	1.62	-
21 C-phycocyanin-rich extract	0.004	4	0.13	0.03	0.006	-	0.18
22 After MF-101 stream	0.003	3	-	-	-	-	0.18
23 After UF-101 stream	0.001	1	-	-	-	-	0.18
24 Final C-phycocyanin product	-	-	-	-	-	-	0.18

4.3.2 Economic performance and feasibility

The estimated CAPEX and OPEX of the small-scale sequential heterotrophic and mixotrophic scenario are equal to 0.36 M€ and 0.62 M€, respectively. Compared with the heterotrophic small-scale scenario, the addition of the mixotrophic cultivation and downstream recovery sections causes only a limited increase in CAPEX, but a much more pronounced rise in OPEX. This increase is mainly associated with the electricity demand for artificial illumination and with the additional operating requirements of homogenisation, membrane filtration, and freeze-drying. However, the sequential configuration also leads to a substantial increase in revenues, which rise from 205,471.52 € y^{-1} to 932,103.68 € y^{-1}, corresponding to an increase of approximately 354%. A detailed breakdown of the cost items is reported in Appendix D.1, while the annual cash-flow components are provided in Appendix D.2.

The discounted cash-flow profile of the sequential configuration is shown in Figure 4.3.

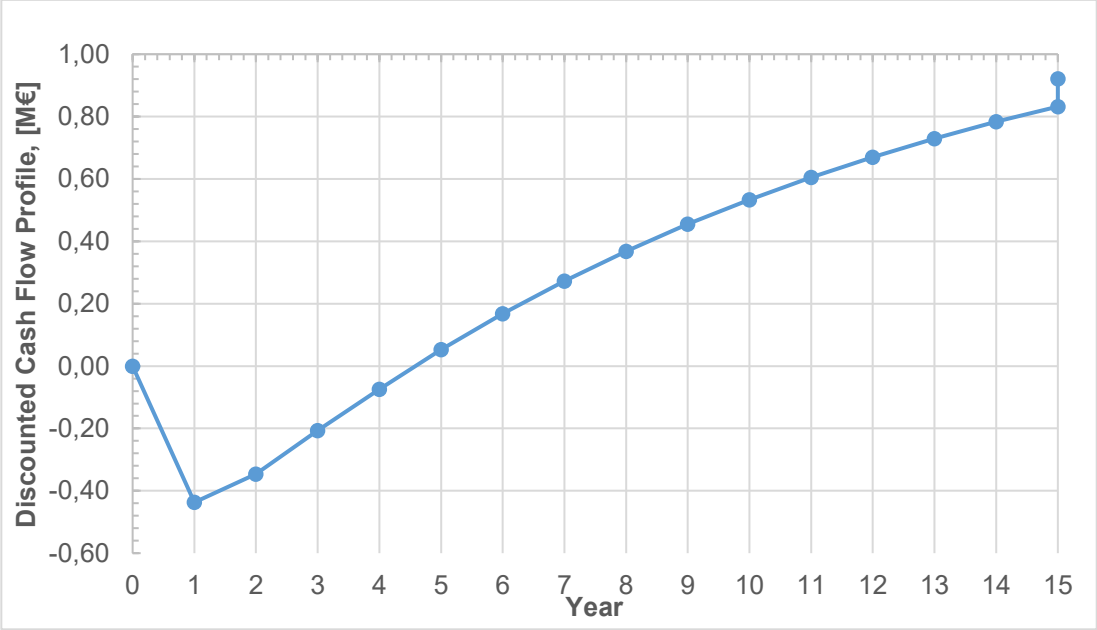

Figure 4.3. *Discounted cash-flow profile over the project lifetime for the sequential heterotrophic and mixotrophic small-scale scenario.*

The scenario yields an NPV of 0.83 M€, and the discounted payback period is equal to 5.46 years. These results indicate that the introduction of the mixotrophic stage and of C-phycocyanin recovery substantially improves the economic performance of the small-scale process. Although the sequential configuration is more expensive to operate than the just heterotrophic scenario, the additional value generated through pigment recovery is sufficient to offset this increase and make the overall process economically attractive.

From a broader perspective, this result confirms that the economic weakness of the small-scale heterotrophic scenario can be overcome by extending the valorisation strategy beyond biomass

production alone. On this basis, the small-scale sequential heterotrophic and mixotrophic scenario can be regarded as techno-economically feasible under the selected assumptions.

4.3.3 Sensitivity analysis

Although the small-scale sequential heterotrophic and mixotrophic scenario shows a positive economic performance under the base-case assumptions, some of the parameters adopted in the analysis are subject to uncertainty. In particular, the profitability of this configuration depends strongly on assumptions related to operating costs and product yield. For this reason, a sensitivity analysis is carried out in order to assess the robustness of the economic results and to evaluate how variations in selected parameters affect the feasibility of the process. Special attention is given to electricity price and C-phycocyanin content in the biomass, since the first directly affects the operating cost of the mixotrophic and downstream sections, while the second has a direct impact on product revenues. In this way, the analysis makes it possible to determine whether the positive profitability obtained for the sequential configuration remains valid under less favourable assumptions.

4.3.3.1 Electricity price

In the base case analysis, an electricity price of 0.23 €/kWh is adopted (Eurostat, 2025). Since electricity prices for industrial users may vary significantly depending on annual consumption level and market conditions, a sensitivity analysis is carried out by considering values between 0.17 and 0.31 €/kWh. The lower bound represents a more favourable condition, whereas the upper bound reflects the higher electricity prices observed in Italy during the energy crisis period (CEIC Data, 2025). This analysis is particularly relevant because artificial illumination is a key element of the integrated small-scale process and therefore contributes significantly to electricity consumption.

Figure 4.4 shows the cumulative discounted cash-flow profiles obtained under the different electricity price scenarios considered in the sensitivity analysis.

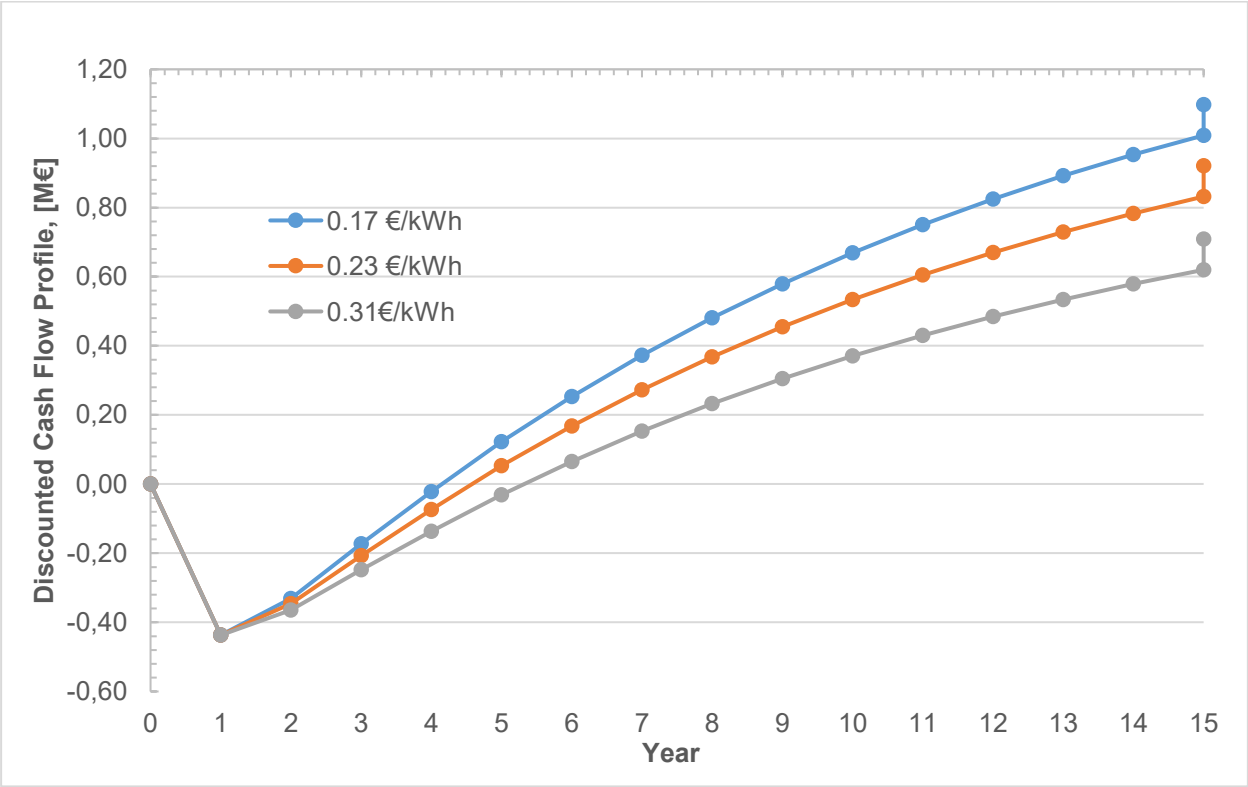

Figure 4.4. *Cumulative discounted cash-flow profiles for different electricity price scenarios considered in the sensitivity analysis.*

As shown in Figure 4.4, lower electricity prices improve the economic performance of the process, although the overall effect remains moderate. In the base case, corresponding to an electricity price of 0.23 € kWh^{-1}, the final discounted cash flow at the end of the project lifetime is about 0.83 M€. When the electricity price is reduced to 0.17 € kWh^{-1}, this value increases to about 1.01 M€, corresponding to an improvement of approximately 0.18 M€, or about 21.7%, relative to the base case. By contrast, when the electricity price is increased to 0.31 € kWh^{-1}, the final discounted cash flow decreases to about 0.61 M€, which is about 0.22 M€, or approximately 26.5%, lower than in the base case. Therefore, electricity cost has a noticeable effect on profitability, but the process remains economically feasible throughout the analysed range.

4.3.3.2 C-phycocyanin content

As already mentioned, the C-phycocyanin content is assumed to be equal to 10.1% w/w of biomass, according to Abiusi et al. (2022). Nevertheless, this value may vary depending on the cultivation conditions, and complete recovery of the pigment during downstream processing cannot be guaranteed. Therefore, a sensitivity analysis is performed in order to assess the impact of different C-phycocyanin contents on the economic performance of the process.

As shown in Figure 4.5, the profitability of the sequential configuration is highly sensitive to this parameter. At the lowest value considered (5% w/w), the cumulative discounted cash flow remains negative over the entire project lifetime, reaching a final value of approximately −0.45 M€. A negative result is also obtained at 6% w/w, for which the final discounted cash flow is still around −0.20 M€. When the C-phycocyanin content is increased to 7% w/w, the process becomes only marginally profitable, with a final discounted cash flow of about 0.06 M€. For higher pigment contents, the economic performance improves progressively, with final discounted cash-flow values of about 0.30 M€ at 8% w/w, 0.56 M€ at 9% w/w, and 0.83 M€ for the base-case assumption of 10.1% w/w.

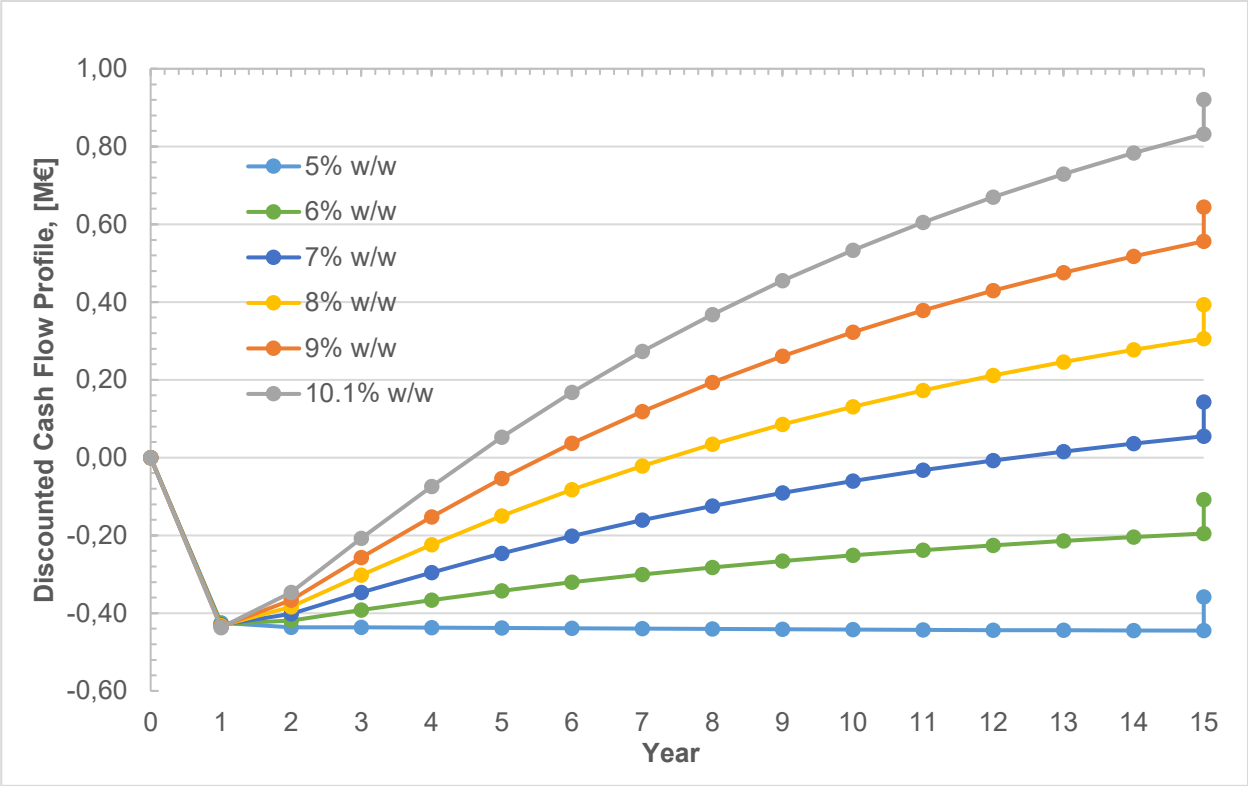

Figure 4.5. *Cumulative discounted cash-flow profiles for the different C-phycocyanin content scenarios considered in the sensitivity analysis.*

Overall, these results indicate that the economic feasibility of the sequential configuration depends strongly on the assumed C-phycocyanin content in the biomass. This confirms that pigment recovery represents the main factor enabling the improved profitability of the integrated process compared with the standalone small-scale heterotrophic scenario.

4.4 Comparative discussion of the three scenarios

This section compares the main economic results of the three scenarios in order to highlight the effect of process scale, configuration, and product portfolio on overall feasibility.

4.4.1 CAPEX and OPEX

The estimated CAPEX and OPEX of the three scenarios are reported in Table 4.4, while the detailed cost breakdown is provided in Appendix D.1.

Table 4.4. *Estimated CAPEX and OPEX of the analysed process scenarios.*

Scenario	*CAPEX*	*OPEX*
Heterotrophic large-scale	12.77 M€	5.37 M€
Heterotrophic small-scale	0.32 M€	0.16 M€
Heterotrophic and mixotrophic small-scale	0.36 M€	0.62 M€

As shown in Table 4.4, the large-scale heterotrophic scenario has the highest CAPEX and OPEX in absolute terms, owing to its much larger treatment capacity. The small-scale heterotrophic scenario shows the lowest costs, reflecting its reduced scale and simpler layout. The small-scale sequential heterotrophic and mixotrophic scenario involves only a limited increase in CAPEX compared with the standalone small-scale heterotrophic case, but a much larger increase in OPEX. This is mainly due to the additional operating requirements associated with artificial illumination and downstream processing. Overall, scale mainly affects absolute capital cost, whereas process complexity has a stronger impact on operating cost.

4.4.2 Comparison of profitability indicators

Table 4.5 compares the main profitability indicators of the three analysed scenarios, namely the net present value (NPV), the discounted payback period (DPB), and the present value ratio (PVR). In addition to NPV and DPB, the PVR is included in order to normalise the economic return with respect to the total capital investment (TCI), thus making the comparison between scenarios of very different scale more straightforward. On this basis, the large-scale heterotrophic scenario remains the most attractive option, as it combines the highest NPV, the shortest discounted payback period, and the highest PVR. By contrast, the small-scale heterotrophic scenario is not economically attractive, since it shows a negative NPV, a negative PVR, and no discounted payback within the project lifetime. The sequential small-scale heterotrophic and mixotrophic scenario shows intermediate performance: although less attractive than the large-scale option, it achieves a positive NPV, a discounted payback period of 5.46 years, and a positive PVR. Overall, these results confirm that scale strongly supports profitability, but also that, at small scale,

economic performance can be significantly improved by adopting a multiproduct strategy based on the recovery of a higher-value product such as C-phycocyanin.

Table 4.5. *Comparison of the main profitability indicators for the analysed scenarios.*

Scenario	***NPV***	***DPB***	***PVR***	***Key result***
Heterotrophic large-scale	65.5 M€	2.62 y	4.17	Most attractive
Heterotrophic small-scale	-0.15 M€	-	-0.38	Not feasible
Heterotrophic and mixotrophic small-scale	0.83 M€	5.46	1.90	Feasible with multiproduct strategy

Conclusions

This thesis investigated the potential valorisation of two dairy industry by-products, milk permeate and second cheese whey (SCW), through the cultivation of the microalga *Galdieria sulphuraria*. The aim was to assess whether these streams could serve as suitable substrates for microalgal growth and, on this basis, to evaluate the technical feasibility and preliminary economic viability of producing biomass and value-added products. Particular attention was given to the comparison between heterotrophic and mixotrophic cultivation, since heterotrophic conditions could favour biomass production, whereas mixotrophic cultivation could broaden the valorisation potential of the process through the synthesis of higher-value compounds such as C-phycocyanin.

The work combined experimental investigation with process design and techno-economic assessment. First, the selected by-products were characterised in terms of carbon, nitrogen, and phosphorus content, and continuous cultivation experiments with *G. sulphuraria* were carried out on milk permeate under heterotrophic and mixotrophic conditions. The experimental results were then used to derive the biomass productivities and elemental yield coefficients required for process calculations. In a second stage, these data were applied to process simulation, mass and energy balances, conceptual plant design, and techno-economic analysis. On this basis, three configurations were evaluated: a large-scale heterotrophic process based on milk permeate, a small-scale heterotrophic process based on SCW, and a sequential small-scale heterotrophic and mixotrophic process based on SCW with C-phycocyanin recovery.

The compositional analysis confirmed that both by-products contained significant amounts of recoverable nutrients and organic matter. Milk permeate showed experimental concentrations of 18.81 ± 0.39 g_C L^{-1}, 0.22 ± 0.01 g_N L^{-1}, and 0.28 ± 0.01 g_P L^{-1}, while SCW showed 20.25 ± 0.46 g_C L^{-1}, 0.44 ± 0.01 g_N L^{-1}, and 0.21 ± 0.01 g_P L^{-1}. These values confirmed that both streams are potentially suitable substrates for microalgal cultivation. The experimental results also showed that *G. sulphuraria* grew successfully on permeate-derived media under acidic conditions. Under heterotrophic operation, continuous cultivation reached a biomass concentration of 5.71 ± 0.11 g L^{-1} and a productivity of 2.83 ± 0.05 g L^{-1} d^{-1}. Under mixotrophic conditions, the best performance among the tested cases was obtained at 6 g L^{-1} and 215 μmol m^{-2} s^{-1}, where biomass concentration reached 2.33 ± 0.24 g L^{-1} and productivity 1.56 ± 0.16 g L^{-1} d^{-1}. Therefore, under the operating conditions investigated in this thesis, heterotrophic cultivation proved to be more effective than mixotrophic cultivation when the main objective was to maximise biomass production.

The main technical conclusion was that milk permeate and SCW could be considered promising substrates for microalgal cultivation, as they contained valuable nutrients that could support the growth of *G. sulphuraria*. The experimental results showed that *G. sulphuraria* was able to grow successfully on permeate-derived media under acidic conditions. Future work would be useful to assess whether the microalga could also grow efficiently when permeate or SCW was used directly, without dilution. Under the operating conditions investigated in this thesis, heterotrophic cultivation proved to be more effective than mixotrophic cultivation for biomass production. In particular, at a nominal influent carbon concentration of 6 g_C L^{-1}, heterotrophic cultivation achieved higher biomass concentration and higher productivity than the corresponding mixotrophic case. These results indicated that heterotrophic cultivation was the most suitable option when the main objective was to maximise biomass production.

From a process-design perspective, the results indicated that both dairy by-products could be converted into microalgal biomass, although the economic outcome depended strongly on scale and process configuration. The large-scale heterotrophic permeate scenario, based on an inlet flow rate of 30 m^3 h^{-1}, produced 453 kg h^{-1} of biomass, corresponding to 3691.95 t y^{-1}, and proved to be the most favourable configuration among those analysed. Its profitability indicators were particularly strong, with an NPV of 65.5 M€ and a discounted payback period of 2.62 years. By contrast, the small-scale heterotrophic SCW scenario produced 3.81 kg h^{-1} of biomass, corresponding to 31.05 t y^{-1}, but remained economically unattractive in its current form, with an NPV of −0.15 M€.

The comparison between the permeate- and SCW-based heterotrophic cases showed that the estimated biomass productivities did not differ substantially. In particular, permeate gave 2.83 g L^{-1} d^{-1}, whereas SCW gave 2.39 g L^{-1} d^{-1}, based on the complementary results available within the laboratory research group. This meant that the better economic performance of the permeate-based case was not mainly explained by higher biological productivity, but rather by the effect of process scale.

The sequential small-scale heterotrophic and mixotrophic scenario showed that the addition of a second stage increased process complexity and operating costs, but also allowed the recovery of a higher-value product. In this case, the mixotrophic section produced 1.80 kg h^{-1} of biomass, corresponding to 14.6 t y^{-1}, together with 0.18 kg h^{-1} of C-phycocyanin, equivalent to 1.48 t y^{-1}. Thanks to this additional product, the economic performance improved significantly compared with the heterotrophic small-scale configuration, reaching an NPV of 0.83 M€ and a discounted payback period of 5.46 years. These results indicated that the small-scale valorisation of SCW was more promising when based on a multiproduct strategy rather than on biomass production alone.

Overall, this thesis showed that the valorisation of dairy by-products through the cultivation of *Galdieria sulphuraria* was technically feasible and could also be economically promising. However, the final outcome depended strongly on the cultivation regime, the selected by-product, the process scale, and the value of the final products. More specifically, the results indicated that heterotrophic cultivation was the most suitable option for maximising biomass productivity, while mixotrophic cultivation became attractive when the recovery of value-added compounds such as C-phycocyanin was included in the process design. From a broader perspective, the work confirmed that microalgal cultivation could represent a viable route for supporting circular economy strategies in the dairy sector, contributing both to waste reduction and to the generation of valuable biobased products.

However, further advancements are necessary. For instance, from an experimental point of view, it would be useful to conduct other cultivation trials on just permeate and SCW with nutrient additions based on the assumptions made in the process design. It would also be beneficial to construct or validate the performance of a pilot-scale unit, which could help confirm the productivity estimates as well as identify any potential scale-up challenges. Furthermore, it would be intriguing to explore the possibility of using the biomass directly in making a bioproduct, instead of treating it solely as a marketable biomass resource, and to determine if such a bioproduct can be used for certain applications in the dairy sector itself. Finally, a more comprehensive environmental analysis, such as a life cycle assessment, can supplement the techno-economic results to provide a more holistic understanding of the process sustainability.

In conclusion, this study showed that *Galdieria sulphuraria* represented a promising platform for the valorisation of dairy waste streams and demonstrated how the combination of experimental investigation and preliminary techno-economic assessment provided a valuable basis for future developments.

Appendix

A Survey for inlet determination

In collaboration with the University of Bologna, a survey is conducted among three dairy plants in order to investigate their production processes and the generation, management, and quantities of dairy by-products. The main objective is to better understand how cheese whey (CW) and second cheese whey (SCW) are generated and managed, and to identify potential opportunities for improving sustainability and resource valorisation. The participating companies request anonymity and confidentiality regarding their identity.

The questionnaire gathers general information on each dairy plant, including production capacity, product types, and processing techniques. Particular attention is paid to the quantity and management of by-products generated during cheese production. The survey shows that all dairy plants produce significant quantities of whey as a primary by-product of cheese manufacture. In many cases, whey is reused internally for ricotta production, whereas SCW is generally not further processed and is instead disposed of or transferred to third parties, such as farms, for use as animal feed. No advanced treatment technologies, such as drying, fermentation, or filtration, are reported for the by-products currently generated. These results indicate that, although part of the whey is already valorised through ricotta production, a considerable fraction of the residual by-products remains underutilised and may therefore represent an opportunity for further exploitation. The quantities of by-products reported by each dairy factory are summarised in Table A.1.

Table A.1. *Survey carried out by the University of Bologna on the quantities of by-products produced by different dairy industries.*

Company	***Whey (Liters/week)***	***Second Cheese Whey (SCW) (Liters/week)***
Dairy factory 1	105600	104400
Dairy factory 2	7000	7000
Dairy factory 3	-	9000

For the milk permeate case study, the supplier is assumed to be a large dairy company. By contrast, for the SCW case study, the by-product is assumed to originate from a small dairy plant. In

addition, one company provides laboratory samples of both permeate and SCW for compositional analysis, and the process design presented in this work is based on these samples.

B Estimation procedure for productivity and light intensity evaluation in mixotrophic conditions

This appendix describes the interpolation procedure adopted only for the specific mixotrophic case considered in the small-scale SCW process. In this configuration, direct experimental data are not available under the exact operating conditions selected for the case study. For this reason, the biomass productivity and the corresponding light intensity are estimated from the available experimental dataset by interpolation and extrapolation. The procedure is therefore applied specifically to the mixotrophic SCW scenario used in the process design and does not represent a general calculation method for all the configurations analysed in this thesis.

B.1 Productivity

Since biomass productivity is not experimentally available for all the operating conditions considered in the process design, the missing values are estimated from the available experimental data through a stepwise interpolation procedure. In particular, the estimation is carried out for the mixotrophic cultivation case with SCW as substrate at an influent carbon concentration of 2.513 $g_C\ L^{-1}$ and a residence time of 2 d.

First, the productivity values obtained under mixotrophic conditions with glucose at τ=1.5 d and inlet carbon concentrations ranging between 1.3 $g_C\ L^{-1}$ and 3 $g_C\ L^{-1}$ are used as the reference dataset, and the value at 2.51 $g_C\ L^{-1}$ is estimated by interpolation. Then, a correction factor is introduced to account for the lower productivity observed when SCW is used instead of glucose. This factor is calculated from the ratio between the productivity obtained with SCW and that obtained with glucose under the same conditions at τ=1.5 and 1.3 $g_C\ L^{-1}$, and resulted equal to 0.66. The interpolated productivity for glucose at 2.513 $g_C\ L^{-1}$ and τ=1.5 d is then multiplied by this factor to estimate the corresponding value for SCW at the same residence time. Finally, this value is converted to τ=2 d by applying a residence-time correction factor derived from the productivity ratios obtained for glucose at τ=2 d and τ=1.5 d (equal to 0.86).

In this way, the final productivity value for SCW at 2.513 $g_C\ L^{-1}$ and τ=2 d is obtained consistently from the available experimental trends.

This part of the study is conducted in collaboration with the laboratory research group.

B.2 Light intensity

In this approach, the average light intensity inside the photobioreactor is estimated by first deriving a biomass-specific light attenuation coefficient from autotrophic data and then applying it to the mixotrophic conditions under analysis. In this approach, light attenuation is characterised by a biomass-specific coefficient, k_I, expressed in $m^2\ g_X^{-1}$, while the overall attenuation in the culture depends on the biomass concentration through the product $C_X\ k_I$. On this basis, the local light intensity along the reactor depth is calculated using the Beer–Lambert law, according to:

$$I_{(Z)} = I_{(0)} e^{-k_1 \cdot C_x \cdot z} \tag{B.1}$$

where $I_{(0)}$ is the incident light intensity, C_X is the biomass concentration, and z is the distance from the illuminated surface.

The average light intensity within the reactor is then obtained by integrating the light profile over the whole PBR depth. Since the profile is evaluated at discrete depth intervals, the integral is approximated numerically by means of the trapezoidal rule. In practice, the area under the $I_{(z)}$ profile is calculated as the sum of trapezoids defined between consecutive depth points, and the average light intensity is finally obtained by dividing this total area by the reactor depth.

C Economic formulas

C.1 Reactor installed cost calculation

$$C_{inst} = C_p^0 \cdot F_{BM}$$

C_{inst}: Installation cost (Bare module cost) [US$];

C_p^0: Purchase cost at year 0, retrieved from tables (Turton et al., 2018) [US$];

F_{BM}: Bare module factor [-].

C.2 Heat exchangers and impellers installed cost calculation

$$C_{inst} = C_p^0 (B_1 + B_2 F_p F_m)$$

C_{inst}: Installation cost (Bare module cost) [US$];

C_p^0: Purchase cost at year 0 [US$];

B_1,B_2 : Constants for Bare Module Factor, retrieved from [36] tables of Appendix A [-];

F_p: Pressure factor [-];

F_m: Material factor [-].

With the purchase cost to be calculated as:

$$log_{10}C_p^0 = C_1 + C_2 log_{10}A + C_3 (log_{10}A)^2$$

Where:

C_1, C_2 and C_3: retrieved from tables (Turton et al., 2018).

C.3 Heating water stream calculations for heat exchangers

Starting from the exchanger's duty:

$$Q = c_p * \dot{m} * \Delta T, \text{ consequently } \dot{m} = \frac{Q}{c_p * \Delta T}$$

Q: heat exchanger's duty, [kW];

c_p: water's specific heat, 4.186 [kJ/kg°C];

$\dot{m}$: cooling water's flowrate [kg/s];

ΔT: temperature difference between inlet and outlet heating water [°C].

Afterwards, the required amount of natural gas to heat the specified quantity of water is calculated.

$$\dot{m}_{NG} = \frac{Q}{\eta * LHV_{NG}}$$

$\dot{m}_{NG}$*:* natural gas mass flowrate [kg/s];

Q: required heat duty [kJ/s];

η: thermal efficiency of the heating system [-];

LHV_{NG}: lower heating value of natural gas [kJ/kg].

C.4 Reactor and other equipment's scale-up costs

$$\frac{CostA}{CostB} = \left(\frac{SizeA}{SizeB}\right)^n$$

The exponent n is taken as 0.6 following the 'six-tenths rule,' a commonly used approximation that reflects average cost-capacity scaling behaviour when detailed process specific data are unavailable.

D Detailed economic results

This appendix reports the detailed economic results of the three process scenarios analysed in this work, namely the heterotrophic large-scale scenario, the heterotrophic small-scale scenario, and Heterotrophic and mixotrophic sequential small-scale scenario.

D.1 Capital and operating cost breakdown

This appendix includes the breakdown of the installed cost of the main equipment items, together with the detailed composition of capital expenditure and annual operating costs used for the economic assessment presented in Chapter 4. The heterotrophic and mixotrophic sequential small-scale scenario is denominated integrated small-scale in this section.

Table D.1 reports the installed cost of the main equipment units considered in each process configuration. Table D.2 summarises the total capital investment for the three scenarios. Table D.3 presents the main annual revenues and operating cost items.

Table D.1. *Installed cost of the main equipment items for the analysed process scenarios.*

Equipment	*Large-scale [€]*	*Small-scale [€]*	*Integrated small-scale [€]*
Heterotrophic reactor(s)	4,351,594.03	122,297.23	122,297.23
Tubular photobioreactor system	-	-	16,528.88
Heat exhanger(s)	239,983.07	4,151.38	4,151.38
Impellers	1,168,383.22	2,809.33	2,809.33
Disk-stack centrifuge S-101	107,267.53	6,139.31	6,139.31
Disk-stack centrifuge S-102	-	-	17,431.00
Disk-stack centrifuge S-103	-	-	1,558.37
High-pressure homogeniser	-	-	1,968.32
Extraction vessel	-	-	2,396.56
Microfiltration and ultrafiltration units	-	-	1,419.89

Freeze-drying unit FD-101	-	-	15,688.24
Artificial illumination system	-	-	11,436.75
Total installed equipment cost	5,867,227.85	135,397.25	203,825.26

Table D.2. *Total capital investment for the analysed process scenarios.*

Investment item	***Large-scale [€]***	***Small-scale [€]***	***Integrated small-scale [€]***
Direct costs (ISBL + OSBL)	9,357,407.02	235,714.37	296,085.94
Indirect costs	1,871,481.40	53,577.97	59,217.19
Fixed capital investment (FCI)	12,769,710.23	321,367.82	355,303.13
Working capital (WC)	1,915,456.53	48,220.17	53,295.47
Start-up capital	1,021,576.82	25,717.43	28,424.25
Total capital investment (TCI)	15,706,743.58	395,405.42	437,022.85

Table D.3. *Annual revenues and main operating cost items for the analysed process scenarios.*

Item	***Large-scale [€/y]***	***Small-scale [€/y]***	***Integrated small-scale [€/y]***
Revenues	24,551,956.50	205,471.52	932,103.68
-Biomass	24,256,111.50	203,992.29	203,992.29
-C-phycocyanin	-	-	680,421.66
- Residual biomass as biofertilizer	-	-	46,210.50
-By-prod. not to wastewater treatment	295,845.00	1,479.23	1,479.23
Raw materials	318,147.24	2,315.16	4,737.29
- Ammonium sulphate	300,147.24	2,162.16	4,218.88
-Sulfuric Acid	18,000	153	153

-Monoammonium phosphate	-	-	365.41
Utilities	2,485,435.29	21,630.2	208,385.28
-Electricity	1,407,601.61	482.18	482.18
- Natural gas + water	799,865.76	19,819.07	19,819.07
- Wastewater treatment	277,967.91	1,328.95	1,328.95
-PBR + harvest utilities	-	-	186,753.28
Labour	1,050,000.00	63,840.00	191,520.00

D.2 Profitability analysis results

This section presents the detailed profitability results of the analysed scenarios. Table D.4 summarises the main annual profitability indicators, including depreciation allowance, profit before tax, income tax, profit after tax, and net cash flow. Figures D.1, D.2 and D.3 report the detailed annual cash-flow components used for the discounted cash-flow analysis of the heterotrophic large-scale scenario, the heterotrophic small-scale scenario, and Heterotrophic and mixotrophic sequential small-scale scenario.

***Table D.4**. Annual profitability and cash-flow results for the analysed scenarios.*

Cash flow item	***Large-scale [€/y]***	***Small-scale [€/y]***	***Integrated small-scale [€/y]***
Depreciation amount	766,182.61	19,288.07	21,318.19
Before tax profit	19,185,969.12	42,199.85	313,831.40
Income tax	8,633,686.10	18,989.93	141,224.13
After tax profit	10,552,283.02	23,209.92	172,607.27
Net cash flow	11,318,465.63	42,497.99	193,925.46

Process Profitability - NPV Analysis | PERMEATE

"Reference time" = end of year zero

Land:	*Investment year 1*	*Investment year 2*	*Investment year 3*	*Working capital*
1.276.971,02 €	15.706.743,58 €	- €	- €	1.915.456,53 €

Salvage	*Taxation rate*	*Interest rate*	*Plant life (years)*
- €	45	10	15

End of year (k)	Capital for depreciation	Capital not for depreciation	Depreciation allowance d_k	Book value $FCI_L - \Sigma d_k$	Revenues R	Total manufact. cost (excl. deprec.) C'	After tax profit $(R-C'-d_k)\times(1-t)+d_k$	Cash flow	Annualised cash flow	Cumulative cash flow
0	- €	- €	- €	- €	- €	- €	- €	- €	- €	- €
1	- 15.706.743,58 €	- €	- €	15.706.743,58 €	- €	- €	- €	- 15.706.743,58 €	- 15.706.743,58 €	- 15.706.743,58 €
2	- €	- €	1.047.116,24 €	14.659.627,34 €	24.551.956,50 €	5.365.987,38 €	11.023.485,32 €	11.023.485,32 €	10.021.350,29 €	- 5.685.393,29 €
3	- €	- €	1.047.116,24 €	13.612.511,10 €	24.551.956,50 €	5.365.987,38 €	11.023.485,32 €	11.023.485,32 €	9.110.318,45 €	3.424.925,16 €
4	- €	- €	1.047.116,24 €	12.565.394,87 €	24.551.956,50 €	5.365.987,38 €	11.023.485,32 €	11.023.485,32 €	8.282.107,68 €	11.707.032,84 €
5	- €	- €	1.047.116,24 €	11.518.278,63 €	24.551.956,50 €	5.365.987,38 €	11.023.485,32 €	11.023.485,32 €	7.529.188,80 €	19.236.221,64 €
6	- €	- €	1.047.116,24 €	10.471.162,39 €	24.551.956,50 €	5.365.987,38 €	11.023.485,32 €	11.023.485,32 €	6.844.717,09 €	26.080.938,73 €
7	- €	- €	1.047.116,24 €	9.424.046,15 €	24.551.956,50 €	5.365.987,38 €	11.023.485,32 €	11.023.485,32 €	6.222.470,08 €	32.303.408,81 €
8	- €	- €	1.047.116,24 €	8.376.929,91 €	24.551.956,50 €	5.365.987,38 €	11.023.485,32 €	11.023.485,32 €	5.656.790,98 €	37.960.199,80 €
9	- €	- €	1.047.116,24 €	7.329.813,67 €	24.551.956,50 €	5.365.987,38 €	11.023.485,32 €	11.023.485,32 €	5.142.537,26 €	43.102.737,06 €
10	- €	- €	1.047.116,24 €	6.282.697,43 €	24.551.956,50 €	5.365.987,38 €	11.023.485,32 €	11.023.485,32 €	4.675.033,87 €	47.777.770,93 €
11	- €	- €	1.047.116,24 €	5.235.581,19 €	24.551.956,50 €	5.365.987,38 €	11.023.485,32 €	11.023.485,32 €	4.250.030,79 €	52.027.801,72 €
12	- €	- €	1.047.116,24 €	4.188.464,96 €	24.551.956,50 €	5.365.987,38 €	11.023.485,32 €	11.023.485,32 €	3.863.664,36 €	55.891.466,08 €
13	- €	- €	1.047.116,24 €	3.141.348,72 €	24.551.956,50 €	5.365.987,38 €	11.023.485,32 €	11.023.485,32 €	3.512.422,14 €	59.403.888,22 €
14	- €	- €	1.047.116,24 €	2.094.232,48 €	24.551.956,50 €	5.365.987,38 €	11.023.485,32 €	11.023.485,32 €	3.193.111,04 €	62.596.999,26 €
15	- €	- €	1.047.116,24 €	1.047.116,24 €	24.551.956,50 €	5.365.987,38 €	11.023.485,32 €	11.023.485,32 €	2.902.828,22 €	65.499.827,48 €
15										68.692.255,03 €

Figure D.1. *Annual cash-flow components used for the profitability analysis of large-scale scenario.*

Process Profitability - NPV Analysis | **SCW Second cheese whey**

"Reference time" = end of year zero

Land:	*Investment year 1*	*Investment year 2*	*Investment year 3*	*Working capital*
32.146,78 €	395.405,42 €	- €	- €	48.220,17 €

Salvage	*Taxation rate*	*Interest rate*	*Plant life (years)*
- €	45	10	15

End of year (k)	Capital for depreciation	Capital not for depreciation	Depreciation allowance d_k	Book value $FCI_L - \Sigma d_k$	Revenues R	Total manufact. cost (excl. deprec.) C'	After tax profit $(R-C'-d_k)\times(1-t)+d_k$	Cash flow	Annualised cash flow	Cumulative cash flow
0	- €	- €	- €	- €	- €	- €	- €	- €	- €	- €
1	- 395.405,42 €	- €	- €	395.405,42 €	- €	- €	- €	- 395.405,42 €	- 395.405,42 €	- 395.405,42 €
2	- €	- €	26.360,36 €	395.405,42 €	123.282,91 €	106.126,59 €	21.298,14 €	21.298,14 €	19.361,95 €	- 376.043,48 €
3	- €	- €	26.360,36 €	395.405,42 €	184.924,36 €	146.944,50 €	32.751,09 €	32.751,09 €	27.067,01 €	- 348.976,46 €
4	- €	- €	26.360,36 €	369.045,06 €	195.197,94 €	155.108,09 €	33.911,58 €	33.911,58 €	25.478,27 €	- 323.498,19 €
5	- €	- €	26.360,36 €	342.684,70 €	205.471,52 €	163.271,67 €	35.072,08 €	35.072,08 €	23.954,70 €	- 299.543,49 €
6	- €	- €	26.360,36 €	316.324,34 €	205.471,52 €	163.271,67 €	35.072,08 €	35.072,08 €	21.777,00 €	- 277.766,49 €
7	- €	- €	26.360,36 €	289.963,98 €	205.471,52 €	163.271,67 €	35.072,08 €	35.072,08 €	19.797,27 €	- 257.969,21 €
8	- €	- €	26.360,36 €	263.603,62 €	205.471,52 €	163.271,67 €	35.072,08 €	35.072,08 €	17.997,52 €	- 239.971,69 €
9	- €	- €	26.360,36 €	237.243,25 €	205.471,52 €	163.271,67 €	35.072,08 €	35.072,08 €	16.361,38 €	- 223.610,31 €
10	- €	- €	26.360,36 €	210.882,89 €	205.471,52 €	163.271,67 €	35.072,08 €	35.072,08 €	14.873,98 €	- 208.736,32 €
11	- €	- €	26.360,36 €	184.522,53 €	205.471,52 €	163.271,67 €	35.072,08 €	35.072,08 €	13.521,80 €	- 195.214,52 €
12	- €	- €	26.360,36 €	158.162,17 €	205.471,52 €	163.271,67 €	35.072,08 €	35.072,08 €	12.292,55 €	- 182.921,97 €
13	- €	- €	26.360,36 €	131.801,81 €	205.471,52 €	163.271,67 €	35.072,08 €	35.072,08 €	11.175,05 €	- 171.746,92 €
14	- €	- €	26.360,36 €	105.441,45 €	205.471,52 €	163.271,67 €	35.072,08 €	35.072,08 €	10.159,13 €	- 161.587,79 €
15	- €		26.360,36 €	79.081,08 €	205.471,52 €	163.271,67 €	35.072,08 €	35.072,08 €	9.235,57 €	- 152.352,22 €
15										- 71.985,26 €

Figure D.2. *Annual cash-flow components used for the profitability analysis of small-scale scenario.*

Process Profitability - NPV Analysis — **SCW Second cheese whey**

"Reference time" = end of year zero

Land:	*Investment year 1*	*Investment year 2*	*Investment year 3*	*Working capital*
35.530,31 €	437.022,85 €	- €	- €	53.295,47 €

Salvage	*Taxation rate*	*Interest rate*	*Plant life (years)*
- €	45	10	15

End of year (k)	Capital for depreciation	Capital not for depreciation	Depreciation allowance d_k	Book value FCI_L-Σd_k	Revenues R	Total manufact. cost (excl. deprec.) C'	After tax profit $(R\text{-}C'\text{-}d_k)\times(1\text{-}t)+d_k$	Cash flow	Annualised cash flow	Cumulative cash flow
0	- €	- €	- €	- €	- €	- €	- €	- €	- €	- €
1	- 437.022,85 €	- €	- €	437.022,85 €	- €	- €	- €	- 437.022,85 €	- 437.022,85 €	- 437.022,85 €
2	- €	- €	29.134,86 €	437.022,85 €	559.262,21 €	401.876,98 €	99.672,56 €	99.672,56 €	90.611,42 €	- 346.411,43 €
3	- €	- €	29.134,86 €	437.022,85 €	838.893,31 €	556.445,05 €	168.457,23 €	168.457,23 €	139.220,85 €	- 207.190,58 €
4	- €	- €	29.134,86 €	407.887,99 €	885.498,50 €	587.358,67 €	177.087,59 €	177.087,59 €	133.048,53 €	- 74.142,06 €
5	- €	- €	29.134,86 €	378.753,14 €	932.103,68 €	618.272,28 €	185.717,95 €	185.717,95 €	126.847,86 €	52.705,81 €
6	- €	- €	29.134,86 €	349.618,28 €	932.103,68 €	618.272,28 €	185.717,95 €	185.717,95 €	115.316,24 €	168.022,04 €
7	- €	- €	29.134,86 €	320.483,42 €	932.103,68 €	618.272,28 €	185.717,95 €	185.717,95 €	104.832,94 €	272.854,99 €
8	- €	- €	29.134,86 €	291.348,57 €	932.103,68 €	618.272,28 €	185.717,95 €	185.717,95 €	95.302,68 €	368.157,66 €
9	- €	- €	29.134,86 €	262.213,71 €	932.103,68 €	618.272,28 €	185.717,95 €	185.717,95 €	86.638,80 €	454.796,46 €
10	- €	- €	29.134,86 €	233.078,85 €	932.103,68 €	618.272,28 €	185.717,95 €	185.717,95 €	78.762,54 €	533.559,00 €
11	- €	- €	29.134,86 €	203.944,00 €	932.103,68 €	618.272,28 €	185.717,95 €	185.717,95 €	71.602,31 €	605.161,31 €
12	- €	- €	29.134,86 €	174.809,14 €	932.103,68 €	618.272,28 €	185.717,95 €	185.717,95 €	65.093,01 €	670.254,32 €
13	- €	- €	29.134,86 €	145.674,28 €	932.103,68 €	618.272,28 €	185.717,95 €	185.717,95 €	59.175,46 €	729.429,79 €
14	- €	- €	29.134,86 €	116.539,43 €	932.103,68 €	618.272,28 €	185.717,95 €	185.717,95 €	53.795,88 €	783.225,66 €
15	- €		29.134,86 €	87.404,57 €	932.103,68 €	618.272,28 €	185.717,95 €	185.717,95 €	48.905,34 €	832.131,01 €
15										920.956,79 €

Figure D.3. *Annual cash-flow components used for the profitability analysis of integrated small-scale scenario.*

Glossary

ATP: Adenosine Triphosphate

BAT: Best Available Techniques

BOD: Biochemical Oxygen Demand

CAPEX: Capital Expenditure

CEPCI: Chemical Engineering Plant Cost Index

COD: Chemical Oxygen Demand

CSTR: Continuous Stirred-Tank Reactor

CW: Cheese Whey

DPB: Discounted Payback Period

DW: Dry Weight

EU: European Union

FCI: Fixed Capital Investment

HTST: High-Temperature Short-Time

IC: Inorganic Carbon

IED: Industrial Emissions Directive

ISBL: Inside Battery Limits

LTLT: Low-Temperature Long-Time

LED: Light-Emitting Diode

MAM: Modified Allen Medium

MAP: Monoammonium Phosphate

MF: Microfiltration

NO_X: Nitrogen Oxides

SO_X: Sulphur Oxides

NPV: Net Present Value

OD: Optical Density

OPEX: Operating Expenditure

OSBL: Outside Battery Limits

PBR: Photobioreactor

PHA: Polyhydroxyalkanoates

REEs: Rare Earth Elements

SCW: Second Cheese Whey

TC: Total Carbon

TCI: Total Capital Investment

TN: Total Nitrogen

TOC: Total Organic Carbon

TP: Total Phosphorus

TSS: Total Suspended Solids

UF: Ultrafiltration

WC: Working Capital

List of symbols

[A−]: Molar concentration of the conjugate base in the Henderson–Hasselbalch equation [mol L^{-1}]

[HA]: Molar concentration of the undissociated acid in the Henderson–Hasselbalch equation [mol L^{-1}]

A: Absorbance [–]

Abs_{705}: Absorbance at 705 nm [–]

A_{HX}: Heat transfer area of the heat exchanger [m^2]

A_w: Heat transfer area through the reactor wall [m^2]

B_1, B_2: Constants for the bare module factor [–]

C: Sample concentration in the Beer–Lambert law [g L^{-1}]

C_1, C_2 and C_3: Purchase cost factors used in the equipment cost correlation [–]

C_{BIO}: Carbon concentration in the reactor sample, including biomass-associated and dissolved organic carbon [g L^{-1}]

C_{FIL}: Carbon concentration in the filtrate [g L^{-1}]

C_{IN}: Carbon concentration in the inlet culture medium [g L^{-1}]

C_{inst}: Installed cost (bare module cost) [US$]

C_p^0: Purchase cost at the reference year [US$]

C_p: Specific heat capacity of water [kJ kg^{-1} $°C^{-1}$]

C_x: Biomass concentration [g L^{-1}]

D: Diameter of the reactor [m]

D_t: Tube diameter of the photobioreactor [m]

F_{BM}: Bare module factor [–]

F_{ds}: Mass fraction of dry biomass in the recovered wet paste [–]

F_m: Material factor [–]

F_p: Pressure factor [–]

h_0: External heat transfer coefficient [W m^{-2} K^{-1}]

h_i: Internal heat transfer coefficient [W m^{-2} K^{-1}]

I(0): Incident light intensity at the illuminated surface [µmol m^{-2} s^{-1}]

I(center): Light intensity at the centre of the photobioreactor tube [µmol m^{-2} s^{-1}]

I(z): Local light intensity at a distance z from the illuminated surface [µmol m^{-2} s^{-1}]

k_I: Biomass-specific light attenuation coefficient [$m^2\ g_X^{-1}$]

k_{316L}: Thermal conductivity of stainless steel 316L [$W\ m^{-1}\ K^{-1}$]

K_a: Symbol used in the thesis for the acid dissociation constant and, in a different context, for the biomass absorption coefficient in the light attenuation equation [$m^2\ g_X^{-1}$]

l: Optical path length [cm]

LHV_{NG}: Lower heating value of natural gas [$kJ\ kg^{-1}$]

$\dot{m}$: Mass flow rate [$kg\ s^{-1}$]

$\dot{m}_{NG}$: Natural gas mass flow rate [$kg\ s^{-1}$]

n: Lifetime of the plant in the economic analysis; the same symbol is also used as the cost-capacity exponent in scale-up correlations [years]

N_{BIO}: Nitrogen concentration in the reactor sample [$g\ L^{-1}$]

N_{FIL}: Nitrogen concentration in the filtrate [$g\ L^{-1}$]

N_{IN}: Nitrogen concentration in the inlet culture medium [$g\ L^{-1}$]

P: Operating pressure [bar]

P_{IN}: Phosphorus concentration in the inlet stream [$g\ L^{-1}$]

P_{OUT}: Phosphorus concentration in the outlet stream [$g\ L^{-1}$]

pH: Measure of acidity/alkalinity [–]

P_X: Biomass productivity [$g\ L^{-1}\ d^{-1}$]

pK_a: Negative logarithm of the acid dissociation constant [–]

Q: Volumetric flow rate in the residence-time equation; the same symbol is also used in Appendix C for heat exchanger duty [$L\ d^{-1}$ or kW]

$\dot{Q}_{HX}$: Heat supplied by the heat exchanger [kW]

$\dot{Q}_{shaft}$: Mechanical energy input provided by agitation [kW]

$\dot{Q}_{wall}$: Heat dissipated through the reactor wall [kW]

R: Revenues from the sale of by-products or products [€ $year^{-1}$]

R^2: Coefficient of determination [–]

r: Discount rate [%]

S: Maximum allowable stress [bar]

T: Reactor or process temperature [°C]

T_{amb}: Ambient temperature [°C]

T_{IN}: Inlet stream temperature [°C]

t_{min}: Minimum allowable vessel thickness [m]

U_{HX}: Overall heat transfer coefficient of the heat exchanger [$W\ m^{-2}\ K^{-1}$]

U_w: Overall heat transfer coefficient through the reactor wall [$W\ m^{-2}\ K^{-1}$]

V: Reactor volume [L or m^3]

$\dot{V}$: Volumetric flow rate used in the energy balance [$m^3\ s^{-1}$ or $m^3\ h^{-1}$]

X_C: Overall carbon conversion [–]

$Y_{C/X}$: Carbon-in-biomass yield coefficient [$g_C\ g_X^{-1}$]

$Y_{CO2/X}$: Yield coefficient of carbon converted into carbon dioxide per unit biomass formed [$g_C\ g_X^{-1}$]

$Y_{N/X}$: Nitrogen-in-biomass yield coefficient [$g_N\ g_X^{-1}$]

$Y_{P/X}$: Phosphorus-in-biomass yield coefficient [$g_P\ g_X^{-1}$]

z: Distance from the illuminated surface [m]

δ: Wall thickness [m]

ΔT: Temperature difference between inlet and outlet heating water [°C]

$\Delta T_{lm,HX}$: Logarithmic mean temperature difference in the heat exchanger [°C]

ε: Attenuation coefficient in the Beer–Lambert law [$L\ g^{-1}\ cm^{-1}$]

η: Thermal efficiency of the heating system [–]

ρ: Density [$kg\ m^{-3}$]

τ: Residence time [d]

References

Abiusi, F., P. Moñino Fernández, S. Canziani, M. Janssen, R. H. Wijffels e M. Barbosa (2022). Mixotrophic Cultivation of *Galdieria sulphuraria* for C-Phycocyanin and Protein Production. Algal Research, 61, 102603. https://doi.org/10.1016/j.algal.2021.102603

Akzarkhanam, A. R., D. Cysneiros, A. Chatzifragkou, K. A. G. Karatzas e M. Kennedy (2025). From Waste to Resource: A Review on Advancing Whey Permeate Valorization Through Anaerobic Digestion. International Journal of Dairy Technology. https://doi.org/10.1016/j.jclepro.2025.127695

Albenzio, M. e A. Santillo (2025). Ricotta Cheese. In: Dairy Foods Processing: Methods and Protocols (A. G. da Cruz, Ed.), Springer, p. 139. https://doi.org/10.1007/978-1-0716-4144-6_10

Allakhverdiev, S. I., V. D. Kreslavski, V. V. Klimov, D. A. Los, R. Carpentier e P. Mohanty (2008). Heat Stress: An Overview of Molecular Responses in Photosynthesis. Photosynthesis Research, 98(1–3), 541–550. https://doi.org/10.1007/s11120-008-9331-0

Allen, M. M. (1968). Simple Conditions for Growth of Unicellular Blue-Green Algae on Plates. Journal of Phycology, 4(1), 1–4. https://doi.org/10.1111/j.1529-8817.1968.tb04667.x

Arezzo Parcheggi (2025). Quali Sono i Costi dell'Acqua al Metro Cubo in Italia. https://arezzoparcheggi.it/quali-sono-i-costi-dellacqua-al-metro-cubo-in-italia/

Bandler, D. K. (2025). Cheese Making. Britannica, Encyclopaedia Britannica, Inc. Accessed November 15, 2025. https://www.britannica.com/topic/cheese-making

Banihashemi, F., A. F. M. Ibrahim, S. Deng e J. Y. S. Lin (2023). Pyrolysis and Gasification Characteristics of *Galdieria sulphuraria* Microalgae. BioEnergy Research, 16, 616–621. https://doi.org/10.1007/s12155-022-10449-7

Barba, F. J. (2021). An Integrated Approach for the Valorization of Cheese Whey. Foods, 10(3), 564. https://doi.org/10.3390/foods10030564

Benner, P., L. Meier, A. Pfeffer, K. Krüger, J. E. Orepeza Vargas e D. Weuster-Botz (2022). Lab-Scale Photobioreactor Systems: Principles, Applications, and Scalability. Bioprocess and Biosystems Engineering, 45, 791–813. https://doi.org/10.1007/s00449-022-02711-1

Bezzo, F. (2024). Process Design Course: Class Slides. University of Padova.

Borowitzka, M. A. (2013). High-Value Products from Microalgae — Their Development and Commercialisation. Journal of Applied Phycology, 25(3), 743–756. https://doi.org/10.1007/s10811-013-9983-9

Brennan, L. e P. Owende (2010). Biofuels from Microalgae—A Review of Technologies for Production, Processing, and Extractions of Biofuels and Co-Products. Renewable and Sustainable Energy Reviews, 14(2), 557–577. https://doi.org/10.1016/j.rser.2009.10.009

Buchanan, D., W. Martindale, E. Romeih e E. Hebishy (2023). Recent Advances in Whey Processing and Valorisation: Technological and Environmental Perspectives. International Journal of Dairy Technology, 76(2), 291–312.

Bumbak, F., S. Cook, V. Zachleder, S. Hauser e K. Kovar (2011). Best Practices in Heterotrophic High-Cell-Density Microalgal Processes: Achievements, Potential and Possible Limitations. 1, 31–46. https://doi.org/10.1007/s00253-011-3311-6

Bylund, G. (1995). Dairy Processing Handbook. Tetra Pak Processing Systems AB, Lund (Sweden).

Caporgno, M. P. e A. Mathys (2018). Trends in Microalgae Incorporation into Innovative Food Products with Potential Health Benefits. Frontiers in Nutrition, 5, 58. https://doi.org/10.3389/fnut.2018.00058

Carvalho, A. P., S. O. Silva, J. M. Baptista e F. X. Malcata (2011). Light Requirements in Microalgal Photobioreactors: An Overview of Biophotonic Aspects. Applied Microbiology and Biotechnology, 89(5), 1275–1288. https://doi.org/10.1007/s00253-010-3047-8

CEIC Data (2025). Italy Electricity Price: Non-Household Consumers. Retrieved April 2, 2026, from CEIC Data website. https://www.ceicdata.com/en/italy/electricity-price-nonhousehold-consumers

Chandola, G., M. Muthuraj, S. Mandal, V. P. S. e B. Bhunia (2026). Engineering Advances in Tubular Photobioreactors for Microalgae Cultivation: Design, Scale-Up, Optimization, and Operational Challenges. Renewable and Sustainable Energy Reviews, 231, 116776. https://doi.org/10.1016/j.rser.2026.116776

Chanquia, S. N., G. Vernet e S. Kara (2021). Photobioreactors for Cultivation and Synthesis: Specifications, Challenges, and Perspectives. Engineering in Life Sciences, 21(11–12), 712–724. https://doi.org/10.1002/elsc.202100044

Chemical Engineering (2025). 2025 CEPCI Updates: January (Prelim.) and December 2024 (Final). https://www.chemengonline.com/2025-cepci-updates-january-prelim-and-december-2024-final/

Chemanalyst (2025). Ammonium Sulphate Price Trend and Forecast. https://www.chemanalyst.com/Pricing-data/ammonium-sulphate-64

Chen, Q., S. Li, H. Xiong e Q. Zhao (2022). Effect of Different Extraction Methods on Physicochemical Characteristics and Antioxidant Activity of C-Phycocyanin from Dry Biomass of Arthrospira platensis. Foods, 11(9), 1296. https://doi.org/10.3390/foods11091296

Chiklakhan, R., N. Chirasuwan, V. Loha, S. Tid e B. Bunnag (2018). Stepwise Extraction of High-Value Chemicals from Arthrospira (Spirulina) and an Economic Feasibility Study. Biotechnology Reports, 20, e00280. https://doi.org/10.1016/j.btre.2018.e00280

Chisti, Y. (2007). Biodiesel from Microalgae. Biotechnology Advances, 25(3), 294–306. https://doi.org/10.1016/j.biotechadv.2007.02.001

Coelho, M. C., F. X. Malcata e C. C. G. Silva (2022). Lactic Acid Bacteria in Raw-Milk Cheeses: From Starter Cultures to Probiotic Functions. 15, 2276. https://doi.org/10.3390/foods11152276

Cozzolino, S., P. Caputo, O. De Castro, A. Moretti e G. Pinto (2000). Molecular Variation in *Galdieria sulphuraria* (Galdieri) Merola and Its Bearing on Taxonomy. Hydrobiologia, 433(1–3), 145–150. https://doi.org/10.1023/A:1004066823140

Culture Collection of Algae at Göttingen University (SAG) (1992). *Galdieria sulphuraria* SAG 21.92. https://sagdb.uni-goettingen.de/detailedList.php?str_number=21.92

Curien, G., D. Lagrange, S. Brugière, D. Da Silva, J. Decelle, A. Falciatore, G. Finazzi et al. (2021). Mixotrophic Growth of the Extremophile *Galdieria sulphuraria* Reveals the Flexibility of Its Carbon Assimilation Metabolism. New Phytologist, 231(1), 326–338. https://doi.org/10.1111/nph.17359

Davis, R., A. Aden e P. T. Pienkos (2011). Techno-Economic Analysis of Autotrophic Microalgae for Fuel Production. Applied Energy, 88(10), 3524–3531. https://doi.org/10.1016/j.apenergy.2011.04.018

Del Campo, J. A., M. García-González e M. G. Guerrero (2007). Outdoor Cultivation of Microalgae for Carotenoid Production: Current State and Perspectives. Applied Microbiology and Biotechnology, 74(6), 1163–1174. https://doi.org/10.1007/s00253-007-0844-9

Eilertsen, H. C., G. K. Eriksen, J.-S. Bergum, J. Strømholt, E. Elvevoll, K.-E. Eilertsen, E. S. Heimstad, I. H. Giæver, L. Israelsen e G.-H. Wintervoll (2022). Mass Cultivation of Microalgae: I. Experiences with Vertical Column Airlift Photobioreactors, Diatoms and CO_2 Sequestration. Applied Sciences, 12(6), 3082. https://doi.org/10.3390/app12063082

Eurostat (2025). Electricity Price Statistics. European Commission. https://ec.europa.eu/eurostat/statistics-explained/index.php?title=Electricity_price_statistics

European Commission, Joint Research Centre (2019). Best Available Techniques (BAT) Reference Document for the Food, Drink and Milk Industries. Industrial Emissions Directive 2010/75/EU (Integrated Pollution Prevention and Control). Publications Office of the European Union, Luxembourg.

European Parliament and Council of the European Union (2010). Directive 2010/75/EU of the European Parliament and of the Council of 24 November 2010 on Industrial Emissions (Integrated Pollution Prevention and Control). Official Journal of the European Union, L334, 17-119. Publications Office of the European Union, Luxembourg.

Fancello, F., G. Zara, F. Hatami, E. A. Scano e I. Mannazzu (2024). Unlocking the Potential of Second Cheese Whey: A Comprehensive Review on Valorisation Strategies. Reviews in Environmental Science and Bio/Technology, 23, 411–441. https://doi.org/10.1007/s11157-024-09687-2

Fasaei, F., J. H. Bitter, P. M. Slegers e A. J. B. van Boxtel (2018). Techno-Economic Evaluation of Microalgae Harvesting and Dewatering Systems. Algal Research, 31, 347–362. https://doi.org/10.1016/j.algal.2017.11.038

Ferro, L. (2019). Wastewater Treatment and Biomass Generation by Nordic Microalgae: Growth in Subarctic Climate and Microbial Interactions. Doctoral Dissertation, Umeå University. https://www.researchgate.net/publication/331487610_Wastewater_treatment_and_biomass_generation_by_Nordic_microalgae_Growth_in_subarctic_climate_and_microbial_interactions

Figueroa Pires, A., N. Garcia Marnotes, O. Díaz Rubio, A. Cobos Garcia e C. Dias Pereira (2021). Dairy By-Products: A Review on the Valorization of Whey and Second Cheese Whey. Foods, 10(5), 1067. MDPI. https://doi.org/10.3390/foods10051067

Foegeding, E. A., P. Luck e B. Vardhanabhuti (2011). Whey Protein Products. In: Encyclopedia of Dairy Sciences (2nd ed.), Elsevier.

Food and Agriculture Organization of the United Nations (FAO) (2025). Guide to Good Dairy Farming Practice. FAO Animal Production and Health Guidelines No. 8. FAO. https://openknowledge.fao.org/server/api/core/bitstreams/eb6570d4-c820-428b-bdee-fca1aa2d430f/content

Fox, P. F. e P. L. H. McSweeney (2002). Pasteurized Milk. In: Encyclopedia of Dairy Sciences (H. Roginski, J. W. Fuquay e P. F. Fox, Eds.), Academic Press. https://www.sciencedirect.com/topics/food-science/pasteurized-milk

Gaber, K., C. Rösch e N. Biondi (2022). Life Cycle Assessment of Total Fatty Acid (TFA) Production from Microalgae Nannochloropsis oceanica at Different Sites and Under Different Sustainability Scenarios. BioEnergy Research, 15, 1595–1615. https://doi.org/10.1007/s12155-021-10279-z

Geider, R. J. e J. La Roche (2002). Redfield Revisited: Variability of C:N:P in Marine Microalgae and Its Biochemical Basis. European Journal of Phycology, 37(1), 1–17. https://doi.org/10.1017/S0967026201003456

Glass, L. e T. I. Hedrick (1977). Nutritional Composition of Sweet- and Acid-Type Dry Wheys. I. Major Factors Including Amino Acids. Journal of Dairy Science, 60(2), 185–189. https://doi.org/10.3168/jds.S0022-0302(77)83852-6

GlobalPetrolPrices.com (2026). Italy Natural Gas Prices. https://www.globalpetrolprices.com/Italy/natural_gas_prices/

Goldman, J. C., C. B. Riley e M. R. Dennett (1982). The Effect of pH in Intensive Microalgal Cultures. II. Species Competition. Journal of Experimental Marine Biology and Ecology, 57, 15–24. https://doi.org/10.1016/0022-0981(82)90017-5

Gramegna, G., A. Scortica, V. Scafati, F. Ferella, L. Gurrieri, M. Giovannoni, R. Bassi, F. Sparla, B. Mattei e M. Benedetti (2020). Exploring the Potential of Microalgae in the Recycling of Dairy Wastes. Bioresource Technology Reports, 12, 100604. https://doi.org/10.1016/j.biteb.2020.100604

Gross, W. e C. Schnarrenberger (1995). Heterotrophic Growth of Two Strains of the Acido-Thermophilic Red Alga *Galdieria sulphuraria*. Plant and Cell Physiology, 36(4), 633–638. https://doi.org/10.1093/oxfordjournals.pcp.a078803

Guilherme, J.-B., C. Couteau e L. Coiffard (2017). Applications for Marine Resources in Cosmetics. Cosmetics, 4(3), 35. https://doi.org/10.3390/cosmetics4030035

Haifa Group (2026). Mono Ammonium Phosphate Fertilizer 12-61-0 - Haifa MAP™. https://www.haifa-group.com/haifa-map%E2%84%A2-mono-ammonium-phosphate-12-61-0

Huang, Q., F. Jiang, L. Wang e C. Yang (2017). Design of Photobioreactors for Mass Cultivation of Photosynthetic Organisms. Engineering, 3(3), 318–329. https://doi.org/10.1016/J.ENG.2017.03.020

Innamorati, M., I. Ferrari, D. Marino e M. Ribera d'Alcalà (Eds.) (1990). Metodi nell'Ecologia del Plancton Marino. Nova Thalassia, Vol. 11, Edizioni LINT.

Jaeschke, D. P., I. R. Teixeira, L. D. F. Marczak e G. D. Mercali (2021). Phycocyanin from Spirulina: A Review of Extraction Methods and Stability. Food Research International, 143, 110314. https://doi.org/10.1016/j.foodres.2021.110314

Keymer, P. C., P. A. Lant e S. Pratt (2013). Modelling Microalgal Activity as a Function of Inorganic Carbon Concentration: Accounting for the Impact of pH on the Bicarbonate System. Journal of Applied Phycology.

Kiełczewska, K., O. Brożek, P. Rudkowska, A. Garczewska-Murzyń e M. Smoczyński (2022). The Effects of Full-Stream and Partial High-Pressure Homogenisation on the Properties of Milk Emulsion. International Journal of Food Science & Technology, 57(11), 7167–7174. https://doi.org/10.1111/ijfs.16059

Kim, J., G. Yoo, H. Lee, J. Lim, K. Kim, C. W. Kim, M. S. Park e J.-W. Yang (2013). Methods of Downstream Processing for the Production of Biodiesel from Microalgae. Biotechnology Advances, 31(6), 862–876. https://doi.org/10.1016/j.biotechadv.2013.04.006

Kumar, M., A. Brar, R. Kumari, V. Vivekanand e N. Pareek (2025). Advancements in Photobioreactor Designs for Development of Microalgal Biorefinery Toward Integrated Remediation of Industrial Wastewater and Product Recovery. 3 Biotech, 15, 274. https://doi.org/10.1007/s13205-025-04433-z

Kurniawan, S. B., M. Čížková, A. Ahmad, Y. G. Wibowo, N. S. Mohd Said, H. H. Wan Jusoh, A. Ismail e M. F. Imron (2025). Autotrophic vs. Heterotrophic Microalgae: Juxtaposition of Performances in Treating Organic-Rich Effluent. Desalination and Water Treatment. https://doi.org/10.1016/j.dwt.2025.101159

Lam, M. K. e K. T. Lee (2012). Microalgae Biofuels: A Critical Review of Issues, Problems and the Way Forward. Biotechnology Advances, 30(3), 673–690. https://doi.org/10.1016/j.biotechadv.2011.11.008

Legrand, J., A. Artu e J. Pruvost (2021). A Review on Photobioreactor Design and Modelling for Microalgae Production. Reaction Chemistry & Engineering, 6, 1134–1151. https://doi.org/10.1039/D0RE00450B

Liang, Y., N. Sarkany e Y. Cui (2009). Biomass and Lipid Productivities of Chlorella vulgaris Under Autotrophic, Heterotrophic and Mixotrophic Growth Conditions. Biotechnology Letters, 31(7), 1043–1049. https://doi.org/10.1007/s10529-009-9975-7

Lohrey, C. e V. Kochergin (2012). Biodiesel Production from Microalgae: Co-Location with Sugar Mills, 76–82. https://doi.org/10.1016/j.biortech.2011.12.035

Maltsev, Y., K. Maltseva, M. Kulikovskiy e S. Maltseva (2021). Influence of Light Conditions on Microalgae Growth and Content of Lipids, Carotenoids, and Fatty Acid Composition. Biology, 10(10), 1060. https://doi.org/10.3390/biology10101060

MarkNtel Advisors (2024). Whey Protein Market Growth. https://www.marknteladvisors.com/press-release/whey-protein-market-growth

MarkNtel Advisors (n.d.). Whey Protein Market Size, Share, Growth, and Forecast. https://www.marknteladvisors.com/research-library/whey-protein-market.html

Markou, G., D. Vandamme e K. Muylaert (2014). Microalgal and Cyanobacterial Cultivation: The Supply of Nutrients. Biotechnology Advances, 32(6), 1238–1248. https://doi.org/10.1016/j.watres.2014.07.025

McCarthy, K. S., K. Lopetcharat e M. A. Drake (2017). Milk Fat Threshold Determination and the Effect of Milk Fat Content on Consumer Preference for Fluid Milk. Journal of Dairy Science, 100(3), 1702–1711. https://doi.org/10.3168/jds.2016-11417

McGinn, P. J., K. E. Dickinson, S. Bhatti, J.-C. Frigon, S. R. Guiot e S. J. B. O'Leary (2011). Integration of Microalgae Cultivation with Industrial Waste Remediation for Biofuel and Bioenergy Production: Opportunities and Limitations. Photosynthesis Research, 109(1–3), 231–247. https://doi.org/10.1007/s11120-011-9638-0

Mediboina, M. K., N. M. Holden, S. O'Neill, K. Routledge, B. Morrissey, F. Lawless e F. Murphy (2022). Upscale Fermenter Design for Lactic Acid Production from Cheese Whey Permeate Focusing on Impeller Selection and Energy Optimization. Journal of Food Science and Technology, 59(6), 2263–2273. https://doi.org/10.1007/s13197-021-05239-6

Meyer, H.-P., W. Minas e D. Schmidhalter (2017). Industrial-Scale Fermentation. In: Industrial Biotechnology: Products and Processes (C. Wittmann e J. C. Liao, Eds.), Wiley-VCH Verlag GmbH & Co. KGaA.

Microfluidics (n.d.). M700 Microfluidizer® Processor. https://www.microfluidics-mpt.com/microfluidizers/m700

Minj, S. e S. Anand (2020). Whey Proteins and Its Derivatives: Bioactivity, Functionality, and Current Applications. Dairy, 1(3), 233–258. https://doi.org/10.3390/dairy1030016

Naik, S. N., V. V. Goud, P. K. Rout e A. K. Dalai (2010). Production of First and Second Generation Biofuels: A Comprehensive Review. Renewable and Sustainable Energy Reviews, 14(2), 578–597. https://doi.org/10.1016/j.rser.2009.10.003

Najjar, Y. S. H. e A. Abu-Shamleh (2020). Harvesting of Microalgae by Centrifugation for Biodiesel Production: A Review. Algal Research, 51, 102046. https://doi.org/10.1016/j.algal.2020.102046

Narala, R. R., S. Garg, K. K. Sharma, S. R. Thomas-Hall, M. Deme, Y. Li e P. M. Schenk (2016). Comparison of Microalgae Cultivation in Photobioreactor, Open Raceway Pond, and a Two-Stage Hybrid System. Frontiers in Energy Research, 4, 29. https://doi.org/10.3389/fenrg.2016.00029

New Life Scientific (2024). Microfluidics M700 Microfluidizer Processor 7125-20 Production Scale Homogenizer. eBay listing, November 19, 2024. Retrieved March 27, 2026, from https://www.ebay.com/itm/276720448054

O'Donoghue, L. T. e E. G. Murphy (2023). Nondairy Food Applications of Whey and Milk Permeates: Direct and Indirect Uses. Comprehensive Reviews in Food Science and Food Safety, 22, 2625–2677. https://doi.org/10.1111/1541-4337.13157

Occhipinti, P. S., F. Del Signore, S. Canziani, C. Caggia, V. Mezzanotte e N. Ferrer-Ledo (2023). Mixotrophic and Heterotrophic Growth of *Galdieria sulphuraria* Using Buttermilk as a Carbon Source. Journal of Applied Phycology, 35, 2631–2643. https://doi.org/10.1007/s10811-023-03012-0

Oliveira, D., P. Fox e J. A. O'Mahony (2019). Byproducts from Dairy Processing. In: Byproducts from Agriculture and Fisheries: Adding Value for Food, Feed, Pharma and Fuels (B. K. Simpson, A. N. A. Aryee e F. Toldrá, Eds.), Wiley, pp. 57–106.

Omokaro, G. O., Z. S. Nafula, N. E. Iloabuchi, A. A. Chikukula, O. G. Osayogie e E. C. Nnoli (2025). Microalgae as Biofactories for Sustainable Applications: Advancing Carbon Sequestration, Bioenergy, and Environmental Remediation. Sustainable Chemistry for Climate Action, 7, 100098. https://doi.org/10.1016/j.scca.2025.100098

Ostardo, N. (2024). Utilizzo di Scarti dell'Industria Lattiero-Casearia per la Coltivazione di *Galdieria sulphuraria*: Ottimizzazione della Resa in Reattori Continui. Master's Thesis, Università degli Studi di Padova.

Otari, S., V. A. Bapat, J. Lakkakula, U. S. Kadam e P. Suprasanna (2024). Xanthan Gum Produced from Milk Permeate and Deproteinized Cheese Whey: A Comparative Analysis with Commercial Xanthan Gums. Biocatalysis and Agricultural Biotechnology, 56, 103053.

Ozelcik, D., S. Suwal, C. Ray, B. K. Tiwari, P. E. Jensen e Y. Pouliot (2024). Valorization of Dairy Side-Streams for the Cultivation of Microalgae for Value-Added Food Products. Trends in Food Science & Technology, 146, 104454. https://doi.org/10.1016/j.tifs.2024.104454

Pahmeyer, M. J., S. A. Siddiqui, D. Pleissner, J. Gołaszewski, V. Heinz e S. Smetana (2022). An Automated, Modular System for Organic Waste Utilization Using Heterotrophic Alga *Galdieria sulphuraria*: Design Considerations and Sustainability. Bioresource Technology, 348, 126800. https://doi.org/10.1016/j.biortech.2022.126800

Parveen, A., P. Bhatnagar, P. Gautam, B. Bisht, M. Nanda, S. Kumar, M. S. Vlaskin e V. Kumar (2023). Enhancing the Bio-Prospective of Microalgae by Different Light Systems and Photoperiods. Photochemical & Photobiological Sciences, 22, 2687–2698. https://doi.org/10.1007/s43630-023-00471-9

Patel, R. S. e B. K. Sakhale (n.d.). By-Products of Dairy Industry and Their Utilization. Government College for Women, Gandhinagar. https://gcwgandhinagar.com/econtent/document/15871824941FSTSE0601_ByProductsOfDairyIndustryAndTheirUtilization.pdf

Penloglou, G., A. Pavlou e C. Kiparissides (2024). Recent Advancements in Photo-Bioreactors for Microalgae Cultivation: A Brief Overview. Processes, 12(6), 1104. https://doi.org/10.3390/pr12061104

Penn, M. R., J. J. Pauer e J. R. Mihelcic (2006). Biochemical Oxygen Demand. In: Environmental and Ecological Chemistry, Vol. 2 (J. M. Lehr e J. Keeley, Eds.), Encyclopedia of Life Support Systems (EOLSS), UNESCO.

Perez-Garcia, O., T. M. E. Escalante, L. E. de-Bashan e Y. Bashan (2011). Heterotrophic Cultures of Microalgae: Metabolism and Potential Products. Water Research, 45(1), 11–36. https://doi.org/10.1016/j.watres.2010.08.037

Pleissner, D. e S. Smetana (2020). Estimation of the Economy of Heterotrophic Microalgae- and Insect-Based Food Waste Utilization Processes. Waste Management, 102, 198–203. https://doi.org/10.1016/j.wasman.2019.10.031

Pleissner, D., N. Händel, S. Schönfelder, J.-I. Petrusan, B. Queiroz Silva, J. Schröder, J. Müller, K. Cowan e S. Smetana (2025). Long-Term Heterotrophic Cultivation of *Galdieria sulphuraria* at Technical Scale Under Non-Sterile Conditions. Sustainable Chemistry One World, 8, 100116.

Pontonio, E., M. Montemurro, G. V. De Gennaro, V. Miceli, C. G. Rizzello et al. (2021). Antihypertensive Peptides from Ultrafiltration and Fermentation of the Ricotta Cheese Exhausted Whey: Design and Characterization of a Functional Ricotta Cheese. Foods, 10(11), 2573. https://doi.org/10.3390/foods10112573

Poonia, A. e A. Trajkovska Petkoska (Eds.) (2023). Whey Valorization: Innovations, Technological Advancements and Sustainable Exploitation. Chapter 2, Springer Singapore. https://doi.org/10.1007/978-981-99-5459-9

Powell, N., A. N. Shilton, S. Pratt e Y. Chisti (2008). Factors Influencing Luxury Uptake of Phosphorus by Microalgae in Waste Stabilization Ponds. Environmental Science & Technology, 42(16), 5958–5962. https://doi.org/10.1021/es703118s

Prabhu, S. (n.d.). Industrial Lubricant Recovery Using a Disc Stack Centrifuge. Machinery Lubrication. https://www.machinerylubrication.com/Read/31902/disc-stack-centrifuge

Prazeres, A. R., F. Carvalho e J. Rivas (2012). Cheese Whey Management: A Review. Journal of Environmental Management, 110, 48–68. https://doi.org/10.1016/j.jenvman.2012.05.018

Pugliese, A., G. Cabassi, E. Chiavaro, M. Paciulli, E. Carini e G. Mucchetti (2017). Physical Characterization of Whole and Skim Dried Milk Powders. Journal of Food Science and Technology, 54(11), 3433–3442. https://doi.org/10.1007/s13197-017-2795-1

Quiroz, D., J. A. McGowen e J. C. Quinn (2025). Techno-Economic Analysis of Microalgae Cultivation Strategies: Batch and Semi-Continuous Approaches. Algal Research, 104109. https://doi.org/10.1016/j.algal.2025.104109

Quispe-Chávez, N. (2004). Conceptual Methodology for the Design of Dairy Processes. Doctoral Dissertation, University of Canterbury. https://toaz.info/doc-view-3

Rahman, A., S. Pan, C. Houston e T. Selvaratnam (2021). Evaluation of *Galdieria sulphuraria* and Chlorella vulgaris for the Bioremediation of Produced Water. Water, 13, 1183. https://doi.org/10.3390/w13091183

Rahman, T., W. L. Ebert e J. E. Indacochea (2018). Effect of Molybdenum Additions on the Microstructures and Corrosion Behaviours of 316L Stainless Steel-Based Alloys. Corrosion Engineering, Science and Technology, 53(3), 1–8. https://doi.org/10.1080/1478422X.2018.1443991

Ras, M., J.-P. Steyer e O. Bernard (2013). Temperature Effect on Microalgae: A Crucial Factor for Outdoor Production. Reviews in Environmental Science and Biotechnology, 12, 153–164. https://doi.org/10.1007/s11157-013-9310-6

Raven, J. A., J. Beardall e M. Giordano (2014). Energy Costs of Carbon Dioxide Concentrating Mechanisms in Aquatic Organisms. Photosynthesis Research, 121(2–3), 111–124. https://doi.org/10.1007/s11120-013-9962-7

Razzak, S. A., K. Bahar, K. M. O. Islam, S. M. Z. Hossain, A. Hanif, M. O. Faruque e M. M. Hossain (2017). Microalgae Cultivation in Photobioreactors: Sustainable Solutions for a Greener Future. Green Chemical Engineering. https://doi.org/10.1016/j.gce.2017.04.001

Retta, B., M. Iovino e C. Ciniglia (2024). Significance and Applications of the Thermo-Acidophilic Microalga *Galdieria sulphuraria* (Cyanidiophytina, Rhodophyta). Plants, 13(13), 1786. https://doi.org/10.3390/plants131317886

Ritchie, H. e M. Roser (2023). Milk Consumption. Our World in Data. https://ourworldindata.org/milk-production

Romero-García, J. M., C. V. González-López, C. Brindley, J. M. Fernández-Sevilla e F. G. Acíen-Fernández (2022). Simulation and Techno-Economical Evaluation of a Microalgal Biofertilizer Production Process. Biology, 11(9), 1359. https://doi.org/10.3390/biology11091359

Russo, G. L., A. L. Langelotti, M. Oliviero, M. Baselice, R. Sacchi e P. Masi (2021). Valorization of Second Cheese Whey Through Cultivation of Extremophile Microalga *Galdieria sulphuraria*. AIMS Environmental Science, 8(5), 435–448. https://doi.org/10.3934/environsci.2021028

Rybak, K., O. Parniakov, K. Samborska, A. Wiktor, D. Witrowa-Rajchert e M. Nowacka (2021). Energy and Quality Aspects of Freeze-Drying Preceded by Traditional and Novel Pre-Treatment Methods as Exemplified by Red Bell Pepper. Sustainability, 13(4), 2035. https://doi.org/10.3390/su13042035

Salbitani, G. e S. Carfagna (2020). Different Behaviour Between Autotrophic and Heterotrophic *Galdieria sulphuraria* (Rhodophyta) Cells to Nitrogen Starvation and Restoration: Impact on Pigment and Free Amino Acid Contents. International Journal of Plant Biology, 11(1), 8567. https://doi.org/10.4081/pb.2020.8567

Santiago-López, L., M. A. Zabat, E. Fleming, S. M. Jay, R. L. Hettich e D. Shukla (2021). A Review on the General Cheese Processing Technology, Flavor Biochemical Pathways and the Influence of Yeasts in Cheese. Frontiers in Microbiology, 12, 703284. Frontiers Media S.A. https://doi.org/10.3389/fmicb.2021.703284

Sar, T., S. Harirchi, M. Ramezani, G. Bulkan, M. Yesilcimen Akbas, A. Pandey e M. J. Taherzadeh (2022). Potential Utilization of Dairy Industries By-Products and Wastes Through Microbial Processes: A Critical Review. Science of the Total Environment, 810, 152253. https://doi.org/10.1016/j.scitotenv.2021.152253

Sarıtaş, S., A. E. Kalkan, K. Yılmaz, S. Gürdal, T. Göksan, A. M. Witkowska, M. Lombardo e S. Karav (2025). Biological and Nutritional Applications of Microalgae. Nutrients, 17(1), 93. https://doi.org/10.3390/nu17010093

Sciuto, G., N. Russo, C. L. Randazzo e C. Caggia (2025). Valorization of Second Cheese Whey Through Microalgae-Based Treatments: Advantages, Limits, and Opportunities. BioTech, 14, 79. MDPI, Basel (Switzerland).

Shenzhen Igrow Bio-Tech Co., Ltd. (2026). 2.5umol/J 600w LED Grow Lights. Ecer. https://mart.ecer.com/fullspectrum-growlights/pz66513b3-2-5umol-j-600w-led-grow-lights.html

Sierra, E., F. G. Acíen, J. M. Fernández, J. L. García, C. González e E. Molina (2008). Characterization of a Flat Plate Photobioreactor for the Production of Microalgae. Chemical Engineering Journal, 138(1–3), 136–147. https://doi.org/10.1016/j.cej.2007.06.004

Silva, M., P. Geada, R. N. Pereira e J. A. Teixeira (2025). Microalgae Biomass—A Source of Sustainable Dietary Bioactive Compounds Towards Improved Health and Well-Being. Food Chemistry Advances, 6, 100926. https://doi.org/10.1016/j.focha.2025.100926

Singh, S. P. e P. Singh (2015). Effect of Temperature and Light on the Growth of Algae Species: A Review. Renewable and Sustainable Energy Reviews, 50, 431–444.

Sodini, I., P. Morin, A. Olabi e R. Jiménez-Flores (2006). Compositional and Functional Properties of Buttermilk: A Comparison Between Sweet, Sour, and Whey Buttermilk. Journal of Dairy Science, 89(2), 525–536. https://doi.org/10.3168/jds.S0022-0302(06)72151-4

Somers, M. D., P. Chen, J. Clippinger, J. R. Cruce, R. Davis, P. J. Lammers e J. C. Quinn (2021). Techno-Economic and Life-Cycle Assessment of Fuel Production from Mixotrophic *Galdieria sulphuraria* Microalgae on Hydrolysate. Algal Research, 59, 102419. https://doi.org/10.1016/j.algal.2021.102419

SPX Flow (2019). APV General Milk Processing. SPX Flow, Inc. https://www.spxflow.com/assets/pdf/apv-general-milk-processing-wp-gb-1019.pdf

Spolaore, P., C. Joannis-Cassan, E. Duran e A. Isambert (2006). Commercial Applications of Microalgae. Journal of Bioscience and Bioengineering, 101(2), 87–96. https://doi.org/10.1263/jbb.101.87

Stasinakis, A. S., P. Charalambous e I. Vyrides (2022). Dairy Wastewater Management in EU: Produced Amounts, Existing Legislation, Applied Treatment Processes and Future Challenges. Journal of Environmental Management, 303, 114152. Elsevier, Amsterdam (The Netherlands).

Tetra Pak International S.A. (2026). Tetra Pak® UF System P. Tetra Pak. Retrieved February 22, 2026, from https://www.tetrapak.com/en-sg/solutions/integrated-solutions-equipment/processing-equipment/membrane-filtration/uf-system-p

Thoré, E. S. J., K. Muylaert, M. G. Bertram e T. Brodin (2023). Microalgae. Current Biology, 33(3), PR91–PR95. https://doi.org/10.1016/j.cub.2022.12.025

Tounsi, L., H. Ben Hlima, F. Hentati, O. Hentati, H. Derbel, P. Michaud e S. Abdelkafi (2023). Microalgae: A Promising Source of Bioactive Phycobiliproteins. Marine Drugs, 21(8), 440. https://doi.org/10.3390/md21080440

Trucent (2021). Milk Centrifugation Process Overview. https://www.trucent.com/milk-centrifugation-process-overview/

Tsermoula, P., G. Barone e J. A. O'Mahony (2024). Physicochemical Properties and Stability of Milk Permeate as Influenced by Ultrafiltration Processing Parameters. International Dairy Journal, 157, 106005. https://doi.org/10.1016/j.idairyj.2024.106005

Turton, R., J. A. Shaeiwitz, D. Bhattacharyya e W. B. Whiting (2018). Analysis, Synthesis, and Design of Chemical Processes (5th ed.). Pearson.

Tuson, J. A. e R. E. Coffey (1976). Feasibility Evaluation of Cheese Whey Processing in Small Plants. Journal of Dairy Science, 59(12), 2127–2133. https://doi.org/10.3168/jds.S0022-0302(76)84367-6

U.S. Dairy Export Council (2025). U.S. Whey and Milk Permeate: Cost Saving, Flavor Enhancing Ingredient. https://usdairyexcellence.org/wp-content/uploads/2025/02/en_2025-US-Whey-and-Milk-Permeate.pdf

U.S. Department of Agriculture, Agricultural Marketing Service (2026). Pacific Northwest Production Cost Report (Bi-Weekly). Report, March 20, 2026. https://www.ams.usda.gov/mnreports/ams_3657.pdf

Utilitatis (2025). Blue Book 2025 (Executive Summary). https://www.utilitatis.org/wp-content/uploads/2025/03/BLUE-BOOK-2025-EXS-ENG.pdf

Uyar, B., M. D. Ali e G. E. O. Uyar (2024). Design Parameters Comparison of Bubble Column, Airlift and Stirred Tank Photobioreactors for Microalgae Production. Bioprocess and Biosystems Engineering. https://doi.org/10.1007/s00449-023-02952-8

Valdovinos-García, E. M., M. G. Bravo-Sánchez, M. de los Á. Olán-Acosta, J. Barajas-Fernández, A. Guzmán-López e M. A. Petriz-Prieto (2022). Technoeconomic Evaluation of Microalgae Oil Production: Effect of Cell Disruption Method. Fermentation, 8(7), 301.

Van Etten, J. (2020). Red Algal Extremophiles: Novel Genes and Paradigms. Microscopy Today, 28(6), 28–35. https://doi.org/10.1017/S1551929520001534

Verma, R., K. V. L. Kumari, A. Srivastava e A. Kumar (2020). Photoautotrophic, Mixotrophic, and Heterotrophic Culture Media Optimization for Enhanced Microalgae Production. Biochemical Engineering Journal, 163, 107702. https://doi.org/10.1016/j.bej.2020.107702

Vuppaladadiyam, A. K., P. Prinsen, A. Raheem, R. Luque e M. Zhao (2018). Microalgae Cultivation and Metabolites Production: A Comprehensive Review. Biofuels, Bioproducts and Biorefining, 12(2), 304–324. https://doi.org/10.1002/bbb.1864

Walstra, P., J. T. M. Wouters e T. J. Geurts (2006). Dairy Science and Technology (2nd ed.). CRC Press. https://biot409.wordpress.com/wp-content/uploads/2014/02/16-dairy-science-and-technology.pdf

Wang, J., H. Yang e F. Wang (2014). Mixotrophic Cultivation of Microalgae for Biodiesel Production: Status and Prospects. Applied Biochemistry and Biotechnology, 172(7), 3307–3329. https://doi.org/10.1007/s12010-014-0729-1

Yu, Z., W. Zhao, H. Sun, H. Mou, J. Liu, H. Yu, L. Dai, Q. Kong e S. Yang (2024). Phycocyanin from Microalgae: A Comprehensive Review Covering Microalgal Culture, Phycocyanin Sources and Stability. Food Research International, 186, 114362. https://doi.org/10.1016/j.foodres.2024.114362

Zhu, L. (2015). Microalgal Culture Strategies for Biofuel Production: A Review. Biofuels, Bioproducts and Biorefining, 9, 801–814. https://doi.org/10.1002/bbb.1576